Timing and amount of southern Cascadia earthquake subsidence over the past 1,700 years at northern Humboldt Bay, California, USA

Jason S. Padgett[1,2], Simon E. Engelhart[1], Harvey M. Kelsey[3], Robert C. Witter[4], Niamh Cahill[5] and Eileen Hemphill-Haley[3]

[1]*Department of Geography, Durham University, Durham DH1 3LE,, UK*
[2]*Department of Geosciences, University of Rhode Island, Kingston, Rhode Island 02881, USA*
[3]*Department of Geology, Humboldt State University, Arcata, California 95524, USA*
[4]*U.S. Geological Survey, Alaska Science Center, Anchorage, Alaska 99508, USA*
[5]*Department of Mathematics and Statistics, Maynooth University, Kildare, Ireland*

ABSTRACT

Stratigraphic, lithologic, foraminiferal, and radiocarbon analyses indicate that at least four abrupt mud-over-peat contacts are recorded across three sites (Jacoby Creek, McDaniel Creek, and Mad River Slough) in northern Humboldt Bay, California (~44.8°N, -124.2°W). The stratigraphy records subsidence during past megathrust earthquakes at the southern Cascadia subduction zone, ~40 km north of the Mendocino Triple Junction. Maximum and minimum radiocarbon ages on plant macrofossils from above and below laterally extensive (>6 km) contacts suggest regional synchroneity of subsidence. The shallowest contact has radiocarbon ages consistent with the most recent great earthquake at Cascadia in 250 cal yr BP (1700 CE). Using Bchron and OxCal software, we model ages for the three older contacts of ~875, ~1,120 and ~1,620 cal yr BP.

For each of the four earthquakes, we analyze foraminifera across representative mud-over-peat contacts selected from McDaniel Slough. Changes in fossil foraminiferal assemblages across all four contacts reveal sudden relative sea-level (RSL) rise (land subsidence) with lasting submergence (decades to centuries). To estimate subsidence during each earthquake, we reconstructed RSL rise across the contacts using the fossil foraminiferal assemblages in a Bayesian transfer function. The coseismic subsidence

estimates are 0.85 ±0.46m for the 1700 CE earthquake, 0.42±0.37 m for the ~875 cal yrs BP earthquake, 0.79±0.47 m for the ~1,120 cal yrs BP earthquake, and ≥0.93 m for the ~1,620 cal yrs BP earthquake. The subsidence estimate for the 1,620 cal yrs BP earthquake is a minimum because the pre-subsidence paleoenvironment likely was above the upper limit of foraminiferal habitation. The subsidence estimate for the ~875 cal yrs BP earthquake is less than (<50%) the subsidence estimates for other contacts and suggests that subsidence magnitude varied over the past four earthquake cycles in southern Cascadia.

1. INTRODUCTION

Many of Cascadia's coastal wetlands host extensive stratigraphic evidence for coseismic subsidence induced by earthquake rupture on the subduction megathrust. Over three decades of coastal paleogeodetic research on these natural archives has greatly improved our understanding of Cascadia plate boundary processes (Atwater, 1987; Darienzo, 1987; Peterson and Darienzo, 1991; Atwater et al., 1992; Nelson, 1992; Nelson et al., 1996; Shennan et al. 1996; Atwater and Hemphill-Haley, 1997; Kelsey et al., 2002; Witter et al., 2003; Hawks et al., 2010; 2011; Engelhart et al., 2013, Wang et al., 2013; Milker et al., 2017). However, current coastal datasets do not resolve fundamental questions in Cascadia subduction zone (CSZ) science, such as estimation and variability in past earthquake magnitude and the potential for persistent earthquake rupture boundaries. These questions require in part better earthquake chronologies and thus prompt the first question, given adequate radiocarbon age determinations for contacts that represent subduction zone earthquakes, which Bayesian age models optimally model earthquake ages? Additionally, one of the challenges of better defining the variability in rupture length and magnitude for past subduction zone earthquakes bears on the uncertainty of evidence used to correlate paleoearthquake histories from one paleoseismic site to others along the margin. Thus, the other outstanding question we address is, what is the needed level of resolution, both of age ranges for specific paleoearthquakes and subsidence amounts for specific paleoearthquakes, to correlate earthquake records within study areas at one paleoseismic site, or correlate of earthquake records among different coastal paleoseismic sites.

Stratigraphic correlation of wetland stratigraphy within a marsh, over tens to hundreds of meters, can often be straightforward. However, it becomes increasingly difficult with distance, both across multiple marshes within a single estuary and over tens to hundreds of kilometers between estuaries (Nelson et al., 1996; Milker et al., 2016). For evidence of earthquakes prior to the well-documented 1700 CE earthquake, radiocarbon dating techniques can test models of stratigraphic correlation within and across sites. Yet in many cases radiocarbon age errors can be on the order of several hundred years, which presents difficulties when attempting to correlate stratigraphic contacts among estuaries recording earthquakes that have 200-500 year recurrence intervals, (Atwater, 1987; Adams, 1990; Nelson, 1992; Nelson et al., 1996; Shennan et al. 1996; Atwater and Hemphill-Haley, 1997; Kelsey et al., 2002; Witter et al., 2003; Nelson et al., 2008; Goldfinger et al., 2012; Enkin et al., 2013; Milker et al., 2016). Promisingly, new methods that incorporate multiple minimum and maximum limiting ages of in-situ plant macrofossils found above and below subsidence contacts (Nelson et al., 2006; 2008; Kemp et al., 2013; Milker et al., 2017) and Bayesian statistics (e.g., Bronk Ramsey, 2008;

Parnell et al., 2008) produce more accurate chronologies with better precision of stratigraphic ages to aid in correlation (Kelsey et al., 2005; Goldfinger, 2012; Enkin et al., 2013; Garrett et al., 2013; Milker et al., 2016; Dura et al., 2017; Witter et al., 2019; Nelson et al., 2019).

Equally as important to defining the timing of past plate boundary rupture is quantifying the amount of coseismic vertical deformation. Early Cascadia coastal research utilized qualitative and quantitative methods to estimate coseismic subsidence with accompanying errors that were either poorly defined for qualitative approaches or typically ±0.5–1.0 m for early quantitative methods (e.g., TWINSPAN, DCA; Shennan et al, 1996). Such errors are generally too large to distinguish differences between earthquakes or between sites. In order to improve estimates of coseismic subsidence, subsequent research at Cascadia has focused on the development of quantitative microfossil-based transfer functions primarily using foraminifera (e.g., Jennings and Nelson, 1992; Guilbault et al., 1995; 1996; Nelson et al., 2008; Hawkes et al., 2010; 2011; Engelhart et al., 2013; 2015; Milker et al., 2015; 2016). Foraminiferal-based transfer functions use the modern species-elevation relationships to relate fossil assemblages to past tidal elevations and enable researchers to assess differences in coseismic subsidence estimates. Cascadia foraminiferal transfer function analysis has been applied to one earthquake at many sites (Hawkes et al., 2011; Wang et al., 2013; Kemp et al., 2018) and over multiple earthquake cycles at a single site (e.g., Milker et al., 2016; Nelson et al., 2019). For example, Wang et al. (2013) use foraminiferal transfer function subsidence estimates to model along-strike slip heterogeneity during the 1700 CE earthquake and highlight large spatial gaps within the paleogeodetic database, e.g., northern California and Washington. Recent refinement and expansion of the Cascadia foraminiferal-based transfer function has led to development of a Bayesian transfer function (BTF), which can model non-unimodal taxa-elevation relationships, improves the availability of modern analogues for fossil samples, and is capable of handling sediment and microfossil mixing through assigning simple informative priors based on lithology (Kemp et al., 2018).

Northern Humboldt Bay was one of the first locations recognized to contain stratigraphic evidence of past Cascadia subduction zone earthquakes (Vick, 1988; Clarke and Carver, 1992; Valentine 1992). However, the complicated stratigraphic record has led to disparate interpretations by various research groups that are yet to be clarified. For example, there remains no consensus on the number of past CSZ earthquake-induced subsidence contacts or the magnitude of coseismic deformation archived within the wetland stratigraphy. These open questions have resulted in paleoseismic interpretations that range from three to six earthquakes over the past ~1900 yrs, (e.g., Vick 1988, Clark and Carver 1992; Valentine, 1992; Pritchard, 2004; Valentine et al., 2012). Both limited radiocarbon constraints and a general lack of microfossil analysis likely contribute towards inconsistent stratigraphic correlations and lack of criteria to distinguish contacts caused by megathrust earthquakes or other mechanisms. However, the development of improved chronostratigraphic methods and quantitative foraminiferal-based transfer functions makes it timely to refine the northern Humboldt Bay paleoseismic history.

The goals of this paper are, first, to provide high-quality age determinations for times of wetland subsidence within the northern Humboldt Bay estuary, second, to construct a paleoseismic chronology for the site, third, to provide high-precision estimates of subsidence during past subduction zone earthquakes, and fourth, to reevaluate and update regional (43.5°-40.5°N) correlations of paleoearthquakes in the southern Cascadia subduction zone. Our results suggest that northern Humboldt Bay has recorded four CSZ earthquakes over the past 1,700 years and that the amount of coseismic subsidence and possibly earthquake magnitude varied in the past four Cascadia earthquakes.

2. SETTING

The southern Cascadia subduction zone, from the Coos Bay coastal area to Cape Mendocino (Fig 1), is a portion of the subduction zone where improved paleoseismic data would enable better informed models of along-strike heterogeneity during the most recent (1700 CE), and older, subduction zone earthquakes (Wang et al., 2013; Milker et al., 2016; Kemp et al., 2018). Southern Cascadia archives the temporally longest onshore paleoseismic records observed along the whole subduction zone with earthquake histories extending back to 6,700 years documented at the Sixes River, Bradley Lake, and Coquille River sites (Kelsey et al., 2002; 2005; Witter et al., 2003; Fig. 1). However, the two largest spatial data gaps with no paleoseismic information along the entire subduction zone are also in southern Cascadia (Fig. 1). These spatial data gaps are the ~75-km-long coastal reach north of Humboldt Bay and the ~85-km-long coastal reach north of the Crescent City area (Fig. 1b). These spatial data gaps occur because the coastal environments appear to lack a stratigraphic record that preserves RSL changes (Hemphill-Haley et al., 2019). Even though investigations at Lagoon Creek (<20 km south of Crescent City) have reported evidence for tsunami inundation as much as 3,500 yrs ago (Abramson, 1998; Garrison-Laney, 1998), many of the freshwater lacustrine and wetland environments near Crescent City record a limited extent of stratigraphic evidence for coseismic subsidence, e.g., Sand Mine marsh (Peterson et al., 2011; Simms et al., 2019; Hemphill-Haley et al., 2019). Finding subsidence stratigraphy in the spatial gaps north and south of Crescent City may not be realized, even with more field reconnaissance, if conditions preclude the accommodation space required to document stratigraphic evidence of late Holocene RSL changes (Kelsey et al., 2015; Dura et al., 2016). We chose an alternative approach to ultimately improving models of along-strike heterogeneity in southern Cascadia; namely, we reevaluate the paleoseismic record in northern Humboldt Bay, a site where subsidence stratigraphy has been documented but where previous legacy studies did not attain scientific consensus on the subduction zone earthquake record.

Despite northern Humboldt Bay being a focal point of southern Cascadia paleoseismic research over the past 30 years, the stratigraphic framework and paleoseismic history has remained unresolved. Vick (1988) was the first to describe the tidal wetland stratigraphy at northern Humboldt Bay and focused on the stratigraphy at Mad River Slough. Even though Vick (1988) observed five submergence contacts, based on stratigraphic mapping and six radiocarbon ages, he concluded that at least four submergence contacts represent coseismic subsidence. Subsequent investigations extended stratigraphic mapping and paleoseismic correlations beyond Mad River Slough and consequently developed both similar (Valentine, 1992; Clarke and Carver, 1992;) and diverging (Pritchard, 2004; Valentine et al., 2012) interpretations. Valentine (1992), Clarke and Carver (1992), and Valentine et al., (2012) correlate stratigraphic contacts and ages to other paleoseismic data from proximate trenching and wetland sites and conclude that four-to-six megathrust events have occurred over the past 2,000 yrs. In contrast, Pritchard (2004) focused solely on the tidal wetland stratigraphic record within the northern Humboldt Bay estuary and conclude that the tidal wetland stratigraphy records evidence for three-to-four megathrust earthquakes over the past 1,900 yrs. Even though specific correlations and conclusions have differed, the common theme throughout the research conducted at northern Humboldt Bay is that the complicated stratigraphy has restricted conclusionary findings and further research is required to refine the understanding of the paleoseismic history.

We studied stratigraphy beneath three tidal marshes that fringe the northern portion of Humboldt Bay: Mad River Slough, McDaniel Creek, and Jacoby Creek. These areas are protected and managed by U.S. Fish & Wildlife Service Humboldt Bay National Wildlife Refuge or the City Arcata, California (Fig. 2). Northern Humboldt Bay is separated from the Pacific Ocean by the ~20-25 m high Lanphere-Ma-le'l Dunes (Fig. 2c; Vick, 1988; Pickart and Hesp, 2019). At the mouth of Mad River Slough, a NOAA tide gauge station registers the semidiurnal tidal range (Mean Highest High Water, MHHW – Mean Lowest Low Water, MLLW) at 2.36 m (Fig. 2c; ID: 9418865). Because over half of northern Humboldt Bay surface area is exposed at low tide, most of the environments of the lagoon system are tidal channels and low-tide mud flats (Eicher, 1987). Low marshes form at elevations around mean high water (MHW) and high marshes form at elevations around mean higher high water (MHHW; Pritchard, 2004).

Flora and fauna within northern Humboldt Bay are typical for Cascadia tidal wetland plant and animal distributions (Pritchard, 2004; Hawkes et al., 2010; Engelhart, 2015; Kemp et al., 2018). Plant communities of lower marsh environments, around mean tide level (MTL), include *Distichlis spicata*, *Salicornia virginica*, *Spartina densiflora*, and *Triglochin maritimum* (Eicher, 1987). In high marsh environments plant communities include *Castilleja exserta*, *Distichlis spicata*, *Grindelia spp*., *Jaumea carnosa, Spartina alterniflora*, and *Triglochin maritimum* (Eicher, 1987). Kemp et al. (2018) show that intertidal benthic foraminiferal communities are comparable along the west coast of North America from ~35.5 -50° N. Benthic foraminiferal communities differ along an intertidal gradient such that higher marsh environments, around MHHW, are often dominated by *Trochaminita spp.*, *Haplophragmoides spp.*, *Balticammina pseudomacrescens*, *Trochammina inflata*, and *Jadammina macrescens*. Whereas at elevations from ~MHW down to MTL, increasing percentages of *Miliammina fusca*, *Ammobaculites spp.*, *Reophax spp.,* and calcareous foraminifera species are reported (Guilbault et al., 1995; 1996; Nelson et al., 2008; Hawkes et al., 2010; 2011; Engelhart et al., 2013a, 2013b; Pilarcyk et al., 2014; Milker et al., 2015a, 2015b; 2016; Kemp et al., 2018).

We selected three study sites because the existing wetland stratigraphic framework reflects a complicated stratigraphic record of earthquake subsidence. The stratigraphic sections typically consist of repeated abrupt mud-over-peat and mud-over-upland soil contacts, where a peat or upland soil is sharply overlain by tidal mud and then the tidal mud gradually grades upward into an overlying organic-rich unit.

3. RESEARCH APPROACH AND METHODS

In order to evaluate if stratigraphy is evidence of megathrust-induced land-level changes, we utilize a strategy refined by over three decades of research along the Cascadia margin through the context of land-level changes expressed by contrasting stratigraphic units within intertidal sediments (Atwater, 1987; Hemphill-Haley, 1995; Nelson et al., 1996; Kelsey et al., 2002; Witter et al., 2003; Hawkes et al., 2011; Engelhart et al., 2013; Shennan et al., 2016; Milker et al., 2017). Our approach utilizes four of the criteria proposed by Nelson et al., (1996) and Shennan et al., (2016) to test for identifying coseismic subsidence in tidal-wetland stratigraphic sequences. These criteria include 1) lateral extent of stratigraphic contacts, 2) suddenness of submergence, 3) amount of submergence, 4) regional synchroneity of submergence, which are determined by employing stratigraphic mapping, lithostratigraphic analysis, foraminiferal analysis, and radiocarbon dating techniques combined with potential correlations with other plate boundary earthquake records in southern Cascadia. We do not discuss the "coincidence of tsunami deposit" criterion because we found no evidence for a tsunami deposit above any buried organic-rich units. The ~20-25 m high, Lanphere-Ma-le'l Dunes may have protected northern Humboldt Bay from tsunami inundation (Vick, 1988; Pickart and Hesp, 2019).

Our research approach is three-fold; 1) lithostratigraphic analysis (describe subsurface stratigraphy at multiple core locations across three sites), 2) Chronologic analysis using Bayesian age models (constrained by radiocarbon AMS ages of plant macrofossils) and 3) relative sea-level reconstructions (estimate paleoenvironmental elevation changes using fossil foraminiferal data and an existing BTF; Kemp et al., 2018).

3.1 Lithostratigraphic analysis

3.1.1 Stratigraphic description and sampling

We compiled stratigraphic descriptions from 31 core locations over a >6 km transect at Mad River Slough (6), McDaniel Creek (15), and Jacoby Creek (10) moving west to east (landward) along the northern shore of northern Humboldt Bay (Fig. 2). Wetland stratigraphy consists of clastic mud and interbedded organic-rich units. A clastic "mud" refers to a grey to olive grey massive to finely (1-3mm) bedded silt and clay. An "organic-rich unit" refers to a dark oxidized salt marsh peat or an upland soil. A "submergence contact" is either a mud-over-peat or mud-over-upland soil contact.

Using a 30 mm wide gouge core, we mapped abrupt (1 mm), sharp (1-5 mm), clear (5-10 mm), and gradual (>10mm) submergence contacts up to ~4 m depth below the ground surface. Grain size, sedimentary structures, contacts, thickness, and facies changes were described in the field using general stratigraphic methods in combination with the Troels-Smith (1955) method for describing organic-rich sediment. Stratigraphic unit descriptions include peat, muddy peat, peaty mud, and mud. Organic percentages determined by qualitative field assessment (Troels-Smith, 1955) for peat, muddy peat, and peaty mud are 100%-75%, 75%-50%, and 50%-25%, respectively. Silt and clay units that consist of <25% organics by volume are described as "mud". For lab analyses, we selected representative segments (50 cm) of key stratigraphic intervals that visually contained the sharpest contacts between the mud-over-peat and mud-over-upland soil contacts and/or abundant in-situ plant macrofossils. Samples were collected for radiometric and biostratigraphic analyses using either an Eijkelkamp peat sampler or a 60 mm gouge core.

3.1.2 Stratigraphic Imaging

Contact sharpness and continuity is not always clear from optical inspection. Therefore, we followed recent studies in Cascadia (e.g., Goldfinger et al., 2012; Milker et al., 2016) and Alaska (e.g., Briggs et al., 2014; Witter et al., 2019) and obtained high-resolution imagery in order to analyze fossil core density contrasts. We examined density imagery of multiple representative cores prior to selecting the optimal core and stratigraphic intervals for counting foraminifera as well as selecting material for radiocarbon dating. Computerized tomography (CT) scans were conducted at Oregon State University College of Veterinary Medicine and Rhode Island South County Hospital, following the methods outlined in Rothwell and Rack (2006) and Davies et al. (2011). At Oregon State University, density measurements were collected at 120 kVp and 200 mA and a pitch of 0.5s (100 mAs) using a Toshiba Aquilion 64-slice CT system. For visualization purposes, the resulting images were processed with a "bone" algorithm to generate coronal images every millimeter across the core. At Rhode Island South County Hospital, density scans were collected with 32-slice GE LightSpeed scanner at 120 kVp and 200-600 mA (depending on the fossil core thickness) core and a pitch of 0.969:1. X-radiation (X-ray) images, collected with a Shimadzu UD150B-40 and imaged with a Fuji FCR XL-2 at the University of Rhode Island Health Center, also illuminate density differences within the collected sediment cores. The fossil core images were processed using Horos and Adobe Illustrator software.

3.1.3 Surveying to sea-level datum

Sample elevations for each core were acquired using RTK-GPS. Data collected by the RTK-GPS was post-processed using Online Positioning User Service, (https://www.ngs.noaa.gov/OPUS/) to obtain North American Vertical Datum 1988 (NAVD88) orthometric elevations. To establish elevations with respect to a tidal datum, we took RTK-GPS measurements of the tidal benchmarks associated with the temporary tide gauge installation (12/01/1978 to 03/31/1979) at Mad River Slough (NOAA ID: 9418865). The vertical precision of the RTK measurements are less than 4 cm.

3.2 Chronologic analysis

3.2.1 Radiocarbon dating

Plant macrofossils were collected from above and below key contacts to provide 24 bracketing maximum and/or minimum-ages for each organic-rich unit upper contact at all three sites. We focused on samples that were found in growth position and/or close (<3 cm) to submergence contacts and that have the potential to tightly constrain the timing of the organic-rich unit burial, such as rhizomes of salt-marsh plants that have a known relationship to the surface of the marsh (n=13). We also collected detrital fragments of plants including stems (n=8) and wood fragments (n=1), and seeds and seed casings (n=2). Discrete stratigraphic intervals, that range from 0.5 cm to 1.5 cm, were sampled from cores and disaggregated on a glass plate under a binocular microscope. Occasionally, high-resolution CT scans and X-radiographic images aided in targeting organic materials to be extracted from sediments. Selected material, usually plant rhizome, stem, or seed, was cleaned of all attached sediment particles and rootlets; then oven dried at ~50^{o} C for 24 hrs (Kemp et al., 2013; Nelson et al, 2015; Törnqvist et al., 2015). Once dried and weighed, samples were sent to National Ocean Science

Accelerator Mass Spectrometer (NOSAMS) laboratory at Woods Hole Oceanographic Institute for analysis. The AMS radiocarbon age results were calibrated with OxCal (version 4.2.4; Bronk Ramsey and Lee, 2013) using the IntCal13 calibration curve for terrestrial samples (Reimer et al., 2013) and are reported with the standard two-sigma uncertainty in calendar years before 1950 (cal yr BP).

3.2.2 Bayesian Age-models

We developed a representative, estuary-wide composite stratigraphy to be used in the construction of three Bayesian age models. The composite stratigraphy incorporates maximum and minimum plant macrofossil samples that were selected as close to the upper contacts of the buried organic-rich units as possible. Outlier ages, as well as anomalously older and younger ages than stratigraphic position would suggest, were not incorporated into the composite stratigraphic section used in model development.

Bayesian age-depth modeling has been used by many RSL investigations that seek to refine the timing of past changes in RSL and decrease the error envelopes of sediment accumulation histories (e.g., Garrett et al., 2013; Witter et al., 2015; Dura et al., 2017). Model choice is a vital component of reducing timing uncertainties and the consistency of accumulation rates should be considered (Wright et al., 2017). If deposition is seasonal, steady, and predictable, for example a lake bottom, then an OxCal 'U-sequence' command (Bronk Ramsey, 2008; 2009a) would be a good age model option because deposition is assumed to be fairly uniform. However, if a sedimentation rate is variable then models that can account for randomness in deposition can be more suitable e.g., Bchron (Parnell et al., 2008) or OxCal 'P-sequence'(Bronk Ramsey, 2008; 2009a). In contrast, if only an order is known, a more conservative model such as OxCal

‘Sequence’ command is appropriate, which only defines an order for events and groups of events (Bronk Ramsey, 1995). In regard to the ability to capture sedimentation rate variability, within their confidence intervals OxCal ‘P-sequence’ and Bchron outperform other age modeling programs (Trachsel and Telford, 2016; Wright et al., 2017).

Typically, tidal wetland stratigraphic investigations obtain a chronologic dataset, construct a numerical age-depth model, and test the results to other regional datasets. However, little work has considered the potential differences in the age estimate results that could be imposed by the numerical age-model of choice. Moreover, often only the modeling program is cited without the specific type of model identified and/or explained (Milker et al., 2016; Nelson et al., 2020). We attempt to address this gap by comparing useful Bayesian age-depth models, in order to assess the variability in age estimates that may be imposed by model choice.

Three Bayesian age models with different assumptions are utilized to estimate time of organic-rich unit burial, OxCal ‘Sequence’ and ‘P-sequence’ commands (Bronk Ramsey, 1995; 2008; 2009a), and Bchron (version 4.3.0; Haslett and Parnell, 2008). The OxCal ‘Sequence’ command only incorporates the relative positioning of the age constraints within the composite stratigraphy, i.e., does not incorporate a modeled sedimentation rate to further refine the ages of subsidence contacts. In contrast, OxCal ‘P-sequence’ and Bchron model sedimentation rates based on age constraint depths and accumulation rate parameters (Trachsel and Telford, 2016). OxCal ‘P-sequence’ allows for variable sediment accumulation as a Poisson process controlled by the user defined *‘k-parameter’*. We follow the approach of Bronk Ramsey (2008) and Enkin et al., (2013) for determining the optimal value of *k* by selecting the highest k value to give a satisfactory agreement with the actual dating information. Bchron also incorporates sample depths to further constrain the age estimate by modeling a sedimentation rate between age constraint intervals but, in contrast to OxCal 'P-sequence,' does so without the user defining a sedimentation rate parameter. Instead, Bchron is based on modeling piecewise linear accumulations, where increments are independent and arrive in a Poisson fashion, which allows for abrupt changes in accumulation rates (Haslett and Parnell, 2008; Trachsel and Telford, 2016). Modeled sedimentation rates trim the predicted age resulting in a more precise estimate. However, the accuracy will be dependent on an appropriate density of radiocarbon dates that can identify changes in sedimentation rate that may be expected post-earthquake and that exceed the long-term (centennial-scale) average. Using more than one Bayesian age modeling technique, each with different assumptions, enables us to assess the impacts of model choice on the variability of age estimates.

3.2.3 Regional Paleoseismic Timing Correspondence

Based on our comparison of Bayesian modeling techniques, described below (section 4), we prefer results from the OxCal 'Sequence' modeling technique. Thus, we compare the age distributions derived from OxCal 'Sequence' results from northern Humboldt Bay with the timing of plate-boundary earthquakes at other sites along the southern Cascadia coastal estuarine and lacustrine environments from 43.5°-40.5° N, which include Eel River (Li, 1992), southern Humboldt Bay (Patton, 2004), Lagoon Creek (Abramson, 1998; Garrison-Laney 1998), Bradley Lake (Kelsey et al., 2005), Coquille River (Witter et al., 2003) and Talbot Creek, which is tributary to South Slough in the Coos Bay region of Southern Oregon (Milker et al, 2016). We also compare offshore turbidite data that has been interpreted to reflect shaking produced by great earthquakes (Goldfinger et al., 2012). We do not include paleoseismic data from Sixes River into our comparison because, since about 2000 years ago, the lower Sixes River Valley has not recorded (or minimally recorded) coseismic subsidence. i.e., earthquakes did not drop the lower valley into the intertidal range (Kelsey et al., 2002). Bradley Lake and Lagoon Creek are coastal lacustrine environments that are inferred to have recorded tsunami inundation coincident with plate-boundary earthquakes. Eel River, southern and northern Humboldt Bay, Coquille River, and Talbot Creek are estuarine marshes that have recorded evidence for both coseismic land-level changes and occasionally subsequent tsunami inundation. Offshore turbidite chronology provides the longest stratigraphic records of CSZ paleoseismic history. Each location included in our comparison has recorded evidence of megathrust earthquakes within the past ~2000 years.

3.3 Relative sea-level reconstructions

3.3.1 Foraminifera

Fossil foraminifera species assemblages are indicative of paleo-intertidal environments. We followed standard sample preparation and analysis techniques of fossil foraminiferal found within wetland stratigraphy (e.g. Scott and Medioli, 1982; de Rijk, 1995; Horton and Edwards, 2006). Fossil foraminifera were concentrated by sieving 1 cm intervals of sediment (~3cm^3) from collected cores over 500- and 63-micron sieves and retaining the material between those size fractions. The 500-micron sieve was checked for larger foraminifera before material was discarded. Fossil samples were analyzed until at least 200 dead foraminifera were identified, or until the entire sample was enumerated (Fatela and Taborda, 2002). Following after Kemp et al. (2018), only samples with >30 foraminifera were used in the production of quantitative RSL reconstructions because low abundances may reflect a non in-situ assemblage and/or may not be representative of the depositional environment. Foraminifera were identified following taxonomy based on Hawkes et al. (2010) and Milker et al. (2015). Additionally, we combine *Haplophragmoides spp* following Kemp et al. (2018). We apply a pairwise comparison test of modern and fossil foraminiferal assemblages in order to confirm that all fossil assemblages have modern analogs.

3.3.2 Transfer Function

Sudden RSL change caused by subsidence during past great earthquakes along the Cascadia coastal margin can be quantified using fossil foraminifera (found within subsidence stratigraphy) and a transfer function (Guilbault et al., 1995; 1996; Nelson et al., 2008, Hawkes et al., 2010; 2011; Engelhart et al., 2013; Wang et al., 2013; Milker et al., 2016; Kemp et al., 2018). Early fossil foraminifera transfer functions utilized a local (same site) training set of foraminiferal assemblages and tidal elevations (Guilbault et al., 1995; 1996; Nelson et al., 2008). Later efforts progressed to regional modern training sets where more robust taxa-elevation relationships were constructed based on compilations from several marsh sites (Hawkes et al., 2010; 2011; Engelhart et al., 2013; Wang et al., 2013; Milker et al., 2016). Generally, a larger modern dataset provides a higher diversity of modern analogs and covers more natural variability; but a larger modern dataset is often accompanied with reduced precision (Horton and Edwards, 2005). More recently, Kemp et al. (2018) developed a BTF that incorporates an extended West Coast modern foraminifera training set, allows for flexible species-response curves, and can formally incorporate information about elevation from additional proxies, e.g., other microfossil groups, $\delta^{13}C$, or lithologic/stratigraphic context, which combine to produce more informed estimates of RSL reconstruction and extends applicability of the methodology (Cahill et al., 2016; Holden et al., 2017). We follow Kemp et al. (2018) and use lithology to provide constraints for RSL reconstructions. The lithology ranges from either clastic dominated (tidal flat) to low salt-marsh sediment, which most likely accumulates at elevations between mean low water (MLW) and MHHW (20-200 SWLI; standardized water level index), or organic-rich high salt marsh, which most likely accumulates at elevations around MHW to the Highest Occurrence of Foraminifera (HOF; 180-252 SWLI; Kemp et al., 2018). Although clastic sediment can accumulate at elevations below 20 SWLI, we follow the assumptions of Kemp et al. (2018). The BTF does not incorporate a lithologic constraint of a forest or upland soil unit, as it occurs above HOF and foraminifera cannot inform such elevations. In order to evaluate if a fossil assemblage has a modern analog, we used the Bray-Curtis distance metric. Due to low species diversity, a threshold of less than the 20th percentile is appropriate for salt marsh foraminifera modern and fossil assemblage pairings (Kemp and Telford, 2015).

4. RESULTS

We first describe wetland stratigraphy across the three sites. Then, we present radiocarbon ages that constrain the timing of organic-rich unit burial. Using the radiocarbon age results, we correlate buried organic-rich units among all the sites using lithology, depth, and age. Next, we present radiocarbon age modeling in order to assign age ranges for the submergence contacts. Finally, using foraminiferal analyses, we present estimates of subsidence across submergence contacts at McDaniel Creek.

We focus our foraminiferal analysis on stratigraphic sections collected at McDaniel Creek because it archives the largest spatial extent of subsidence stratigraphy within northern Humboldt Bay. One exception is analysis of a single stratigraphic section from Mad River Slough because of the limited spatial extent of a contact that is not found at McDaniel Creek. To derive a subsidence estimate we use the distributions of the reconstructed RSL elevations from the first unmixed centimeter intervals above and below the subsidence contact.

4.1 Wetland Stratigraphy

In cores, we observed grey mud units sharply overlying dark organic-rich units, which we refer to as a submergence contact (Fig 3; Table 1). The organic-rich units contain humified organic matter and plant macrofossils. The clastic muds contain sparse plant macrofossils and were often massive and occasionally finely bedded. We did not observe any sand layers between an organic-rich unit and overlying mud across the estuary. In general, the shallowest organic-rich units are well defined and widespread, while deeper organic-rich units are often less distinct, more humified, and have a more restricted lateral extent. Stratigraphic mapping identified five submergence contacts at Mad River Slough, four submergence contacts at McDaniel Creek and three submergence contacts at Jacoby Creek (Fig. 3; Table 1). We reoccupied previously described wetland stratigraphic sections (Vick, 1988; Clarke and Carver, 1992; Valentine, 1992; Pritchard, 2004; Valentine et al., 2012) and further extended the spatial extent of wetland stratigraphic mapping in northern Humboldt Bay. In doing so, we document submergence contacts that have not been previously described at McDaniel Creek and Jacoby Creek marshes.

4.1.1 Mad River Slough

We reoccupied six coring sites of Vick (1988) in the southern portion of Mad River Slough and observed similar stratigraphy (Fig. 3b). We observed five submergence contacts at *MR.2* and *MR.7*; but based on lithology and depth, we can correlate four submergence contacts across the six-location survey at Mad River Slough (Figs. 2b and 3b; Table 1). Core top elevations differ from the west to the east side of the main tidal channel, 2.1 m and 1.4 m respectively (NAVD88). The shallowest organic rich unit is a well-developed peat, observed at every core location, and is relatively thick. The second deepest from the surface (all following descriptions follow this orientation) organic-rich unit is a relatively thin peat and observed <8 cm below the lower contact of the overlying peat unit. The second and fifth deepest organic-rich units were only observed at the same two core locations, *MR.2* and *MR.7* (Figs. 2b and 3b; Table 1). The third deepest organic-rich unit was observed at every core location and ranges from a rooted mud to a peat between the core locations. The fourth deepest was observed on both sides of the main channel and described as a peat unit. The deepest organic-rich unit is a humified peat. Although all the submergence contacts are at least clear, the fourth and fifth deepest organic-rich units have less distinct upper contacts (Table 1). In summary, five submergence contacts were observed at two core locations, three submergence contacts were observed at two core locations, and two submergence contacts were observed at two core locations (Fig. 3b). Mad River Slough archives the highest amount of stratigraphic variability throughout the estuary (Fig. 3b; Table 1).

4.1.2 McDaniel Creek

We expanded upon the stratigraphic descriptions of Pritchard (2004) by describing 15 core locations further west-northwest (Figs. 2a and 3c). South of the dike, core elevations range from 2.0 to 2.3 m and north of the dike core elevations range from 1.8 to 2.0 m (NAVD88).

Based on lithology and depth, we correlate four submergence contacts across a 15-core survey at the McDaniel Creek site. The shallowest organic-rich unit was observed at every core location survey and varies from a muddy peat to a peat both across multiple core locations and also within the unit. The second deepest organic-rich unit was overserved at nine locations and varies from a rooted mud to a muddy peat between locations and within the unit. The third deepest organic-rich unit was observed at ten locations and varies from rooted mud to a peat between locations and within the unit. The fourth deepest organic-rich unit was observed at nine core locations and is a humified organic-rich unit. We observed a less distinct upper contact for the fourth deepest organic-rich unit than compared to the shallower organic-rich units (Table 1). In summary, four submergence contacts were observed at five core locations while three submergence contacts were observed at seven core locations. The organic content of both the second and third deepest buried organic-rich units increase to the northeast towards the modern channel. McDaniel Creek archives the largest lateral extent of submergence contacts throughout the estuary.

4.1.3 Jacoby Creek

Similar to previous investigations (Valentine, 1992; Pritchard, 2004), we observed one submergence contact close to the mouth of Jacoby Creek at *JC.6*. We extended stratigraphic mapping ~200-400 m farther to the north at the marsh and observed three submergence contacts within the top 200 cm of the marsh stratigraphy (Figs. 2d and 3c).

Across a ten-core transect, three submergence contacts were correlated based on depth in cores and lithology. Elevations of the core tops range from 1.95 to 2.39 m (NAVD88). At the northern and southern extents of the survey transect in cores only one submergence contact was observed. At four core locations in the mid-section of the marsh, three submergence contacts were observed within 200 cm below the salt marsh surface. The shallowest organic-rich unit was observed at eight core locations and ranges from bold, well-developed peat to a muddy peat within the unit. The second deepest organic rich unit was observed at seven core locations and ranges from a peat to a muddy peat both within the unit and across multiple core locations. The deepest organic rich-unit was observed at six core locations, is a highly-humified upland soil, and overlies pebbly-sand alluvial sediments. In summary, at Jacoby Creek we observed three submergence contacts at four core locations, two submergence contacts at three locations, and one submergence contact at three core locations. Jacoby Creek core sites have the highest core top elevations, cover the smallest surface area, and have the shallowest wetland stratigraphic section in northern Humboldt Bay.

4.1.4 Radiocarbon Ages

We obtained 24 radiocarbon ages of plant macrofossils to determine the timing of paleoenvironmental changes across the upper contacts of buried organic-rich units (Table 2). Whenever possible, we used identifiable plant material. Both minimum and maximum age samples were found above and below the three deepest submergence contacts and constrain the timing of those paleoenvironmental changes. Although we obtained 24 radiocarbon ages, we exclude three dates identified as outliers in stratigraphic sequences. We infer that downward bioturbation and/or root penetration has resulted in a younger age than stratigraphic position would suggest (sample *JC.14.02.D.100-101*), and detrital reworking and deposition has resulted in anomalous older dates than stratigraphic position suggests (*JC.14.02.D.103-104* and *JC.14.02.D.103-105*) (Fig. 3c; Table 2). The calibrated ages range from modern to 1575–1707 cal yr BP, indicating the sediments accumulated over the last two millennia (Table 2).

From Mad River Slough we obtained seven radiocarbon ages that provide a 1700-year chronology (Table 2). One maximum age (307–1 cal yr BP) from the shallowest organic-rich unit falls within last ~300 yr radiocarbon calibration plateau. The age of a *D. spicata* rhizome derived from the second deepest buried organic-rich unit is consistent with previous paleoseismic dating results of the same unit (e.g., Valentine et al., 2012). Previous investigations have suggested that the second deepest submergence contact could represent subsidence from a CSZ earthquake; however, we did not observe similar stratigraphy or radiocarbon age anywhere else within the marsh or across the estuary (Fig. 3; Tables 1 and 2;). Maximum ages from the third deepest organic rich unit are consistent (956–912 cal yr BP and 956–802 cal yr BP, respectively) and aid in correlation of stratigraphy across the marsh. The burial timing of the fourth organic-rich unit is constrained by a minimum age (1057–961 cal yr BP) and a maximum age (1280–1183 cal yr BP). Within the deepest organic-rich unit, we dated roughly 25 *Atriplex* and *Potamogeton* seeds, which provide maximum age constraint (1690–1545 cal yr BP; Table 2).

From McDaniel Creek, nine radiocarbon ages combine to provide a 1700-year chronology (Table 2). One maximum age (283–1 cal yr BP) from the shallowest organic-rich unit falls within last ~300 yr radiocarbon calibration plateau. The timing of burial for the second organic-rich unit is constrained by two maximum ages (965–929 cal yr BP and 951–804 cal yr BP) and one minimum age (926–798 cal yr BP). Two ages (1302–1190 cal yr BP and 1399–1328 cal yr BP) from the third deepest organic-rich unit provide maximum age constraints of the peat unit. Due to the availability of representative stratigraphy during the initial field and dating efforts, one maximum age (1399–1328 cal yr BP) was taken from 15 cm below the upper contact of the unit. Two maximum ages (1708–1614 cal yr BP and 1695–1565 cal yr BP) and a minimum age (1707–1575 cal yr BP) tightly constrain the timing of burial for the fourth deepest organic-rich unit.

From Jacoby Creek we obtained eight radiocarbon ages from a single core (JC.2), which provides a 1700-year chronology (Table 2). One maximum age (289–1 cal yr BP) from the shallowest organic-rich unit falls within last ~300 yr radiocarbon calibration plateau. Maximum ages were derived from the second and third buried organic-rich units (1277–1181 cal yr BP and 1694–1558 cal yr BP, respectively). Two minimum ages, that may be detrital, were derived from plant macrofossils found within mud units directly overlying the two deeper buried organic-rich units (1166–968 cal yr BP and 1692–1561 cal yr BP, respectively).

Also, at *JC.2* we observed a ~7 cm thick slightly organic unit, which was ~5 cm beneath the shallowest organic-rich unit (Fig. 2d). Although we did not recognize a lithological change from visual inspection in the field, a density contrast within the core was identified through CT analysis. Due to the similarity to a contact observed in two cores at Mad River Slough (*MR.2* and *MR.7*) we obtained three maximum ages on this slightly organic-rich unit (modern (post 1950 CE), 1263–1082 cal yr BP, and 1333–1285 cal yr BP). Either downward root penetration, bioturbation, or contamination of the core during extraction may explain the anomalously young modern age. The two older radiocarbon ages are stratigraphically inconsistent (Table 2) with the ages from the deeper two buried organic-rich units, possibly indicating the re-deposition of older material. Therefore, we hypothesize that this contact may have been eroded at Jacoby Creek sometime prior to the 250 yrs BP earthquake. Because these three radiocarbon ages are inconsistent with ages of the rest of the core and are not in stratigraphic order, we do not include them within the composite stratigraphy used in the development of Bayesian age models.

4.1.5 Correlation of Stratigraphy Among the Study Sites

The age results provide context for stratigraphic correlations both within the marsh as well as across the estuary. In total, we observed five mud-over-peat and/or mud-over-upland soil contacts within the tidal wetland stratigraphy at northern Humboldt Bay. However, correlation of only four submergence contacts is supported by stratigraphic mapping, depth and radiocarbon age overlap. We assign submergence contacts with letter designations by depth, e.g., contact A is the shallowest submergence contact. We correlate three submergence contacts, e.g., A, D, and E, across all three marsh sites, contact C across two marsh sites (Mad River Slough and McDaniel Creek), and Contact B was only observed at one marsh (Mad River Slough).

Contact A

Contact A is the upper contact of the shallowest, most distinct, and most wide-spread buried organic-rich unit observed at northern Humboldt Bay. Three maximum-limiting radiocarbon ages, one from each marsh, of an in-growth position rhizome and two herbaceous stems ≤10mm below the contact, range between 283–1 cal yr BP to 307–1 cal yr BP, and corroborate stratigraphic correlation across the estuary (Table 2). Contact A has radiocarbon ages consistent with previous research at Cascadia (Atwater, 1987; Nelson, 1992; Nelson, 1995; Satake et al., 1996; Satake et al., 2003; Atwater et al, 2005), which infers that the contact dates from the 250 cal yr BP (1700 CE) earthquake. For the remainder of the paper, we will refer to Contact A as the contact formed due to subsidence from the 1700 CE earthquake.

Contact B

Contact B has the most limited lateral extent within the estuary as it was only observed in cores *MR.2* and MR.*7* at Mad River Slough, which are less than 30 m apart (Fig. 2b; Table 1). At 161.5 and 166.5 cm core depth at *MR.2* and *MR.7*, the sharp upper contact of organic rich-unit has ~7mm of relief and is <10 cm below the base of the buried 1700 CE peaty unit that forms Contact A. The organic-rich unit of Contact B is 2-4 cm thick and contains 0.25-0.5 cm thick intercalated clastic beds. The overlying 8-10 cm thick mud unit contains~0.25 cm thick intercalated slightly-rooted beds. One maximum age of an in-situ plant macrofossil found within 1 cm below contact B, 511–476 cal yr BP, does not overlap with any other radiocarbon age obtained in our investigation (Table 2).

Contact C

Based on stratigraphic mapping and radiocarbon age overlap, contact C was observed at Mad River Slough and McDaniel Creek. Four maximum ages and one minimum age constrain the timing of contact C. A rhizome in growth position <10 mm above the contact at *MD.06* ranges in age from 926–798 cal yr BP (Table 2). Three rhizomes in growth position and a herbaceous stem each within <10 mm below the contact range in age from 956–802 cal yr BP (Table 2).

Contact D

Based on stratigraphic mapping and radiocarbon age overlap, contact D was observed at every marsh within the northern Humboldt Bay estuary. Two minimum ages and three maximum ages constrain the timing of Contact D, one from each marsh. A *Grindelia spp.* stem <25 mm above the contact and a rhizome in growth position <15mm from the contact range in age from 1166–961 cal yr BP. Three maximum age samples of a rhizome in growth position, rhizome fragments, and stem fragments were each found within 15 mm below the contact and range in age from 1399–1181 cal yr BP (Table 2).

Contact E

Based on stratigraphic mapping and radiocarbon age overlap, contact E was observed at every marsh within the northern Humboldt Bay estuary. Two minimum ages and four maximum ages of plant microfossils constrain the timing of contact E. Minimum ages of wood fragments and a herbaceous stem, both <30 mm above the contacts, have an age range of 1707–1561 cal yr BP. One minimum age, 1707–1575 cal yr BP, is older than three of the four maximum ages. The four maximum ages on two rhizomes in growth position, one rhizome or stem, and ~25 *Atriplex* and *Potamogeton* seeds <20 mm below the contact have a combined age range of 1708–1558 cal yr BP (Table 2).

4.2 Modeling the Timing of Abrupt Submergence

We constructed a representative composite stratigraphic section using 16 radiocarbon ages across the estuary (Fig. DR2). Ages were assigned to appropriate depth intervals relative to the upper contact of buried organic-rich units that were stratigraphically widespread; contacts A, C, D, and E. The composite stratigraphy was based on the stratigraphy observed at MD.5 (Figs. 2c and 3a), where contacts A, C, D, and E, were described at the depths of 126, 173, 246, and 312 cm from the surface, respectively (Fig. DR2). We do not model contact B or include the maximum age constraint obtained at this contact within the composite stratigraphy because of a lack of correlative stratigraphy at McDaniel Creek to allow its placement onto the composite stratigraphic section. We do not model contact A due to the limitations of radiocarbon imposed by a plateau in the calibration curve post 1650 CE (Reimer et al., 2013). The assumption that contact A represents the CSZ 1700 CE megathrust earthquake is consistent with the tsunami modeling of Satake et al., (1996) and Satake et al. (2003), tree ring ages from Nelson et al., (1995), reservoir corrected offshore ages on foraminifera that are not subject to the radiocarbon calibration plateau (Goldfinger et al., 2012; 2013), and our three maximum limiting radiocarbon ages of contact A (Fig. 3 and Table 2).

The estuary-wide composite stratigraphy (Fig. DR2), based on the stratigraphy observed at *MD.5* (Figs. 1 and 2), was used in the construction of the three Bayesian age models (Fig. 4). We employ the OxCal ‘Sequence’ as a simple Bayesian age model using stratigraphic position to order ages as well as the more complicated OxCal ‘P-sequence’ and Bchron age models, which incorporate depths and variable sedimentation rates, to develop paleoseismic chronologies at northern Humboldt Bay and evaluate the effect that model and software choices have on our results (Figs. DR1-7).

In general, each of the Bayesian age models show strong agreement on the timing of burial for each of the modelled contacts (Fig. 4; Table 3). For contacts C, D, and E, the variability of modelled mean ages range over 38 years, 25 years, and 19 years respectively (Table 3). For contacts C and D, Bchron provides narrower age ranges than OxCal 'Sequence' and 'P-sequence' models, which is the result of the model assigned sedimentation rate between age constraints. For contact E, all modelled mean age ranges are essentially identical (within four years; Fig. 4; Table 3). The tight age overlap for contact E result is likely based on the combination of 1) the narrow radiocarbon age range of 147 years between the youngest minimum (1692–1561 cal yr BP) and oldest maximum (1708–1614 cal yr BP) and 2) the close depth distribution of our age constraints, i.e., two minimum ages within the first <3 cm above the contact and four maximum ages within the first 2 cm below the contact (Fig. 3; Table 2; and Fig. DR2).

For each modeled contact age, the OxCal 'P-sequence' age model produces broader age ranges than OxCal 'Sequence' and Bchron models. The relatively broad age range results may be attributed to the assigned *k* value. For the northern Humboldt Bay chronologic data and following Bronk Ramsey (2008) and Enkin et al. (2013), we determined the optimal *k* is 0.1 cm^{-1}, meaning that variations in deposition rate occur on average about every 0.1 cm (Table 2; Table DR 1-27; Fig. DR1-2). A large k value directs a more uniform sedimentation rate (Bronk Ramsey, 2008;), which can over-constrain the age model (i.e., narrower age ranges) and result in low agreement indices

(Enkin et al., 2013; Tables DR1, 15-27). In contrast, a small k value allows for a greater randomness in the deposition rate and weights superposition of samples over sample depth (Bronk Ramsey, 2008), which result in less constrained age ranges (i.e., wider age ranges) and high agreement indices (Enkin et al., 2013; Tables DR1-14). Therefore, when k is small and radiocarbon age constraints are clustered around contacts of interest, OxCal 'P-sequence' models more conservative age ranges (Table 3; Fig. 4; DR4-6). For example, the timing of burial for contact D is constrained by 309 years between the oldest minimum limiting age (1166–968 cal yr BP) and youngest maximum limiting age (1277–1181 cal yr BP); the more conservative OxCal 'P-sequence' modelled age for contact D has the largest range of 277 years, whereas OxCal 'Sequence' and Bchron model less conservative age ranges of 227 and 140 years, respectively (Table 3).

4.3 Foraminiferal Analyses of Buried-soil Subsidence at McDaniel Creek

We selected representative sediment cores for foraminiferal analyses from McDaniel Creek because it archives the largest lateral extent of contacts A, C, D, and E (Fig. 5; Tables DR28-32). Further, we analyzed contact B from Mad River Slough due to the absence of this contact at McDaniel Creek and Jacoby Creek and our aim to identify whether it may be related to a subduction zone earthquake (Table DR29). Sudden and lasting foraminiferal community assemblage changes were found across four abrupt-sharp contacts; A, C, D, and E (Fig. 5; Tables DR28, 30-32). We did not apply the BTF to the fossil data across contact B because there was only a minimal change in fossil foraminiferal assemblages between the organic-rich unit and the overlying clastic mud (Table DR29). The BTF results show that contact A and contact D record a similar amount of subsidence, contact C archives the smallest amount of subsidence, and contact E records the largest magnitude of subsidence. Pairwise comparison of modern and fossil foraminiferal assemblages were well below the 20th percentile threshold, indicating that all fossil assemblages had modern analogs.

For contacts A, C, D, and E, we first describe the lithology around the representative contact and then provide a description of the foraminiferal biostratigraphy.

Contact A

At *MD.03*, the shallowest buried organic-rich unit abrupt upper contact is at 115 cm core depth (Fig. 5a). The organic-rich brown peat unit is 8 cm thick and capped by a grey mud that extends >25cm. The CT scan of *MD.03* shows an abrupt 1-2 mm contact with ~5 mm of relief and fine bedding within the overlying mud unit from 97-115 cm core depth overlying indicated by alternating yellow and orange layers (Fig. 4a) that represent differing densities of sediment.

Foraminiferal assemblages in the brown peat unit are dominated by *B. pseudomacrescens* (27-54%), *T. inflata* (7-39%), and *J. macrescens* (5-33%), which is consistent with a MHHW salt marsh environment. Samples in the mud overlying the peat unit show an increase in the abundance of *M. fusca* (5 to 14%), *Reophax spp.* (0.05-3%), *Ammobaculites spp.* (0-1.4%), and *J. macrescens* (25 to 54%) and a decrease in the abundance of *B. pseudomacrescens* (12 to 29%) and *T. inflata* (16 to 27%). The presence of *Ammobaculites spp*., *Reophax spp*., and increase of *M. fusca* is consistent with a tidal flat environment near MTL (Fig. 4; Kemp et al., 2018). The fossil foraminifera BTF reconstruction suggests 0.85 ±0.46 m of subsidence (Fig. 5a; Table 4; Table DR28).

Contact B

At *MR.2*, we found no distinct change in foraminiferal assemblages across contact B (Table DR29). Within the organic-rich unit fossil assemblages are primarily composed of *B. pseudomacrescens* (38-49%), *J. macrescens* (23-32%), *T. inflata* (16-20%) and *M. fusca* (0-1%), which is consistent with a peat soil forming near MHHW. Although samples in the mud overlying the peat unit show a slight increase in the abundance of *M. fusca* (2-3%), *Reophax spp.* (0-1%), and *T. inflata* (22-25%), there are also moderate to high abundances of *B. pseudomacrescens* (38-41%) and *J. macrescens* (21-29%), which is also consistent with an environment forming between mean high water (MHW) and MHHW (Table DR29).

Based on a lack of lateral extent of the contact, lack of radiocarbon age overlap within the estuary, and minimal fossil foraminiferal assemblage change, we do not apply the BTF to the fossil foraminifera assemblage data from contact B and we infer that it does not represent coseismic subsidence induced from megathrust rupture. Instead, we infer that this organic-rich unit is the base of the organic-rich unit below contact A and that the 8-10 cm thick mud that separates these organic rich units could be a local hydrographic event; a possible candidate cause is an overtopping of the Mad River levee that is 6 km to the north-northeast.

Contact C

At *MD.6*, the upper contact of the second deepest buried organic-rich unit at 170.5 cm core depth is sharp and separates a muddy peat from an overlying mud (Fig. 5b). The brown muddy peat unit is 6 cm thick and capped by a grey mud that extends >20cm. CT images show a sharp ~3 mm contact with ~5mm of undulating relief and >6 cm of overlying mud that contains detrital organics and/or paleoburrow. The semi-vertical void that extends across the CT image is possibly a crack that occurred during sediment collection and/or shipping (Fig. 5b).

Foraminifera in the light brown muddy peat unit dominantly consist of *B. pseudomacrescens* (12-40%) and *T. inflata* (24-36%), which is consistent with a MHHW salt marsh environment. Samples in the grey mud overlying the peat unit show an increase in the abundance of *M. fusca* (21 to 33%) and *J. macrescens* (27 to 37%) and a decrease in the abundance of *B. pseudomacrescens* (4 to 9%), which is consistent with an environment below but in close proximity to MHW. The fossil foraminifera BTF reconstruction shows 0.42 ±0.37 m of subsidence (Fig.5b; Table 4, Table DR30).

Contact D

The CT scan of *MD.13* shows a sharp contact at 248 cm to have ~14mm of undulating relief and separates an 8 cm thick organic-rich unit, where the upper 3 cm is a light brown muddy peat and the lower 5 cm are a grey-brown rooted mud, from a >25 cm thick finely bedded grey mud.

Foraminifera in the organic-rich unit dominantly consist of *B. pseudomacrescens* (3-48%), *T. inflata* (9-71%), and *J. macrescens* (22-52%), which is consistent with a MHHW salt marsh environment. Although samples in the grey mud overlying the peat unit are also dominated by *J. macrescens* (27-38%), *T. inflata* (15-19%), and *B. pseudomacrescens* (12-18%) the assemblages show a marked increase in the abundance of *M. fusca* (14 to 17%) and contain *Ammobaculites* spp. (~1%) and *Reophax* spp. (~1%), which are typically associated with a tidal flat environment near MTL (Kemp et al., 2018). For the subsidence estimate we use the distributions of the reconstructed RSL elevations that are 2 cm apart and are the first unmixed centimeter intervals above and below the mud-over-peat contact. The fossil foraminifera BTF reconstruction shows 0.79 ±0.47 m of subsidence across contact D (Fig. 5c; Table 4; Table DR31).

Contact E

At *MD.5*, the sharp upper contact of the deepest buried organic-rich unit is at 308 cm depth, undulates over >15 mm, and separates a dark grey-black organic-rich unit from an overlying grey mud (Fig. 5d). The organic rich unit is 12 cm thick and is overlain by a grey mud that extends thicker than 25 cm. X-ray analysis shows that the overlying grey mud infiltrated into the underlying highly humified and friable organic rich unit below (Fig. 5d).

The fossil foraminifera assemblages further support the interpretation of mixing across contact E. The foraminifera assemblages in the humified organic rich unit have decreasing abundances, from 200 to <30, with distance below (4cm) the contact and are dominated by *M. fusca* (48-52%), *T. inflata* (35-38%) and contain low abundances of *Reophax* spp. (<1%); such an assemblage is typically indicative of an environment that formed below MHW. However, while foraminifera abundances above the deepest organic rich unit are consistent with other analyzed intervals (>200 individuals) the decreasing abundances of foraminifera with distance from the upper contact of the organic-rich unit is consistent with mixing (e.g., Engelhart et al., 2013; Milker et al., 2015). Based on visual appearance in photo and X-ray imagery, decreasing foraminiferal abundances, and similarity to foraminiferal assemblages within the overlying clastic mud unit we interpret that foraminifera assemblages found within the organic-rich unit are not in-situ or indicative of the depositional environment. Moreover, Engelhart et al., (2015) report diatom analysis of core *JC.14.02A* at Jacoby Creek that suggests the organic-rich unit formed as a dry upland surface and not salt marsh. Therefore, considering the diatom data at *JC.14.02A,* correlation of radiocarbon ages, and a lack of in-situ fossil foraminiferal assemblages, we conclude that the fourth deepest organic-rich unit represents a depositional environment that formed above the highest occurrence of foraminifera. Foraminifera in the grey mud above the organic-rich unit are dominated by *M. fusca* (60-65%) and *T. inflata* (25-31%), while *Ammobaculites* spp. and *Reophax* spp. are both present at ~1%, signifying an assemblage that formed are around MTL. Based on the first interval that contains in-situ fossil foraminifera above the organic-rich unit, we subtract the reconstructed RSL elevation for this interval, as predicted by the BTF, from the elevation of the highest occurrence of foraminifera in northern Humboldt Bay which is 2.5 m (NAVD 88). Therefore, fossil foraminifera assemblages can only provide a minimum-limiting estimate for subsidence of ≥0.93 m (Fig. 5d; Table 4: Table DR32).

5. DISCUSSION

We provide multiple lines of evidence for four megathrust earthquakes since 1,700 cal yrs BP in northern Humboldt Bay (Table 5). These results prompt important questions, introduced above, about age modeling techniques that best constrain the ages of past subduction zone earthquakes and questions about needed levels of resolution in both the chronology of paleoearthquakes and the amount of coseismic subsidence during paleoearthquakes such that individual paleoearthquakes can be correlated along the Cascadia margin. In the following, we address the questions in the context of the northern Humboldt Bay tidal wetland stratigraphic record and compare the northern Humboldt Bay paleoearthquake record to other regional paleoseismic sites, and, finally, looking into the possibility of correlating variable subsidence data for different earthquakes among sites in southern Cascadia.

5.1 Northern Humboldt Bay Paleo Subduction Zone Earthquake Record

5.1.1 Revisions to the tidal wetland stratigraphy in northern Humboldt Bay

Our new lithologic, biostratigraphic, and chronologic analyses allow us to provide a refined paleoseismic history of subduction zone earthquakes for northern Humboldt Bay. Tidal wetland stratigraphic records are a proven means for reconstructing paleoearthquakes at subduction zones globally. The record of mud-over-peat and mud-over-upland soil contacts are convincing lines of evidence for land subsidence induced by great (M>8) and giant (M>9) earthquakes (e.g., Atwater, 1987). However, since the stratigraphic record at Cascadia was initially linked to such earthquakes (e.g., Atwater, 1987; 1992; Atwater and Yamaguchi, 1991; Darienzo and Peterson, 1990; Nelson, 1992), there has been continued focus on other processes that may cause similar stratigraphy to coseismic subsidence (Long and Shennan, 1994; Allen, 1997; 2000; Nelson et al., 1998), which has led to the development of the rigorous stratigraphic research framework that underpins modern coastal subduction zone paleoseismology (Nelson et al., 1996; Shennan et al., 2016). Many of the foundational tidal wetland stratigraphic papers for northern Humboldt Bay preceded the development of this framework (e.g., Vick, 1988; Clark and Carver 1992, Valentine, 1992) so that even later review articles (e.g., Valentine et al., 2012) may not adequately represent the uncertainty in the tidal wetland stratigraphy mapped at different sites by different researchers.

This uncertainty is highlighted by the complicated stratigraphy at Mad River Slough, specifically a contact observed by previous researchers that we refer to as contact B (e.g., Vick 1988, Clark and Carver 1992; Valentine, 1992; Valentine et al., 2012). Previous research was not able to conclude if contact B represents megathrust-induced coseismic subsidence because of the limited spatial extent of the contact, (contact B is observed only at MRS-3 core location of Vick, 1988), no radiocarbon age correlation within the estuary (Clark and Carver, 1992; Valentine 1992; Valentine et al., 2012), and limited qualitative microfossil analysis (Valentine et al., 2012). Additionally, even though Pritchard (2004) reoccupied several core and outcrop stratigraphic description locations of previous researchers (Vick, 1988; Clark and Carver, 1992; and Valentine 1992), including MRS-3 of Vick (1988), contact B was not included within their stratigraphic descriptions. Moreover, several previous researchers correlate contact B to evidence from other proximate paleoseismic wetland stratigraphic and trench investigations (e.g., Valentine, 1992; Clarke and Carver, 1992; Valentine et al., 2012). We contend that across-site/estuary correlations based on the relatively large error range of radiocarbon ages on bulk peat samples (e.g., Clarke and Carver, 1992; Valentine et al. 2012), relative order inferences placed on narrowly supported hypothetical composite stratigraphic sections (e.g., Fig. 16 of Valentine, 1992; Valentine et al. 2012), and a lack of within-site radiocarbon age replications (e.g., Clarke and Carver, 1992; Valentine, 1992; Valentine et al., 2012) provide insufficient evidence for correlation beyond a small area of marsh in a single, potentially complicated stratigraphic section. Therefore, differing stratigraphic observations and limited radiocarbon age constraints are primarily responsible for the previous, differing correlations and conclusions of paleoseismic investigations at northern Humboldt Bay.

However, our extended stratigraphic descriptions (Figs. 2, 3 and Table 1) and robust radiocarbon dataset (Table 2) from new coring at McDaniel Creek and Jacoby Creek allows us to provide further clarification. Our new results do not provide any additional evidence for a contact of the age of contact B at other northern Humboldt Bay sites. Instead, we suggest that contact B is likely the result of a simpler explanation of physical processes within Mad River Slough and could be related to the overtopping of the Mad River levee during an unusual flood event (Cahoon et al., 1996; Friedrichs and Perry, 2001), local marsh-edge slumping (Allen, 1989; Gabet, 1998), or soil creep (Mariotti et al., 2016), which could all potentially create non-seismic induced submergence-like stratigraphy over small spatial scales (Nelson et al., 1996; 2006; Shennan et al., 2016). Barring further evidence from additional sites within northern Humboldt Bay, based solely on our observations we suggest contact B is not representative of a CSZ megathrust-induced subsidence.

However, we acknowledge the maximum ages derived from the organic-rich unit below contact B overlap with the age of the T2 turbidite (Goldfinger et al., 2012). It is possible that subsidence smaller than the threshold required to record it consistently in the salt-marsh sediments across northern Humboldt Bay could be invoked to correlate this very sparse record with T2 (e.g., Nelson et al., 1996; Shennan et al., 2016). Nonetheless the currently available coastal observations, limited spatial evidence for contact B, and a lack of foraminiferal assemblage change across contact B (Table DR29), favor other local processes over megathrust-induced subsidence.

Greater confidence can now be assigned given our estuary-wide stratigraphic correlations based on: 1) an increase in the spatial density and extent of stratigraphic descriptions beyond those from previous northern Humboldt Bay paleoseismic investigations (i.e., at McDaniel Creek and Jacoby Creek sites) and, 2) our robust radiocarbon age dataset, which elucidates stratigraphic correlations throughout the estuary (Tables 1 and 2). At northern Humboldt Bay, four stratigraphic contacts meet the criteria (Hemphill-Haley, 1995; Nelson et al., 1996; Shennan et al., 2016) for coseismic subsidence; contacts A, C, D, and E (Table 5). This result is consistent with portions of the findings from the previous research (Vick, 1988; Clark and Carver 1992, Valentine, 1992; Pritchard, 2004; Valentine et al., 2012). Based on our stratigraphic mapping and radiocarbon ages, McDaniel Creek archives the most consistent wetland stratigraphic record of CSZ rupture in north Humboldt Bay (Figs. 2 and 3). This is in contrast to previous research that has focused on Mad River Slough as the type section in northern Humboldt Bay (Vick, 1988; Valentine, 1992; Clarke and Carver 1992; Valentine et al., 2012). We contend that due to inconsistent and variable stratigraphy, and the potential influence of slough processes (e.g., Nelson et al., 1998), that the Mad River Slough stratigraphic record should be treated with caution.

5.1.2 Radiocarbon age modeling of southern Cascadia earthquake chronology: advantages and disadvantages of alternative Bayesian age models

Our work refining the northern Humboldt Bay radiocarbon dataset and constructing Bayesian age models (Fig. 4 and Table 3) provides opportunity for testing, calibrating, and refining chronologic models. We move beyond traditional radiocarbon-based dating approaches by assessing the results of multiple Bayesian age models, which may improve the accuracy and precision of earthquake chronologies. For earthquakes prior to 1700 CE, even the most conservative age model (OxCal 'Sequence') provides narrower age distributions (age ranges of between 94 and 227 years) than previous paleoseismic investigations at northern Humboldt Bay (e.g., Vick, 1988; Valentine 1992; Clarke and Carver, 1992; Valentine et al., 2012); 924–816 cal yr BP, 1,231–1,004 cal yr BP, and 1,669–1,575 cal yr BP (Table 3). The timing of earthquakes may be refined further by incorporating modeled sedimentation rates between radiocarbon age (OxCal 'P-sequence' and Bchron models).

We select an age-model that ignores sedimentation rate for three reasons. Despite the often narrower age distributions provided by Bchron (which incorporates sedimentation rates), the OxCal 'Sequence' age estimates are the most reliable for the paleoseismic activity at northern Humboldt Bay. First, if the age constraints above (minimum age) and below (maximum age) a contact of interest are derived close (e.g., ~<3-4 cm) to the contact of interest and have considerable age range overlaps then each of the three Bayesian models we tested provide nearly identical age estimates, e.g., contact E (Table 3). Therefore, a modeled sedimentation rate does not always improve the modeled age estimate if the data constraints are consistent. Second, our radiocarbon data set cannot resolve the variations in post-seismic sedimentation in northern Humboldt Bay wetlands. Near Portage, Alaska, Atwater et al., (2001), document environmental changes over three decades after the great 1964 Alaska earthquake. Sedimentation was rapid within the first several months and then slowed in the decades following as the previous vegetation and environments re-established (Atwater et al., 2001). Therefore, post-seismic variable sedimentation rates likely vary over time frames less than the uncertainty of radiocarbon ages. Unlike the use in passive margins of sedimentation-rate-informed age models where sedimentation rates are likely to be more consistent (e.g., Kemp et al., 2009, 2011; Wright et al., 2017), care should be taken in active margins when constructing age models that, perhaps unwittingly, are modelling an uncertain and variable sedimentation rate. Third, the development of a composite stratigraphy (multiple age constraints derived from multiple cores) requires that stratigraphic correlations are accurate and estimates sedimentation rate from a composite stratigraphic section. Although radiocarbon age overlap can provide confidence in stratigraphic correlation, sedimentation/accumulation rates and erosional histories are not consistent throughout an entire wetland environment (Letzsch and Frey, 1980; Allen, 2000). Differences in sedimentation rates will affect the modeled age-estimates (e.g., Tables DR1-27 and Figs. DR1, 3-5) and combining chronologic constraints into a composite chronology (e.g., Fig. DR 2) assumes that the differences in sedimentation/accumulation rates are negligible. By selecting an age-model that doesn't model a sedimentation rate, we avoid this potential error.

Although there are problems with finding a single representative core location with abundant quality dating material (e.g., in-situ plant macrofossils and/or seeds), future research should consider acquiring dates from within a single core where possible. This approach would circumvent the need to build composite chronologies and allow greater confidence in testing the applicability of modeled sedimentation rates to constrain timing of earthquakes at Cascadia. Additional dates from adjacent core sites could be used to verify stratigraphic correlations.

5.2 Correlating the Northern Humboldt Bay Earthquake Record to Other Paleoseismic Records on the Southern Cascadia Subduction Zone

Northern Humboldt Bay may have experienced both full and partial ruptures over the late Holocene (e.g., Goldfinger et al., 2012). Our AMS radiocarbon ages provide an unambiguous chronology for earthquake-induced subsidence at northern Humboldt Bay even without Bayesian age modeling. The precision of the conservative OxCal 'Sequence' age model tightly constrains the timing of earthquake subsidence (Fig. 4; Table 3) and allow for increased confidence in correlation over 10-100 km's (Fig. 6). This refined chronostratigraphic approach provides a means with which to test the interpretation of varying rupture length along strike. In testing models for subduction zone ruptures, we anticipate that sites close together should show the same or similar coseismic inference (Shennan et al., 2016). Therefore, we examine regional southern Cascadia paleoseismic records and correlate age overlap with the paleoseismic chronology at northern Humboldt Bay for earthquake contacts C, D. and E (Fig. 6). Below we highlight age estimate overlap and offer plausible explanations for lack of age estimate overlap when appropriate.

5.2.1 Earthquake Contact C, ~875 cal. yrs. .BP

Although the OxCal 'Sequence' model age distribution for contact C overlaps with age ranges of plate-boundary evidence at Talbot Creek, Bradley Lake, Eel River and the timing of turbidite T3, there is a lack of correlation at Coquille River, Lagoon Creek, and southern Humboldt Bay (Fig. 6). The southern Humboldt Bay site (Patton, 2004) contains earthquake evidence below the inferred CSZ 1700 CE contact and above a deeper and older buried organic-rich unit upper contact. Therefore, the undated contact at southern Humboldt Bay could potentially contain a correlative age distribution with contact C at northern Humboldt Bay. At Lagoon Creek, no tsunami deposit is found with an age distribution that overlaps with contact C (Abramson, 1998; Garrison-Laney, 1998). This may be explained by foredune sequence heights sufficiently high to present a barrier to tsunami inundation, although why that should be an issue for this event and not others is not clear. Another potential explanation may be that because the age of tsunami deposit W at Lagoon Creek is derived from detrital material, the age may not represent a close maximum age.

There are at least three potential explanations why there is a lack of correlation with contact C and evidence at Coquille River (Witter et al., 2003): 1) no earthquake occurrence at Coquille River; 2) formation threshold, where slip on the megathrust was insufficient to cause enough vertical deformation to be recorded by the salt marsh; and 3) preservation threshold, where the coastal system had not fully recovered/reset from the previous earthquake rupture, ~1170-1370 cal. yrs. BP (e.g., Benson et al, 2001). A preservation threshold seems an unlikely cause in that there was >200 years between the previously documented earthquake and our inferred timing for contact C (Witter et al., 2003). There are correlative age distributions further north at Talbot Creek (Fig. 6), southern Washington, and Vancouver Island (Nelson et al., 2006) and also to the south at Eel River (Fig. 6). However, at Talbot Creek, Milker et al., (2016) report little to no subsidence across their correlative contact B, and northern Humboldt Bay contact C also records the least amount of subsidence over the four most recent earthquake cycles. Minimal subsidence at the above two sites does support the inference of insufficient coseismic deformation (i.e., formation threshold) at the Coquille River during the earthquake that caused the formation of contact C. Moreover, because the turbidite evidence for T3 suggests a margin-wide megathrust rupture with a relatively large mass and bed thickness at numerous sites (Goldfinger et al., 2012; 2013), could imply that the majority of slip was shallow and farther offshore, potentially limiting the creation and preservation of onshore evidence during this event in southern Cascadia.

5.2.2 Earthquake Contact D, ~1,120 cal. yrs. BP

The OxCal 'Sequence' model age distribution for contact D overlaps with age ranges for evidence of plate-boundary earthquakes at Eel River, Lagoon Creek, Bradley Lake, Coquille River, Talbot Creek, and the T3a and T4 turbidites. There is no correlation with southern Humboldt Bay (Fig. 6). Although southern Humboldt Bay (Patton, 2004) contains an undated buried organic-rich unit that could potentially correlate with either contact C or D at northern Humboldt Bay, the undated unit cannot correlate to both.

Therefore, a preservation threshold not being met is the most likely explanation for the lack of stratigraphic evidence for a plate-boundary earthquake at southern Humboldt Bay during the earthquake that caused the burial of contact D at northern Humboldt Bay. Southern Humboldt Bay may not have fully recovered/reset from the previous earthquake rupture (i.e., preservation threshold) because the age of buried soil 3 upper contact is estimated to be 1,350-2,150 cal. yrs. BP (Patton, 2004), which is potentially <200 years prior to the age of contact D (Fig. 6). Although a heterogenous slip distribution and/or an insufficient amount of coseismic deformation (i.e., formation threshold) could explain the lack of stratigraphic record at southern Humboldt Bay, such an explanation seems unlikely because we estimate 0.79±0.47 m of subsidence ~20 km away. Additionally, a 'no earthquake occurrence' explanation also seems unlikely because there are correlative ages of stratigraphic evidence for plate-boundary rupture both to the north, e.g., Talbot Creek and Coquille River, and to the south at Eel River as well as corresponding age distributions for tsunami deposits at Bradley Lake and Lagoon Creek. Moreover, Goldfinger et al. (2012) suggest that the earthquake that caused T4 was a full margin rupture and the earthquake that caused T3a turbidite was a southern Cascadia rupture, which extended for 444 km and encompasses basins offshore of all sites south of 43 degrees north (Fig. 6).

5.2.3 Earthquake Contact E, ~1,620 cal. yrs. BP

All seven onshore sites (Fig. 6) record evidence for a plate-boundary earthquake and the offshore turbidite T5 ages overlap with the age distribution for contact E. There are abundant corresponding age distributions for contact E both offshore, throughout southern Cascadia (Fig. 6), and further north along the Cascadia margin including central Oregon and southern Washington (Shennan et al., 1996; Nelson et al., 1996; 1998; Nelson et al., 2004; Atwater et al, 2004: Graehl et al., 2014).

5.2.4 Summary: Southern Cascadia Subduction Zone Ruptured All At Once in Each of the Four Earthquakes Recorded at Humboldt Bay

In summary, in examining the paleoseismic chronology at northern Humboldt Bay for earthquake contacts C, D and E, we document age overlap with earthquakes at the other six paleoseismic sites northward from the Eel River estuary to South Slough, an along-margin distance of ~310 km (Fig. 6). The exceptions are the ~875 cal yr BP earthquake that is not recorded at southern Humboldt Bay and Coquille River and the ~1,120 cal yr BP earthquake that is not recorded at southern Humboldt Bay. Given that preservation threshold (i.e., the system had not fully recovered/reset from the previous earthquake rupture) is a reasonable justification for why these two sites do not have complete overlap of earthquake records, we infer that the southern Cascadia margin, at least from the Eel River estuary north to South Slough, could rupture all at once in each of the four subduction zone earthquakes that we document at northern Humboldt Bay. And our inference leaves open the possibility that all the earthquakes recorded in northern Humboldt Bay may also be full-margin ruptures.

5.3 Implications for understanding spatial and temporal variability in subsidence amounts at Cascadia

5.3.1 Expanding the 1700 CE Subsidence Record

Our BTF coseismic subsidence estimate, 0.85±0.46 cm (Fig. 5; Table 4), extends the latitudinal range of foraminifera-based transfer function estimates for the 1700 CE earthquake (Hawkes et al., 2010; 2011; Wang et al., 2013; Milker et al., 2016; Kemp et al., 2018). Additionally, our 1700 CE coseismic subsidence estimate is consistent with both the "preferred" model of Wang et al., (2013) as well as a previous qualitative subsidence estimate based on diatom analysis at Jacoby Creek of 0-1.64 m (Pritchard, 2004), although with a significant improvement in precision. An increase in the density of coseismic subsidence estimates from southern Cascadia coastline will improve knowledge of a highly complicated and dynamic region of the margin (Goldfinger et al., 2012; Wang et al., 2013; Kemp et al., 2018).

Given the spatial variation observed elsewhere in Cascadia for 1700 CE (Kemp et al., 2018) it is appropriate to investigate the degree of spatial variation along the southern

Cascadia region. For example, the Coquille River and northern Humboldt Bay are separated by ~275 km along strike and in-between there are several coastal paleoseismic sites that do not have quantitative microfossil RSL reconstructions despite potentially containing suitable environments. North of our study site, subsidence stratigraphy of the CSZ 1700 CE earthquake may exist at Euchre Creek (~42.55° N; Witter et al., 2001) and Sand Mine Marsh (~41.74° N; Peterson et al., 2011; Hemphill-Haley et al., 2019), although the prospect remains uncertain. To the south of our study site, there is definite potential to develop new records at southern Humboldt Bay (~40.69° N; Patton, 2004) and at the mouth of the Eel River (~40.62° N; Li, 1992) that would further supplement CSZ 1700 CE paleogeodetic database. The aforementioned spatial gaps are areas that represent areas with large uncertainties of 3-D elastic dislocation models and are close to hypothetical patch boundaries of the "preferred" model of Wang et al., (2013). Our new estimate is the first step in bringing the density of estimates in this region closer to that of coastal Oregon.

5.3.2 Correlating variable subsidence data for different earthquakes among sites in southern Cascadia: significance and uncertainties

Modern instrumented ruptures suggest that slip during large megathrust earthquakes is heterogenous (e.g., Chlieh et al., 2007; Lorito et al., 2011; Lee et al., 2011; Yokota et al., 2011; Wei et al., 2012), a feature that is now also suggested by 15 quantitative microfossil derived coseismic subsidence estimates over ~900 km along the Cascadia margin for the CSZ 1700 CE earthquake (e.g., Wang et al., 2013; Kemp et al., 2018). Heterogenous rupture is also a likely characteristic of earlier earthquakes as well (e.g., Goldfinger et al., 2012; Atwater et al., 2014; Shennan et al., 2016; Goldfinger et al., 2017). Our new results add to data that point to variability in coseismic subsidence estimates by suggesting that the amount of coseismic subsidence has varied between earthquakes. To investigate this temporal variability requires a similar density of quantitative estimates of coseismic land-level changes for earthquakes prior to 1700 CE.

Extending this record back in time is complicated not only by the current sparse record of precise subsidence estimates (e.g., Milker et al., 2016) but also by the inherent uncertainties in correlating chronologies along the margin reconstructed from radiocarbon age estimates that span centuries or greater. However, with recent datasets from Cascadia (e.g., Milker et al., 2016; Nelson et al., 2020) combined with our results, some initial insights may be gleaned about variability in rupture prior to 1700 CE.

The penultimate earthquake recorded in the land-based paleoseismic record at Cascadia apparently produced less subsidence than the 1700 CE earthquake. Our new record from northern Humboldt Bay demonstrates that the penultimate earthquake at 924-816 cal. yrs. BP produced smaller subsidence (0.42 ± 0.37 m) than either the 1700 CE or two older earthquakes at 1,232–1,005 cal yr BP and 1,669–1,575 cal yr BP (estimates of 0.85±0.46, 0.79 ± 0.47 m and ≥0.93 m, respectively). Similarly, at Nehalem River in northern Oregon, subsidence during the 1700 CE and 1568–1361 cal yr BP earthquakes was 1.1 ± 0.5 m and 1.0 ± 0.4 m, but perhaps as low as 0.7 ± 0.4 m during the penultimate earthquake at 942–764 cal yr BP (Nelson et al., 2020), although there is variability in this estimate from a second site (1.0 ± 0.4 m) that may suggest similar amounts of subsidence. The South Slough estuary in southern Oregon shows a similar pattern of variability in subsidence estimates. Evidence from Crown Point (Hawkes et al., 2011) and Talbot Creek (Milker et al., 2016) suggest minimum amounts of subsidence of

(0.85 and 0.36m, respectively) during the 1700 CE earthquake. Yet, a potential earthquake contact recorded at Talbot Creek with a large age range (1020–545 cal yr BP) shows almost no subsidence (0.01 m). This is preceded by an earthquake dated to 1280–1190 cal yr BP that produced 0.63–0.65m of subsidence (Milker et al., 2016). Given the low subsidence estimate for the 1020–545 cal yr BP contact, Milker et al., (2016) are rightly cautious in interpreting this as an earthquake as opposed to formation by hydrodynamic processes. However, if this contact was caused by an earthquake that had smaller subsidence amounts, then the Talbot Creek record provides further support for lower subsidence in the land-based record at Cascadia across much of the margin during the penultimate earthquake compared to the preceding and following earthquakes.

At northern Humboldt Bay the penultimate earthquake at ~875 cal yr BP overlaps with the age distribution of the margin-wide turbidite deposit of T3 (~800 cal yr BP), which is inferred to represent a full margin rupture (Goldfinger et al., 2012). Given the potential evidence for lower subsidence during the ~875 cal yr BP earthquake, an accompanying margin-wide rupture and tsunami implies that either less slip is required to induce a full margin turbidite and/or more slip occurred offshore during this earthquake implying that slip distribution varies between great and giant earthquakes at Cascadia. However because T3 is one of the largest turbidites in the turbidite sequence (Goldfinger et al. 2012), slip distribution seems to be a better explanation for the relatively lower subsidence during the ~875 cal yr BP earthquake rather than less slip being required to produce a full-margin rupture. Further land-based records with high-precision chronologies and microfossil-based estimates of subsidence are required to further evaluate this possibility.

CONCLUSIONS

High-precision chronostratigraphic methods and quantitative RSL reconstructions refine our understanding of the paleoseismic history at northern Humboldt Bay. The tidal wetland stratigraphy at northern Humboldt Bay contains four stratigraphic sequences (three mud-over-peat contacts and one mud-over-upland soil contact) consistent with megathrust induced subsidence. Based on stratigraphic, chronologic, fossil foraminifera analyses, and timing estimate comparisons to evidence of plate boundary earthquakes at other paleoseismic sites, we conclude that contacts A, C, D, and E record subsidence during past CSZ plate boundary earthquakes. Data for contact B, found only at Mad River Slough, are insufficient to infer that contact B records a great earthquake, and we infer that the contact formed through local non-seismic hydrographic processes associated with the slough. Multiple minimum and maximum limiting ages of in-situ plant macrofossils found above and below subsidence contacts, combined with the construction of Bayesian age models, provide the tightest age distributions for three plate boundary earthquakes along the southern Cascadia coastline (the three next-oldest earthquakes after the 1700 CE subduction zone earthquake). These tightly bounded ages are 924–816 cal yr BP, 1,231–1,004 cal yr BP, and 1669–1,575 cal yr BP (Table 3). The stratigraphic evidence for four plate boundary earthquakes at northern Humboldt Bay corresponds with stratigraphic evidence from six proximal coastal paleoseismic locations (43.5°–40.5° N). In the course of investigating earthquake chronology, we had occasion to consider sedimentation-rate-informed Bayesian age models and decided that within the active plate-tectonic setting of coastal wetlands situated on subduction zone margins, an age model using dense sampling around earthquake contacts and no applied sedimentation rate was better than age models that incorporate sedimentation rates.

We reconstruct RSL elevations by applying a foraminiferal Bayesian transfer function to fossil data from representative stratigraphic sequences (three mud-over-peat contacts and one mud-over-upland soil contact) collected at McDaniel Creek marsh and provide the first fully quantitative estimates of coseismic subsidence for northern Humboldt Bay, CA. The coseismic subsidence estimates are 0.85 ±0.46m for the 1700 CE earthquake, 0.42±0.37 m for the ~875 cal yr BP earthquake, 0.79±0.47 m ~1,120 cal yr BP earthquake, and ≥0.93 m for the ~1,620 cal yr BP earthquake (Fig 5; Table 4). The subsidence estimate for the oldest earthquake is a minimum because the paleoenvironment prior to the earthquake likely formed above the upper limit of foraminiferal habitation (Fig 5; Table 4). Our coseismic subsidence estimates provide high-resolution data for future modeling of Cascadia earthquakes and offer insight into the inherent variability in coseismic subsidence over multiple earthquake cycles. In order to further address remaining paleoseismic uncertainties, future Cascadia coastal paleoseismology investigations should seek to address remaining spatial gaps and incorporate high-resolution lithostratigraphic imagery, high-precision dating techniques, and fully quantitative microfossil-based relative sea-level reconstructions. Specifically, our results highlight the need for additional precise paleoseismic chronologies and, if possible, coseismic subsidence estimates from southern Cascadia at sites (Fig. 6) such as at Eel River (~40.65° N), southern Humboldt Bay (~40.7° N), Lagoon Creek (~41.9° N), and Sand Mine Marsh (~41.74° N).

ACKNOWLEDGEMENTS

This work was supported by the Earthquake Hazards Program of the U.S. Geological Survey. Research supported by the U.S. Geological Survey (USGS), Department of the Interior, under USGS award numbers G14AP00128 and G19AP00105 to SEE and G14AP000129 to EHH and HMK. The views and conclusions contained in this document are those of the authors and should not be interpreted as necessarily representing the official policies, either express or implied, of the U.S. Government. Research further supported by the National Science Foundation (EAR–1419844) and the Northern California Geological Society, Richard Chambers Memorial Scholarship 2017 to JSP. We thank Dylan Caldwell for conducting an RTK-GPS survey, Byron Halavik, Erin Quinn, and Casey Loofbourrow for the their field support efforts, Jaime Delano and Alan Nelson for their help with Figure 1A, and the Humboldt State University Geology Department for providing access to field equipment and lab facilities. We thank Science Editor Rob Strachan for overseeing the science review. Reviews by Chris Goldfinger, Lydia Staisch, an anonymous reviewer and Associate Editor Stefano Mazzoli substantially improved the manuscript. This is a contribution to International Geoscience Program 639 (IGCP-639) “Sea-level changes from minutes to millennia”.

REFERENCES

Abramson, H.F., 1998. *Evidence for tsunamis and earthquakes during the last 3500 years from Lagoon Creek, a coastal freshwater marsh, northern California* (M.S. thesis, Humboldt State University).

Adams, J., 1990. Paleoseismicity of the Cascadia subduction zone: Evidence from turbidites off the Oregon-Washington margin. *Tectonics*, *9*(4), pp.569-583.

Allen, J.R.L., 1989. Evolution of salt-marsh cliffs in muddy and sandy systems: a qualitative comparison of British west-coast estuaries. *Earth Surface Processes and Landforms*, *14*(1), pp.85-92.

Allen, J.R.L., 1997. Simulation models of salt-marsh morphodynamics: some implications for high-intertidal sediment couplets related to sea-level change. *Sedimentary Geology*, *113*(3-4), pp.211-223.

Allen, J.R., 2000. Morphodynamics of Holocene salt marshes: a review sketch from the Atlantic and Southern North Sea coasts of Europe. *Quaternary Science Reviews*, *19*(12), pp.1155-1231.

Atwater, B.F., 1987. Evidence for great Holocene earthquakes along the outer coast of Washington State. *Science*, *236*(4804), pp.942-944.

Atwater, B.F., 1992. Geologic evidence for earthquakes during the past 2000 years along the Copalis River, southern coastal Washington. *Journal of Geophysical Research: Solid Earth*, *97*(B2), pp.1901-1919.

Atwater, B.F. and Hemphill-Haley, E., 1997. *Recurrence intervals for great earthquakes of the past 3,500 years at northeastern Willapa Bay, Washington* (No. 1576). USGPO; Information Services [distributor].

Atwater, B.F., Tuttle, M.P., Schweig, E.S., Rubin, C.M., Yamaguchi, D.K. and Hemphill-Haley, E., 2003. Earthquake recurrence inferred from paleoseismology. *Developments in Quaternary Sciences*, *1*, pp.331-350.

Benson, B.E., Atwater, B.F., Yamaguchi, D.K., Amidon, L.J., Brown, S.L., and Lewis, R.C., 2001, Renewal of Tidal Forests in Washington State after a Subduction Earthquake in A.D. 1700: Quaternary Research, v. 56, p. 139–147, doi: 10.1006/qres.2001.2251.

Ramsey, C.B., 1995. Radiocarbon calibration and analysis of stratigraphy: the OxCal program. *Radiocarbon*, *37*(2), pp.425-430.

Bronk Ramsey, C., 2008. Radiocarbon dating: Revolutions in Understanding. *Archaeometry*, *50*(2), pp.249-275.

Ramsey, C.B., 2009, Bayesian analysis of radiocarbon dates: Radiocarbon, v. 51, p. 337–360.

Bronk Ramsey, C., 2009b, Dealing with outliers and offsets in radiocarbon dating: Radiocarbon, v. 51, p. 1023–1045, https:// doi .org /10 .1017 /S0033822200034093.

Ramsey, C.B. and Lee, S., 2013. Recent and planned developments of the program OxCal. *Radiocarbon*, *55*(2), pp.720-730.

Cahill, N., Kemp, A.C., Horton, B.P. and Parnell, A.C., 2016. A Bayesian hierarchical model for reconstructing relative sea level: from raw data to rates of change. *Climate of the Past*, *12*(2), pp.525-542.

Cahoon, D.R., Lynch, J.C. and Powell, A.N., 1996. Marsh vertical accretion in a southern California estuary, USA. *Estuarine, Coastal and Shelf Science*, *43*(1), pp.19-32.

Clarke, S.H. and Carver, G.A., 1992. Late Holocene tectonics and paleoseismicity, southern Cascadia subduction zone. *Science*, *255*(5041), pp.188-192.

Darienzo, M.E. and Peterson, C.D., 1990. Episodic tectonic subsidence of late Holocene salt marshes, northern Oregon central Cascadia margin. *Tectonics*, *9*(1), pp.1-22

Darienzo, M.E., Peterson, C.D. and Clough, C., 1994. Stratigraphic evidence for great subduction-zone earthquakes at four estuaries in northern Oregon, USA. *Journal of Coastal Research*, pp.850-876.

Davies, M.H., Mix, A.C., Stoner, J.S., Addison, J.A., Jaeger, J., Finney, B. and Wiest, J., 2011. The deglacial transition on the southeastern Alaska Margin: Meltwater input, sea level rise, marine productivity, and sedimentary anoxia. *Paleoceanography and Paleoclimatology*, *26*(2).

de Rijk, S., 1995. Salinity control on the distribution of salt marsh foraminifera (Great Marshes, Massachusetts). *The Journal of Foraminiferal Research*, *25*(2), pp.156-166.

Dura, T., Horton, B.P., Cisternas, M., Ely, L.L., Hong, I., Nelson, A.R., Wesson, R.L., Pilarczyk, J.E., Parnell, A.C. and Nikitina, D., 2017. Subduction zone slip variability during the last millennium, south-central Chile. *Quaternary Science Reviews*, *175*, pp.112-137.

Engelhart, S.E., Horton, B.P., Nelson, A.R., Hawkes, A.D., Witter, R.C., Wang, K., Wang, P.L. and Vane, C.H., 2013. Testing the use of microfossils to reconstruct great earthquakes at Cascadia. *Geology*, *41*(10), pp.1067-1070.

Engelhart, S.E., Horton, B.P., Vane, C.H., Nelson, A.R., Witter, R.C., Brody, S.R. and Hawkes, A.D., 2013. Modern foraminifera, δ 13 C, and bulk geochemistry of central Oregon tidal marshes and their application in paleoseismology. *Palaeogeography, Palaeoclimatology, Palaeoecology*, *377*, pp.13-27.

Engelhart, S.E., Hemphill-Haley, E., Kelsey, H.M., and Padgett, J.S. *Refined Estimates of Coseismic Subsidence along the Southern Cascadia Subduction Zone in Northern Humboldt Bay (Arcata Bay): Collaborative Research with University of Rhode Island and Humboldt State University*. No. G14AP00128 and G14AP00129. U.S. Geological Survey.

Enkin, R.J., Dallimore, A., Baker, J., Southon, J.R. and Ivanochko, T., 2013. A new high-resolution radiocarbon Bayesian age model of the Holocene and Late Pleistocene from core MD02-2494 and others, Effingham Inlet, British Columbia, Canada; with an application to the paleoseismic event chronology of the Cascadia Subduction Zone. *Canadian Journal of Earth Sciences*, *50*(7), pp.746-760.

Fairbanks, R.G., Mortlock, R.A., Chiu, T.C., Cao, L., Kaplan, A., Guilderson, T.P., Fairbanks, T.W., Bloom, A.L., Grootes, P.M. and Nadeau, M.J., 2005. Radiocarbon calibration curve spanning 0 to 50,000 years BP based on paired 230Th/234U/238U and 14C dates on pristine corals. *Quaternary Science Reviews*, *24*(16-17), pp.1781-1796.

Fatela, F. and Taborda, R., 2002. Confidence limits of species proportions in microfossil assemblages. *Marine Micropaleontology*, *45*(2), pp.169-174.

Friedrichs, C.T. and Perry, J.E., 2001. Tidal salt marsh morphodynamics: a synthesis. *Journal of Coastal Research*, pp.7-37.

Gabet, E.J., 1998. Lateral migration and bank erosion in a saltmarsh tidal channel in San Francisco Bay, California. *Estuaries*, *21*(4), pp.745-753.

Garrett, E., Shennan, I., Woodroffe, S.A., Cisternas, M., Hocking, E.P. and Gulliver, P., 2015. Reconstructing paleoseismic deformation, 2: 1000 years of great earthquakes at Chucalén, south central Chile. *Quaternary Science Reviews*, *113*, pp.112-122.

Garrison-Laney, C.E., 1998. *Diatom evidence for tsunami inundation from Lagoon Creek, a coastal freshwater pond, Del Norte County, California* (Doctoral dissertation, Humboldt State University).

Gehrels, W.R., Belknap, D.F. and Kelley, J.T., 1996. Integrated high-precision analyses of Holocene relative sea-level changes: lessons from the coast of Maine. *Geological Society of America Bulletin*, *108*(9), pp.1073-1088.

Graehl, N.A., Kelsey, H.M., Witter, R.C., Hemphill-Haley, E. and Engelhart, S.E., 2015. Stratigraphic and microfossil evidence for a 4500-year history of Cascadia subduction zone earthquakes and tsunamis at Yaquina River estuary, Oregon, USA. *Bulletin*, *127*(1-2), pp.211-226.

Goldfinger, C., Nelson, C.H., Morey, A.E., Johnson, J.E., Patton, J.R., Karabanov, E.B., Gutierrez-Pastor, J., Eriksson, A.T., Gracia, E., Dunhill, G. and Enkin, R.J., 2012. *Turbidite event history--Methods and implications for Holocene paleoseismicity of the Cascadia subduction zone* (No. 1661-F). US Geological Survey.

Guilbault, J.P., Clague, J.J. and Lapointe, M., 1995. Amount of subsidence during a late Holocene earthquake—evidence from fossil tidal marsh foraminifera at Vancouver Island, west coast of Canada. *Palaeogeography, Palaeoclimatology, Palaeoecology*, *118*(1), pp.49-71.

Guilbault, J.P., Clague, J.J. and Lapointe, M., 1996. Foraminiferal evidence for the amount of coseismic subsidence during a late Holocene earthquake on Vancouver Island, west coast of Canada. *Quaternary Science Reviews*, *15*(8), pp.913-937.

Haslett, J. and Parnell, A., 2008. A simple monotone process with application to radiocarbon-dated depth chronologies. *Journal of the Royal Statistical Society: Series C (Applied Statistics)*, *57*(4), pp.399-418.

Hawkes, A.D., Horton, B.P., Nelson, A.R. and Hill, D.F., 2010. The application of intertidal foraminifera to reconstruct coastal subsidence during the giant Cascadia earthquake of AD 1700 in Oregon, USA. *Quaternary International*, *221*(1), pp.116-140.

Hawkes, A.D., Horton, B.P., Nelson, A.R., Vane, C.H. and Sawai, Y., 2011. Coastal subsidence in Oregon, USA, during the giant Cascadia earthquake of AD 1700. *Quaternary Science Reviews*, *30*(3), pp.364-376.

Hemphill-Haley, E., 1995. Diatom evidence for earthquake-induced subsidence and tsunami 300 yr ago in southern coastal Washington. *Geological Society of America Bulletin*, *107*(3), pp.367-378.

Hemphill-Haley, E., Kelsey, H.M., Graehl, N., Casso, M., Caldwell, D., Loofbourrow, C., Robinson, M., Vermeer, J., and Southwick, E., 2019, Recent sandy deposits at five northern California coastal wetlands - Stratigraphy, diatoms, and implications for storm and tsunami hazards. *U.S. Geological Survey Scientific Investigations Report 2018–5111*, 187 p., https://doi.org/10.3133/sir20185111.

Holden, P.B., Birks, H.J.B., Brooks, S.J., Bush, M.B., Hwang, G.M., Matthews-Bird, F., Valencia, B.G. and Van Woesik, R., 2017. BUMPER v1. 0: a Bayesian user-friendly model for palaeo-environmental reconstruction.

Horton, B.P. and Edwards, R.J., 2005. The application of local and regional transfer functions to the reconstruction of Holocene sea levels, north Norfolk, England. *The Holocene*, *15*(2), pp.216-228.

Horton, B. P., & Edwards, R. J., 2006. Quantifying Holocene Sea Level Change Using Intertidal Foraminifera: Lessons from the British Isles. Cushman Foundation for Foraminiferal Research Special Publication, 40, 97.

Jull, A.J.T., 2007a. Radiocarbon dating: AMS method. In: Elias, S.A. (Ed.), Encyclopedia of Quaternary Science. Elsevier, Amsterdam, pp. 2911–2918.

Kelsey, H.M., Witter, R.C. and Hemphill-Haley, E., 1998. Response of a small Oregon estuary to coseismic subsidence and postseismic uplift in the past 300 years. *Geology*, *26*(3), pp.231-234.

Kelsey, H.M., Witter, R.C. and Hemphill-Haley, E., 2002. Plate-boundary earthquakes and tsunamis of the past 5500 yr, Sixes River estuary, southern Oregon. *Geological Society of America Bulletin*, *114*(3), pp.298-314.

Kelsey, H. M., Nelson, A. R. Witter, R. C., and Hemphill-Haley, E. 2005, Tsunami history of an Oregon coastal lake reveals a 4,600 year record of great earthquakes on the Cascadia subduction zone, Geological Society of America Bulletin, 117, 1009-1032.

Kelsey, H.M., Engelhart, S.E., Pilarczyk, J.E., Horton, B.P., Rubin, C.M., Daryono, M.R., Ismail, N., Hawkes, A.D., Bernhardt, C.E. and Cahill, N., 2015. Accommodation space, relative sea level, and the archiving of paleo-earthquakes along subduction zones. *Geology*, *43*(8), pp.675-678.

Kemp, A.C., Horton, B.P., Culver, S.J., Corbett, D.R., van de Plassche, O., Gehrels, W.R., Douglas, B.C. and Parnell, A.C., 2009. Timing and magnitude of recent accelerated sea-level rise (North Carolina, United States). *Geology*, *37*(11), pp.1035-1038.

Kemp, A.C., Horton, B.P., Donnelly, J.P., Mann, M.E., Vermeer, M. and Rahmstorf, S., 2011. Climate related sea-level variations over the past two millennia. *Proceedings of the National Academy of Sciences*, *108*(27), pp.11017-11022.

Kemp, A.C., Nelson, A.R. and Horton, B.P., 2013. Radiocarbon dating of plant macrofossils from tidal-marsh sediment. *in:* Shroder, J. F., (ed.) Treatise on Geomorphology, 14, 370-388, Academic Press, San Diego.

Kemp, A.C., Cahill, N., Engelhart, S.E., Hawkes, A.D. and Wang, K., 2018. Revising Estimates of Spatially Variable Subsidence during the AD 1700 Cascadia Earthquake Using a Bayesian Foraminiferal Transfer Function. *Bulletin of the Seismological Society of America*, *108*(2), pp.654-673.

Letzsch, W.S. and Frey, R.W., 1980. Deposition and erosion in a Holocene salt marsh, Sapelo Island, Georgia. *Journal of Sedimentary Research*, *50*(2), pp.529-542.

Li, W.H., 1992. *Evidence for the late Holocene coseismic subsidence in the Lower Eel River valley, Humboldt county, Northern California: An application of foraminiferal zonation to indicate tectonic submergence* (Doctoral dissertation, Humboldt State University).

Lorito, S., Romano, F., Atzori, S., Tong, X., Avallone, A., McCloskey, J., Cocco, M., Boschi, E. and Piatanesi, A., 2011. Limited overlap between the seismic gap and coseismic slip of the great 2010 Chile earthquake. *Nature Geoscience*, *4*(3), p.173.

Mariotti, G., Kearney, W.S. and Fagherazzi, S., 2016. Soil creep in salt marshes. *Geology*, *44*(6), pp.459-462.

Milker, Y., Horton, B.P., Vane, C.H., Engelhart, S.E., Nelson, A.R., Witter, R.C., Khan, N.S. and Bridgeland, W.T., 2015. Annual and seasonal distribution of intertidal foraminifera and stable carbon isotope geochemistry, Bandon Marsh, Oregon, USA. *The Journal of Foraminiferal Research*, *45*(2), pp.146-155.

Milker, Y., Nelson, A.R., Horton, B.P., Engelhart, S.E., Bradley, L-A., and Witter, R.C., 2016. Differences in coastal subsidence in southern Oregon (USA) during at least six prehistoric megathrust earthquakes. *Quaternary Science Reviews*.

Nelson, A.R., 1992. Discordant 14C ages from buried tidal-marsh soils in the Cascadia subduction zone, southern Oregon coast. *Quaternary Research*, *38*(1), pp.74-90.

Nelson, A.R., Shennan, I. and Long, A.J., 1996a. Identifying coseismic subsidence in tidal‐wetland stratigraphic sequences at the Cascadia subduction zone of western North America. *Journal of Geophysical Research: Solid Earth*, *101*(B3), pp.6115-6135.

Nelson, A.R., Jennings, A.E. and Kashima, K., 1996b. An earthquake history derived from stratigraphic and microfossil evidence of relative sea-level change at Coos Bay, southern coastal Oregon. *Geological Society of America Bulletin*, *108*(2), pp.141-154.

Nelson, A.R., Sawai, Y., Jennings, A.E., Bradley, L.A., Gerson, L., Sherrod, B.L., Sabean, J. and Horton, B.P., 2008. Great-earthquake paleogeodesy and tsunamis of the past 2000 years at Alsea Bay, central Oregon coast, USA. *Quaternary Science Reviews*, *27*(7), pp.747-768.

Nelson, A.R., Ota, Y., Umitsu, M., Kashima, K. and Matsushima, Y., 1998. Seismic or hydrodynamic control of rapid late-Holocene sea-level rises in southern coastal Oregon, USA?. *The Holocene*, *8*(3), pp.287-299.

Nelson, A.R., Asquith, A.C. and Grant, W.C., 2004. Great earthquakes and tsunamis of the past 2000 years at the Salmon River estuary, central Oregon coast, USA. *Bulletin of the Seismological Society of America*, *94*(4), pp.1276-1292.

Nelson, A.R., Hawkes, A.D., Sawai, Y., Engelhart, S.E., Witter, R., Grant-Walter, W.C., Bradley, L.A., Dura, T., Cahill, N. and Horton, B., 2020. Identifying the greatest earthquakes of the past 2000 years at the Nehalem River Estuary, Northern Oregon Coast, USA. *OpenQuaternary.*, *6*(2), pp.1-30.

Parnell, A.C., Haslett, J., Allen, J.R., Buck, C.E. and Huntley, B., 2008. A flexible approach to assessing synchroneity of past events using Bayesian reconstructions of sedimentation history. *Quaternary Science Reviews*, *27*(19-20), pp.1872-1885.

Patton, J., 2004, Late Holocene coseismic subsidence and coincident tsunamis, southern Cascadia subduction zone, Hookton Slough, Humboldt Bay, California. M.S. thesis, Humboldt State University, 76p.

Pickart, A.J. and Hesp, P.A., 2019. Spatio-temporal geomorphological and ecological evolution of a transgressive dunefield system, Northern California, USA. *Global and planetary change*, *172*, pp.88-103.

Pritchard, C. J., 2004. *Late Holocene relative sea-level changes, Arcata Bay, California: Evaluation of freshwater syncline movement using coseismically buried soil horizons*. M.S. thesis, Humboldt State University, Department of Geology.

Reimer, P.J., Bard, E., Bayliss, A., Beck, J.W., Blackwell, P.G., Ramsey, C.B., Buck, C.E., Cheng, H., Edwards, R.L., Friedrich, M. and Grootes, P.M., 2013. IntCal13 and Marine13 radiocarbon age calibration curves 0–50,000 years cal BP. *Radiocarbon*, *55*(4), pp.1869-1887.

Rothwell, R.G. and Rack, F.R., 2006. New techniques in sediment core analysis: an introduction. *Geological Society, London, Special Publications*, *267*(1), pp.1-29.

Satake, K., Shimazaki, K., Tsuji, Y. and Ueda, K., 1996. Time and size of a giant earthquake in Cascadia inferred from Japanese tsunami records of January 1700. *Nature*, *379*(6562), p.246.

Satake, K., Wang, K. and Atwater, B.F., 2003. Fault slip and seismic moment of the 1700 Cascadia earthquake inferred from Japanese tsunami descriptions. *Journal of Geophysical Research: Solid Earth*, *108*(B11).

Schlosser, S., and A. Eicher. 2012. The Humboldt Bay and Eel River Estuary Benthic Habitat Project. California Sea Grant Publication T-075. 246 p.

Scott, D.B. and Medioli, F.S., 1980. Living vs. total foraminiferal populations: their relative usefulness in paleoecology. *Journal of Paleontology*, pp.814-831.

Shennan, I., Long, A.J., Rutherford, M.M., Green, F.M., Innes, J.B., Lloyd, J.M., Zong, Y. and Walker, K.J., 1996. Tidal marsh stratigraphy, sea-level change and large earthquakes, I: a 5000 year record in Washington, USA. *Quaternary Science Reviews*, *15*(10), pp.1023-1059.

Trachsel, M. and Telford, R.J., 2017. All age–depth models are wrong, but are getting better. *The Holocene*, *27*(6), pp.860-869.

Troels-Smith, J., 1955. Karakterisering af lose jordarter. Characterization of unconsolidated sediments.

Törnqvist, T.E., de Jong, A.F. and van der Borg, K., 1990. Comparison of AMS 14C ages of organic deposits and macrofossils: a progress report. *Nuclear Instruments and Methods in Physics Research Section B: Beam Interactions with Materials and Atoms*, *52*(3-4), pp.442-445.

van de Plassche, O., 1979, Sea-level research in the provinces of south Holland, Netherlands: Proceedings of the “1978 international symposium of coastal evolution in the Quaternary”, Sao Paulo, Brazil, p. 534-551.

van de Plassche, O., van der Borg, K. and de Jong, A.F., 1998. Sea level–climate correlation during the past 1400 yr. *Geology*, *26*(4), pp.319-322.

Valentine, D.W., 1992. *Late Holocene stratigraphy, Humboldt Bay, California: evidence for late Holocene paleoseismicity of the southern Cascadia subduction zone*. M.S. thesis, Humboldt State University.

Valentine, D.W., Keller, E.A., Carver, G., Li, W.H., Manhart, C. and Simms, A.R., 2012. Paleoseismicity of the southern end of the Cascadia subduction zone, northwestern California. *Bulletin of the Seismological Society of America*, *102*(3), pp.1059-1078.

Vick, G.S., 1988. *Late Holocene paleoseismicity and relative sea level changes of the Mad River Slough, northern Humboldt Bay, California*. M.S. thesis, Humboldt State University.

Wang, P.L., Engelhart, S.E., Wang, K., Hawkes, A.D., Horton, B.P., Nelson, A.R. and Witter, R.C., 2013. Heterogeneous rupture in the great Cascadia earthquake of 1700 inferred from coastal subsidence estimates. *Journal of Geophysical Research: Solid Earth*, *118*(5), pp.2460-2473.

Wirth, E.A. and Frankel, A.D., 2019. Impact of Down-Dip Rupture Limit and High-Stress Drop Subevents on Coseismic Land-Level Change during Cascadia Megathrust Earthquakes. *Bulletin of the Seismological Society of America*, *109*(6), pp.2187-2197.

Witter, R.C., Kelsey, H.M. and Hemphill-Haley, E., 2001. Pacific storms, El Nino and tsunamis: competing mechanisms for sand deposition in a coastal marsh, Euchre Creek, Oregon. *Journal of Coastal Research*, pp.563-583.

Witter, R.C., Kelsey, H.M. and Hemphill-Haley, E., 2003. Great Cascadia earthquakes and tsunamis of the past 6700 years, Coquille River estuary, southern coastal Oregon. *Geological Society of America Bulletin*, *115*(10), pp.1289-1306.

Witter, R.C., Jaffe, B., Zhang, Y. and Priest, G., 2012. Reconstructing hydrodynamic flow parameters of the 1700 tsunami at Cannon Beach, Oregon, USA. *Natural Hazards*, *63*(1), pp.223-240.

Witter, R.C., Zhang, Y.J., Wang, K., Priest, G.R., Goldfinger, C., Stimely, L., English, J.T. and Ferro, P.A., 2013. Simulated tsunami inundation for a range of Cascadia megathrust earthquake scenarios at Bandon, Oregon, USA. *Geosphere*, *9*(6), pp.1783-1803.

Witter, R., Briggs, R., Engelhart, S.E., Gelfenbaum, G., Koehler, R.D., Nelson, A., Selle, S.L., Corbett, R. and Wallace, K., 2019. Evidence for frequent, large tsunamis spanning locked and creeping parts of the Aleutian megathrust. *Bulletin*, *131*(5-6), pp.707-729.

FIGURE CAPTION LIST

Figure 1 A. Physiography and major features of the Cascadia subduction zone (base map data source: GEBCO Compilation Group (2019) GEBCO 2019 Grid, doi:10.5285/836f016a-33be-6ddc-e053-6c86abc0788e) and modified from Nelson et al., (2020). The deformation front of the subduction-zone megathrust fault on the ocean floor (black barbed line) is near the bathymetric boundary between the continental slope and abyssal plain. Dots mark estuaries, lagoons, or lakes with evidence for coastal subsidence, tsunamis, and/or turbidites accompanying subduction-zone earthquakes, B. Location map of the southern Cascadia coastline. Dots mark estuaries or lakes with evidence for coastal subsidence and/or tsunami.

Figure 2. Location maps A. Humboldt Bay, B. Mad River Slough, C. McDaniel Creek, D. Jacoby Creek.

Figure 3. Simplified lithostratigraphy of northern Humboldt Bay at A. McDaniel Creek, B. Mad River Slough and C. Jacoby Creek. Parenthesized numbers below the core site numbers are elevations of individual core sites, accurate to the nearest cm. Core depths are shown relative to present-day elevation. Calibrated ^{14}C ages (ka; mode of ^{14}C distribution rounded to the nearest century) are shown for samples above and below contacts (more complete radiocarbon age data in Table 2).

Figure 4. Alternative age models of subsidence contacts C, D, and E from northern Humboldt Bay using Bchron (green), OxCal Sequence model (orange), and OxCal P-sequence model (blue).

Figure 5. Plots showing McDaniel Creek stratigraphy for four contacts, A. Contact A at MD.3; B. Contact C at MD.6; C. Contact D at MD.13; and D. Contact E at MD.5. The plots include photo images, CT scans (rainbow scale; warm colors=more dense and cool colors=less dense), percent foraminifera (grey bar), and results of BTF reconstructed sea level with error bars that represent 1σ uncertainties. HOF, (highest occurrence of foraminifera). SWLI (standardized water level index).

Figure 6. Comparison of dated mud-over-peat and mud-over-upland soil contacts beneath southern Cascadia salt marshes (Talbot Creek: Milker et al, 2016; Coquille River: Witter et al., 2003; Southern Humboldt Bay: Patton, 2004; Eel River: Li, 1992) and tsunami deposits at Lagoon Creek (Abramson, 1998 and Garrison-Laney, 1998) and Bradley Lake (Kelsey et al., 2005) with OxCal Sequence modeled timing of subsidence contacts for northern Humboldt Bay and ages of marine turbidites (vertical black arrows show 2σ uncertainties from Goldfinger et al., 2012). *Evidence Absent** To date evidence of coseismic subsidence in the time range ca. 500-2000 yrs BP has not been found in the latitude range 41.7-42.9°N. Absence of evidence may be because megathrust slip was insufficient to cause vertical deformation to be recorded by the salt marsh and/or because vertical deformation was further offshore and only minimal vertical deformation occurred

at coastal sites. There is also the possibility that, for the above time and latitude range, further field work in salt marshes may reveal subsidence stratigraphy

Table 1. Attributes of buried organic-rich units from cores.

Numbered (by depth) buried organic-rich unit upper contact	Number of cores that sample the unit	Depth range of buried organic-rich unit upper contact (cm)	Nature of buried organic-rich unit upper contact	Thickness range of organic-rich unit (cm)	Thickness range of mud deposit overlying buried organic-rich unit (cm)
			Mad River Slough		
1	6	94-136	5a, 1s	15-35	68-97
2	2	169-174	1a, 1s	3-4	5-7
3	6	184-227	3a, 2s, 1c	8-20	24-65
4	4	234-275	3s, 3c	15-20	32-72
5	2	295-303	2c	4-12	12-17
			McDaniel Creek		
1	15	78-145	11a, 3s, 1c	5-24	60-110
2	9	171-213	3a, 4s, 2c	4-12	18-62
3	10	226-257	2a, 4s, 4c	4-33	32-110
4	9	250-380	2s, 4c, 2g	4-13	16-196
			Jacoby Creek		
1	8	48-116	6a, 2s	8-18	11-86
2	6	113-133	2s, 4c	5-11	18-70
3	6	163-203	1s, 4c, 1g	4-8	16-118

Note: Depth and thicknesses are rounded to the nearest centimeter: thicknesses <1 cm are rounded to the nearest millimeter.
[*]Contacts: a-abrupt, 1 mm; s-sharp, 1-5 mm; c-clear, >5-10 mm; g-gradual, >10 mm. Number refers to number of observations.

Table 2. Summary of northern Humboldt Bay radiocarbon ages

Calibrated Age (2σ cal yr BP)*	Analytical Age (1σ 14C yrs BP)†	Lab Number	^{13}C (‰)	Site Identifier	Depth (cm)	Description of Dated Material	Age inter-pretation	Contact
				Mad River Slough:				
307 - 1	235±20	OS-117742	-24.84	MR.14.02.B	140.5-141.5	Herbaceous stem	Maximum	A
511 - 476	420±15	OS-117743	-13.89	MR.14.02.B	161.5-162.5	Distichlis rhizome	Maximum	B
956 - 802	990±20	OS-117744	-11.39	MR.14.02.B	225.5-226	2 Distichlis rhizomes	Maximum	C
956 - 912	1000±15	OS-119964	-26.65	MR.14.05.B	188.5-189	Herbaceous stem	Maximum	C
1057 - 961	1100±20	OS-117822	-24.8	MR.14.02.A	273-273.5	Detrital grindelia stem	Minimum	D
1280 - 1183	1290±15	OS-119965	-25.69	MR.14.05.C	246-247	Rhizome	Maximum	D
1690 - 1545	1690±20	OS-118743	-25.57	MR.14.02.A	297.50-298.25	~25 seeds (atriplex and potamogeton)	Maximum	E
				McDaniel Creek:				
283 - 1	170±15	OS-119960	-24.32	MD.14.03.C	117-118	Herbaceous stem	Maximum	A
926 - 798	955±15	OS-119963	-25.64	MD.14.06.C	168.5-169.5	Rhizome	Minimum	C
951 - 804	990±15	OS-117738	-26.03	MD.14.06.C	169.5-170.5	2 rhizomes	Maximum	C
965 - 929	1040±15	OS-117739	-26.82	MD.14.03.C	212.5-213.5	Rhizome	Maximum	C
1399 - 1328	1480±15	OS-119962	-27.84	MD.14.05.A	276-277	Rhizome and stem fragments	Maximum	D
1302-1190	1340±20	OS-134119	-14.11	MD.17.13.D	250-251	Rhizome fragment	Maximum	D
1707 - 1575	1740±15	OS-119961	-27.06	MD.14.05.B1	306.5-307.5	Herbaceous stem (detrital?)	Minimum	E
1695 - 1565	1720±15	OS-117740	-28.02	MD.14.05.B1	308-309	2 rhizomes	Maximum	E
1708 - 1614	1750±15	OS-117741	-15.26	MD.14.04.B	379.5-380.5	Distichlis rhizome	Maximum	E
				Jacoby Creek:				
289 - 1	195±15	OS-117608	-13.5	JC.14.02.C	81-82	Distichlis rhizome	Maximum	A
1263 - 1082	1240±20	OS-123307	-12.82	JC.14.02.D	104-105	Herbaceous stem (detrital?)	Outlier	N/A
1333 - 1285	1390+20	OS-124863	-24.62	JC.14.02.D	103-105	Potamogeton seed casings (detrital?)	Outlier	N/A
Modern	>Modern	OS-125075	-16.36	JC.14.02.B	100-101	Herbaceous stem (detrital?)	Outlier	N/A
1166 - 968	1130±20	OS-119878	-26.64	JC.14.02.D	130-130.5	Rhizome	Minimum	D
1277 - 1181	1280±20	OS-117609	-27.65	JC.14.02.C	125.5-126	Rhizome fragments	Maximum	D
1692 - 1561	1710±15	OS-119959	-28.43	JC.14.02.C	167.5-168	Wood fragment (detrital)	Minimum	E
1694 - 1558	1710±20	OS-117610	-27.4	JC.14.02.C	170-171.5	Rhizome or stem	Maximum	E

*Calibrated ages in calendar years before 1950 (BP) were calculated using OxCal (version 4.3.4, Bronk Ramsey [2009a]; 95% probability distribution at 2σ) with the IntCal13 dataset of Reimer et al. (2013).

†Age, calculated using a radiocarbon half-life of 5568 years and reported at one standard deviation in radiocarbon years before 1950 by the National Ocean Sciences Accelerator Mass Spectrometry Facility, Woods Hole, Massachusetts.

§Site identifier codes: MR, Mad River Slough; MD, McDaniel Creek; JC, Jacoby Creek.

Table 3. Summary of Bayesian age models

Contact	OxCal 4.2 ‘Sequence’ calibrated age (yrs BP)					OxCal 4.2 ‘P_Sequence’ calibrated age (yrs BP)					Bchron calibrated age (yrs BP)				
	From	To	μ*	σ*	m*	From	To	μ	σ	m	From	To	μ	σ	m
C	924	816	874	30	877	935	825	905	24	917	939	845	867	47	880
D	1,231	1,004	1,117	61	1,118	1,280	1,003	1139	85	1,165	1,273	1,133	1,142	96	1,145
E	1,669	1,575	1,618	28	1,615	1,693	1,595	1,637	32	1,620	1,682	1,587	1,630	59	1,625

* μ, mean; σ , one standard deviation; m, mode.

Table 4. Summary of subsidence estimates

Contact	Core site	Depth of contact (cm)	Subsidence estimate (m)
A	MD.3	115	0.85±0.46
C	MD.6	170	0.42±0.37
D	MD.13	222	0.79±0.47
E	MD.5	307	≥0.93

Table 5. Buried organic rich unit attributes consistent with subduction earthquake origin

Contact	Sharp (<3mm) contact between buried organic-rich unit and overlying mud	Long-lasting relative sea-level rise (overlying mud >10cm thick)	Fine to very fine sand layer immediately overlies submergence contact	Foraminifera assemblages consistent with abrupt relative sea-level rise across contact	The contact is laterally extensive, e.g., observed across estuary	Calibrated age range (2σ) of buried organic-rich unit is chronologically consistent with regional record of Cascadia subduction zone earthquakes
A	✓	✓		✓	✓	✓
B	✓					
C	✓	✓		✓	~✓	✓
D	✓	✓		✓	✓	✓
E	✓	✓		✓	✓	✓

~not observed at Jacoby Creek

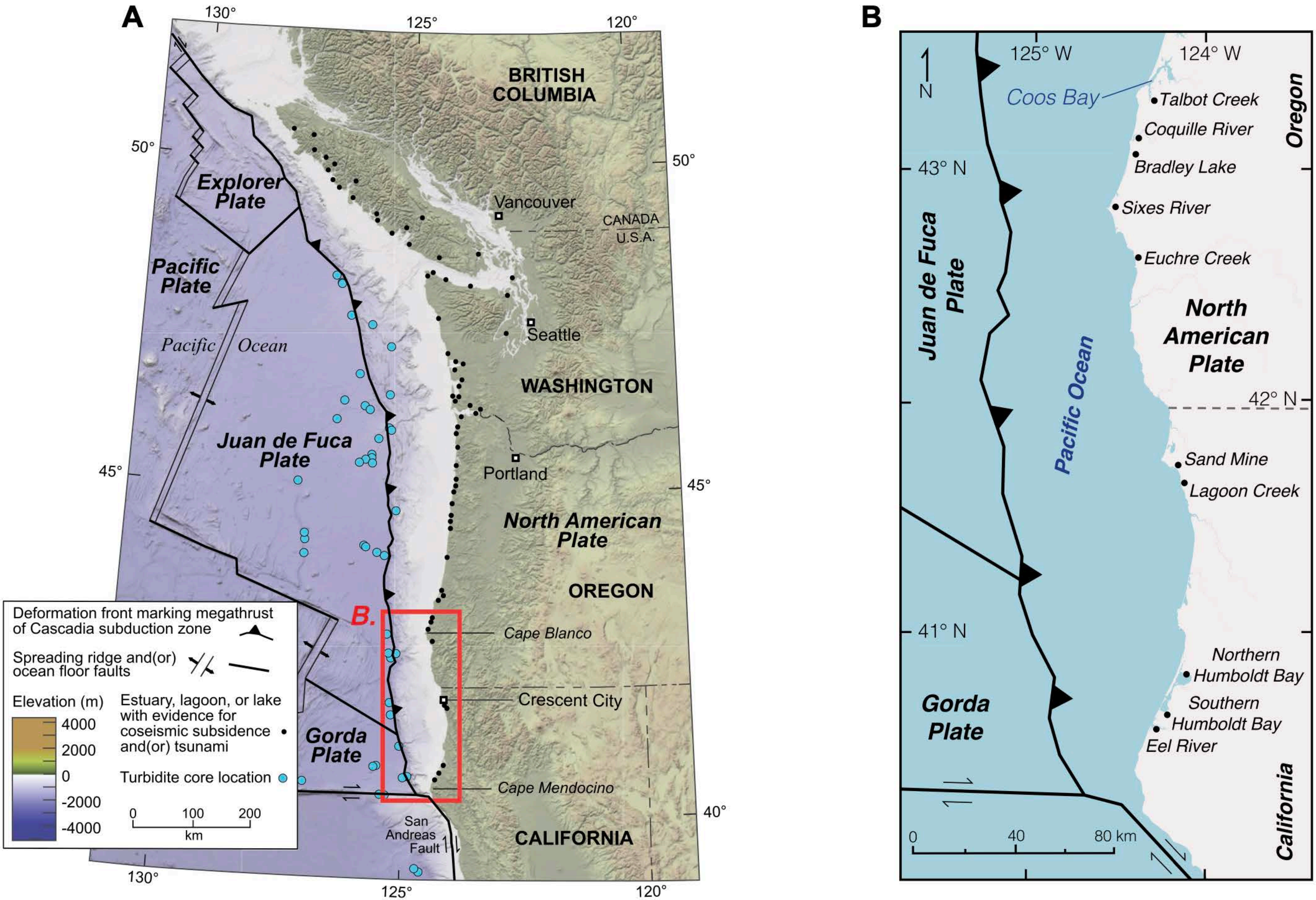

A
B
BRITISH COLUMBIA
Explorer Plate
Pacific Plate
Pacific Ocean
Vancouver
CANADA
U.S.A.
Seattle
WASHINGTON
Juan de Fuca Plate
Portland
North American Plate
OREGON
Cape Blanco
Crescent City
Gorda Plate
Cape Mendocino
San Andreas Fault
CALIFORNIA
Deformation front marking megathrust of Cascadia subduction zone
Spreading ridge and(or) ocean floor faults
Elevation (m)
4000
2000
0
-2000
-4000
Estuary, lagoon, or lake with evidence for coseismic subsidence and(or) tsunami
Turbidite core location
0 100 200 km
130°
125°
120°
50°
45°
40°
125° W
124° W
N
Coos Bay
Talbot Creek
Coquille River
Bradley Lake
Sixes River
Euchre Creek
Oregon
43° N
42° N
41° N
Juan de Fuca Plate
Pacific Ocean
North American Plate
Sand Mine
Lagoon Creek
Northern Humboldt Bay
Southern Humboldt Bay
Eel River
Gorda Plate
California
0 40 80 km

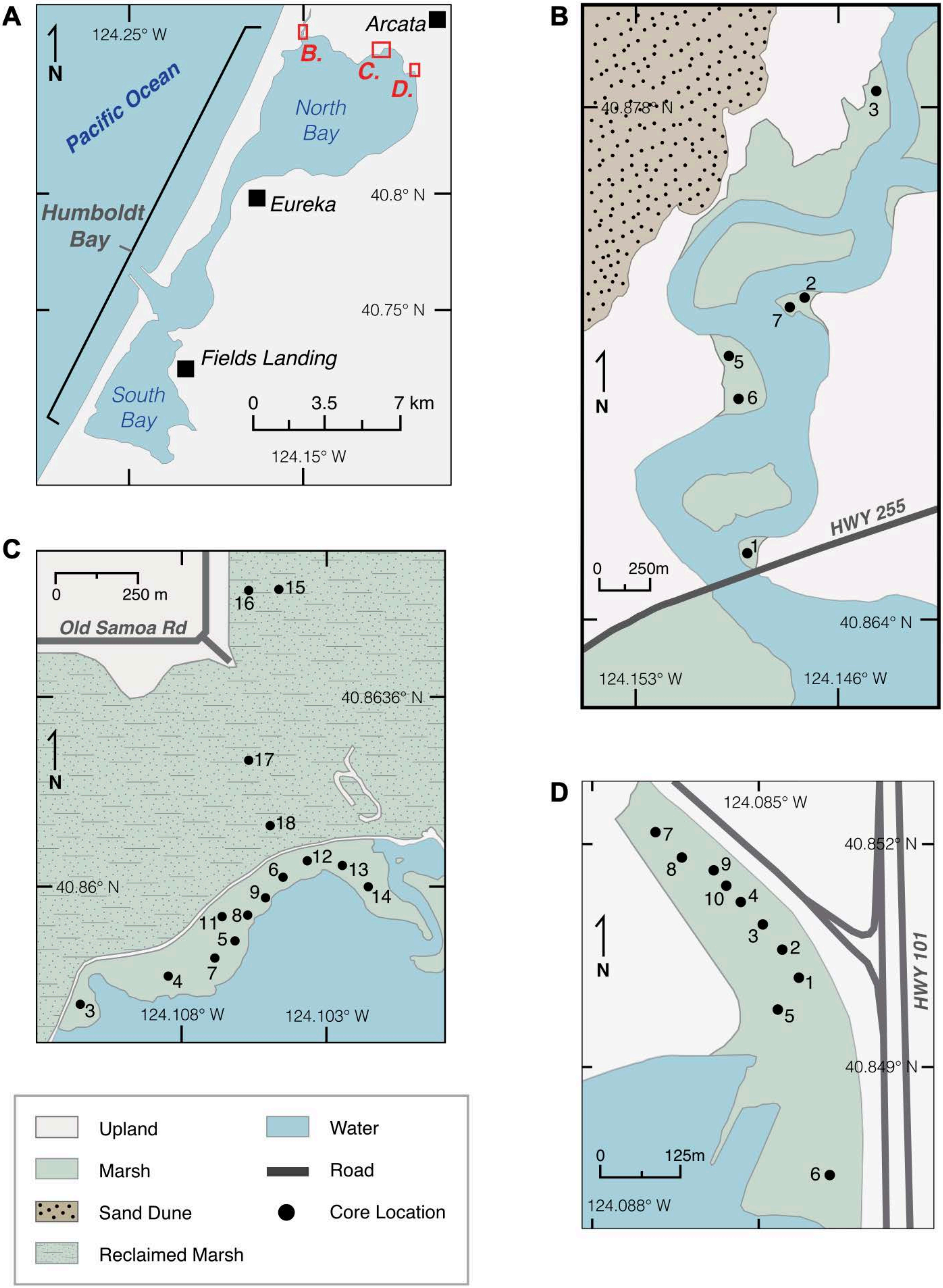
A
124.25° W
N
Pacific Ocean
Arcata
B.
C.
D.
North Bay
40.8° N
Eureka
Humboldt Bay
40.75° N
Fields Landing
South Bay
0 3.5 7 km
124.15° W
B
40.878° N
3
2
7
5
6
N
HWY 255
1
0 250m
40.864° N
124.153° W
124.146° W
C
0 250 m
16
15
Old Samoa Rd
40.8636° N
N
17
18
12
6
13
14
40.86° N
9
11
8
5
7
4
3
124.108° W
124.103° W
D
124.085° W
7
40.852° N
8
9
10
4
N
3
2
1
HWY 101
5
40.849° N
0 125m
6
124.088° W
Upland
Water
Marsh
Road
Sand Dune
Core Location
Reclaimed Marsh

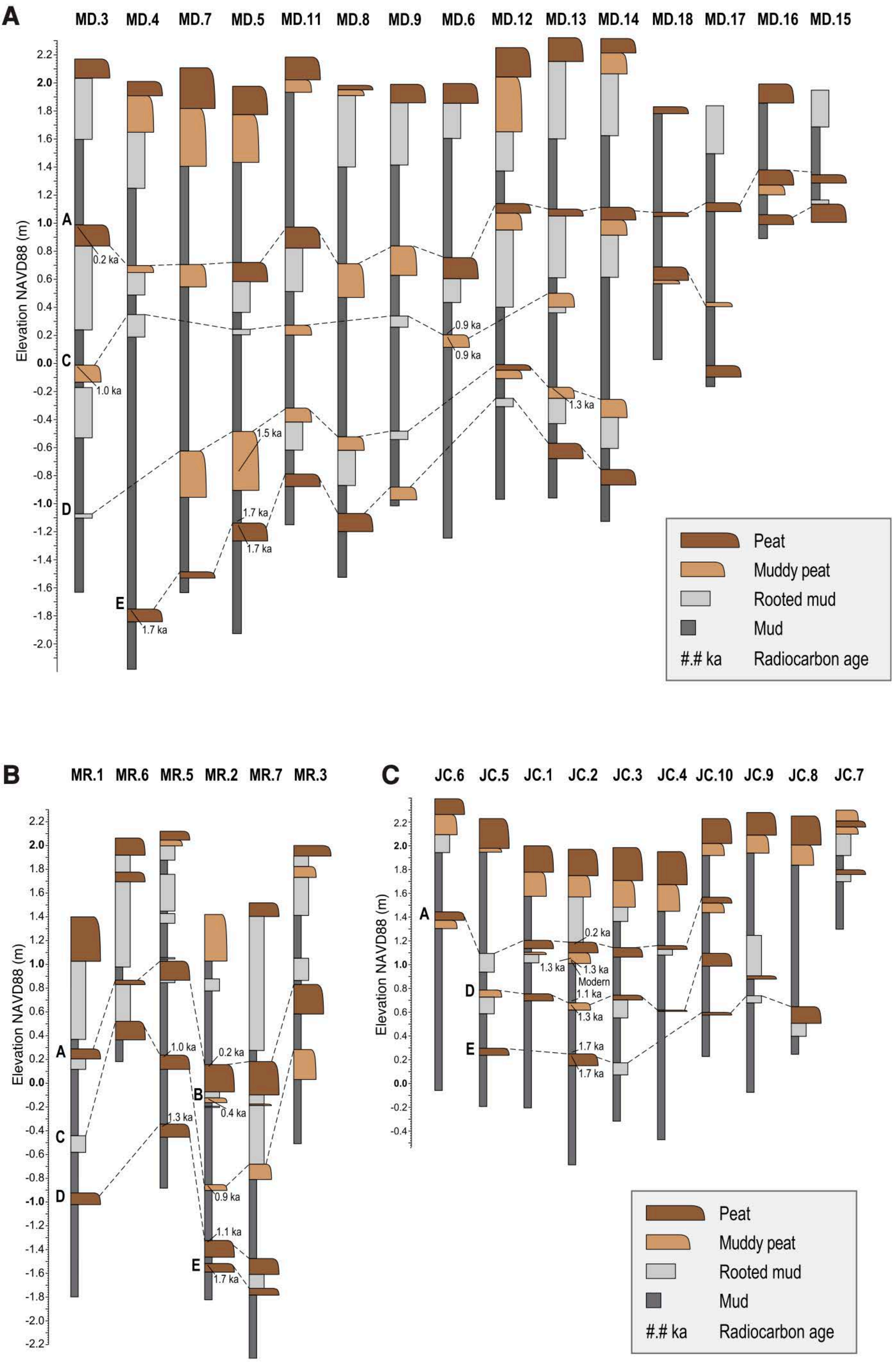

A
MD.3 MD.4 MD.7 MD.5 MD.11 MD.8 MD.9 MD.6 MD.12 MD.13 MD.14 MD.18 MD.17 MD.16 MD.15
Elevation NAVD88 (m)
2.2 2.0 1.8 1.6 1.4 1.2 1.0 0.8 0.6 0.4 0.2 0.0 -0.2 -0.4 -0.6 -0.8 -1.0 -1.2 -1.4 -1.6 -1.8 -2.0
A
C
D
E
0.2 ka
1.0 ka
1.5 ka
1.7 ka
1.7 ka
1.7 ka
0.9 ka
0.9 ka
1.3 ka
Peat
Muddy peat
Rooted mud
Mud
#.# ka
Radiocarbon age
B
MR.1 MR.6 MR.5 MR.2 MR.7 MR.3
Elevation NAVD88 (m)
2.2 2.0 1.8 1.6 1.4 1.2 1.0 0.8 0.6 0.4 0.2 0.0 -0.2 -0.4 -0.6 -0.8 -1.0 -1.2 -1.4 -1.6 -1.8 -2.0 -2.2
A
B
C
D
E
1.0 ka
0.2 ka
0.4 ka
1.3 ka
0.9 ka
1.1 ka
1.7 ka
C
JC.6 JC.5 JC.1 JC.2 JC.3 JC.4 JC.10 JC.9 JC.8 JC.7
Elevation NAVD88 (m)
2.2 2.0 1.8 1.6 1.4 1.2 1.0 0.8 0.6 0.4 0.2 0.0 -0.2 -0.4
A
D
E
0.2 ka
1.3 ka
1.3 ka
Modern
1.1 ka
1.3 ka
1.7 ka
1.7 ka
Peat
Muddy peat
Rooted mud
Mud
#.# ka
Radiocarbon age

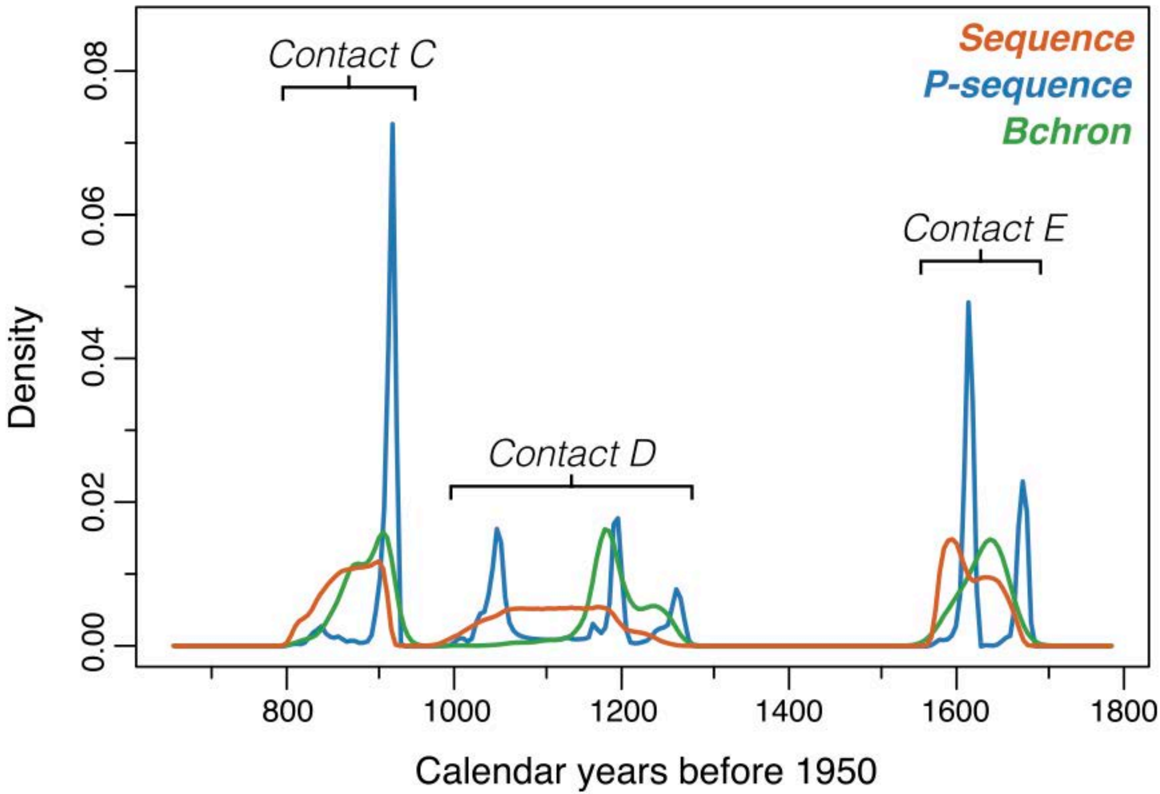

Sequence
P-sequence
Bchron
Contact C
Contact D
Contact E
Density
0.00
0.02
0.04
0.06
0.08
800
1000
1200
1400
1600
1800
Calendar years before 1950

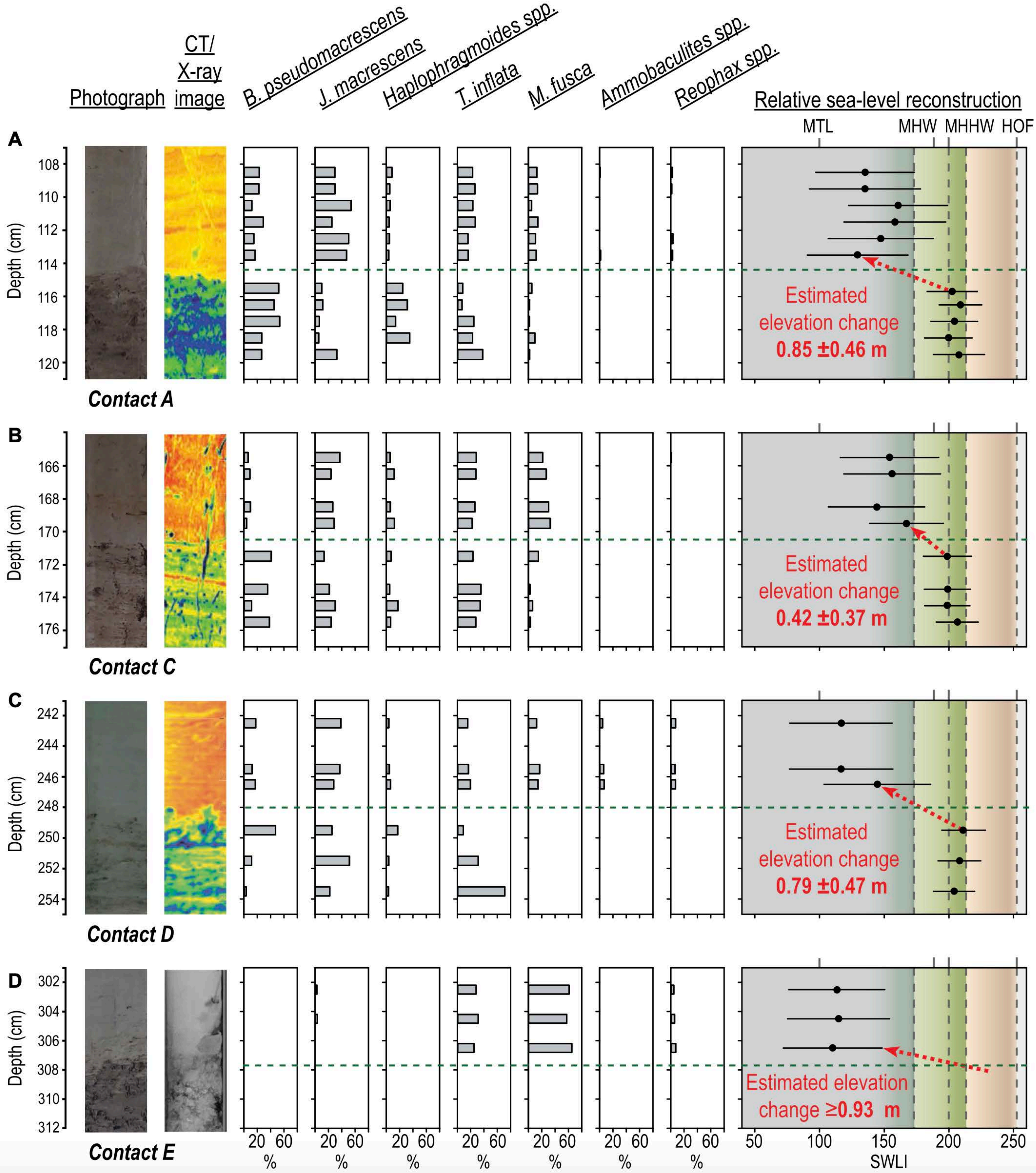

Photograph
CT/ X-ray image
B. pseudomacrescens
J. macrescens
Haplophragmoides spp.
T. inflata
M. fusca
Ammobaculites spp.
Reophax spp.
Relative sea-level reconstruction
MTL
MHW
MHHW
HOF
A
B
C
D
Depth (cm)
Contact A
Contact C
Contact D
Contact E
Estimated elevation change 0.85 ±0.46 m
Estimated elevation change 0.42 ±0.37 m
Estimated elevation change 0.79 ±0.47 m
Estimated elevation change ≥0.93 m
%
SWLI

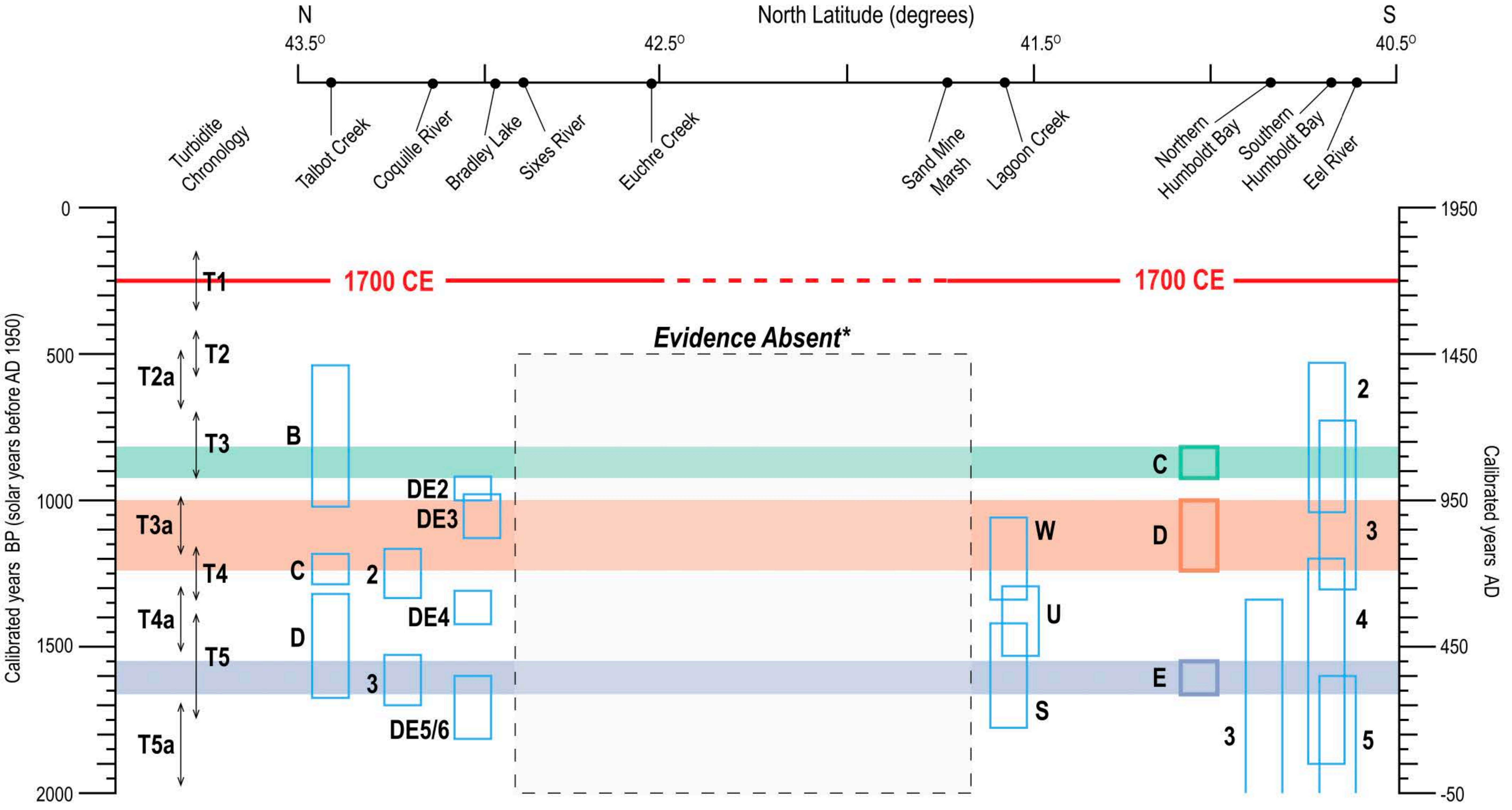
N
North Latitude (degrees)
S
43.5°
42.5°
41.5°
40.5°
Turbidite Chronology
Talbot Creek
Coquille River
Bradley Lake
Sixes River
Euchre Creek
Sand Mine Marsh
Lagoon Creek
Northern Humboldt Bay
Southern Humboldt Bay
Eel River
Calibrated years BP (solar years before AD 1950)
Calibrated years AD
0
500
1000
1500
2000
1950
1450
950
450
-50
1700 CE
1700 CE
Evidence Absent*
T1
T2
T2a
T3
T3a
T4
T4a
T5
T5a
B
C
D
DE2
DE3
DE4
DE5/6
2
3
W
U
S
C
D
E
2
3
4
5
3

GSA Data Repository 2020###

"Timing and amount of southern Cascadia earthquake subsidence over the past 1,700 years at northern Humboldt Bay, California, USA"

Table DR1. This table summarizes criteria used to select the Poisson k parameter. The criteria come from 26 different model runs using different values of k.

k value	Agreement Index (model)	Number of A indices <60%	Mean Confidence Interval (yr)	Standard Deviation	Normalized Age Deviation	Standard Deviation
0.003	70.1	2	89.47	40.09	0.95	1.04
0.005	69.7	3	89.12	39.75	0.76	0.60
0.007	69.9	1	83.88	36.72	0.98	1.03
0.01	71.5	1	83.59	37.01	1.04	1.08
0.02	68.4	2	87.94	40.49	0.99	1.21
0.03	65.6	2	86.18	36.94	1.01	0.95
0.04	65.1	3	85.18	38.26	0.82	0.62
0.05	66.4	2	83.00	39.05	0.95	0.76
0.06	60.6	2	78.00	35.33	1.11	1.10
0.07	59.8	3	66.65	32.26	1.53	1.34
0.08	62.3	3	81.29	39.57	1.22	0.98
0.09	58.3	4	85.88	44.25	1.18	1.24
0.1	56.5	5	87.53	46.50	1.16	1.04
0.2	34.1	5	92.56	44.21	4.35	11.39
0.3	14.2	6	61.06	47.63	3.77	4.69
0.4	6.6	6	55.06	42.38	11.34	19.90
0.5	8.7	6	54.71	42.78	6.19	8.31
0.6	6.1	6	60.94	48.75	8.41	14.84
0.8	8.2	6	55.35	48.56	7.10	9.76
1	5.9	6	59.06	48.26	4.48	6.49
2	4.2	6	79.41	44.14	6.21	10.10
3	3.6	6	56.47	34.85	7.93	11.51
4	1.2	8	56.24	36.50	12.14	17.13
5	1.1	9	55.24	32.31	7.03	12.38
6	0.6	10	51.24	33.82	8.37	8.95
8	0	11	19.47	7.43	20.57	16.90
10	0	11	17.94	5.61	15.46	10.46

Table DR2. This table summarizes the raw OxCal P-sequence output using k = 0.003.

																				Normalized
													Amodel=	70.1						
	UNMODELLED (BP)						MODELLED (BP)						Aoverall=	77.8					Confidence	Age
	from	to	%	µ	σ	m	from	to	%	µ	σ	m	A_{comb}	A	L	P	C		Interval (yr)	Deviation[1]
2014																				
Boundary surface	-63	-64	95.4	-63	0	-63	-63	-64	95.4	-63	0	-63		100			100			
1700 CE							251	250	95.4	250	0	250					100			
R_Date MD.14.06.168.5-169.5	926	798	95.4	860	39	850	934	804	95.5	909	28	920		80.1			80.6		130.00	1.75
EQ2							935	832	95.4	919	18	924					95.5			
R_Date MR.14.02.B.225-226	955	802	95.4	902	40	921	934	915	95.4	924	6	925		161.6			96.3		19.00	3.67
R_Date MD.14.06.C.169.5-170.5	952	803	95.3	913	31	923	934	917	95.4	926	4	926		128.3			93.4		17.00	3.25
R_Date MR.14.05.B.188.5-189.5	959	910	95.4	926	19	927	939	916	95.4	927	5	927		120.9			89.2		23.00	0.20
R_Date MD.14.03.C.212.5-213.5	965	928	95.4	947	11	947	961	921	95.4	937	11	934		70.5			88.3		40.00	0.91
R_Date MR.14.02.A.273-273.5	1058	961	95.4	1008	30	1004	1059	966	95.4	1009	27	1003		98.6			55.6		93.00	0.04
R_Date JC.14.02.D.125.5-126	1072	969	95.4	1025	34	1021	1060	974	95.4	1015	27	1009		99.8			60.6		86.00	0.37
EQ3							1284	967	95.4	1132	116	1132					57.2			
R_Date JC.14.02.D.130-130.5	1278	1181	95.4	1229	29	1233	1284	1184	95.4	1251	28	1263		91.9			71.7		100.00	0.79
R_Date MR.14.05.C.246-247	1281	1182	95.4	1232	31	1240	1285	1185	95.4	1256	27	1266		98.5			76.9		100.00	0.89
R_Date MD.17.13.D.250-251	1302	1190	95.4	1278	20	1283	1298	1188	95.4	1266	24	1272		64.6			87.1		110.00	0.50
R_Date MD.14.05.A.276-277	1401	1326	95.4	1363	18	1363	1395	1320	95.4	1360	18	1361		97.4			100		75.00	0.17
R_Date JC.14.02.C.168.5-169.5	1695	1557	95.4	1618	41	1609	1690	1569	95.4	1629	34	1617		114.6			5		121.00	0.32
R_Date MD.14.05.B1.306.5-307.5	1707	1604	95.4	1654	30	1658	1692	1571	95.4	1632	33	1618		82.2			3.8		121.00	0.67
EQ4							1691	1572	95.4	1632	33	1618					3.5			
R_Date MR.14.02.A.297.5-298	1690	1544	95.4	1594	33	1588	1691	1572	95.4	1633	33	1618		57.4			3.6		119.00	1.18
		Warning! Poor agreement - A= 57.4%(A'c= 60.0%)																		
R_Date JC.14.02.C.170-171.5	1693	1561	95.4	1616	39	1606	1692	1572	95.4	1633	33	1619		106.8			3.6		120.00	0.52
R_Date MD.14.04.B.379.5-380.5	1709	1614	95.4	1659	28	1658	1694	1571	95.4	1636	32	1621		58.5			4.5		123.00	0.72
		Warning! Poor agreement - A= 58.5%(A'c= 60.0%)																		
R_Date MD.14.05.B1.308-309	1695	1565	95.4	1632	40	1622	1695	1571	95.5	1638	33	1621		128			5.4		124.00	0.18
Boundary base of section							1695	1571	95.5	1638	33	1621					5.4			
P_Sequence Northern Humboldt																		Mean=	89.47	0.95
																		StDev=	40.09	1.04

Table DR3. This table summarizes the raw OxCal P-sequence output using k = 0.005.

													Amodel=	69.7						Normalized
	UNMODELLED (BP)						MODELLED (BP)						Aoverall=	78.2					Confidence	Age
	from	to	%	μ	σ	m	from	to	%	μ	σ	m	A_{comb}	A	L	P	C		Interval (yr)	Deviation[1]
2014																				
Boundary surface	-63	-64	95.4	-63	0	-63	-63	-64	95.4	-63	0	-63		100			100			
1700 CE							251	250	95.4	250	0	250					100			
R_Date MD.14.06.168.5-169.5	926	798	95.4	860	39	850	934	805	95.4	908	28	918		87.2			77.2		129.00	1.71
EQ2							935	835	95.4	918	19	923					69.7			
R_Date MR.14.02.B.225-226	955	802	95.4	902	40	921	935	913	95.4	924	11	925		158.1			94		22.00	2.00
R_Date MD.14.06.C.169.5-170.5	952	803	95.3	913	31	923	935	917	95.4	926	7	926		125.3			94.5		18.00	1.86
R_Date MR.14.05.B.188.5-189.5	959	910	95.4	926	19	927	938	916	95.4	928	5	928		122			92		22.00	0.40
R_Date MD.14.03.C.212.5-213.5	965	928	95.4	947	11	947	960	921	95.4	936	10	933		69			92.9		39.00	1.10
R_Date MR.14.02.A.273-273.5	1058	961	95.4	1008	30	1004	1059	969	95.4	1011	26	1005		99			56.9		90.00	0.12
R_Date JC.14.02.D.125.5-126	1072	969	95.4	1025	34	1021	1061	976	95.4	1017	27	1013		100.9			51.7		85.00	0.30
EQ3							1285	971	95.4	1159	108	1198					25.8			
R_Date JC.14.02.D.130-130.5	1278	1181	95.4	1229	29	1233	1283	1185	95.4	1245	30	1258		96.3			73.5		98.00	0.53
R_Date MR.14.05.C.246-247	1281	1182	95.4	1232	31	1240	1284	1186	95.4	1250	30	1263		100.9			77.5		98.00	0.60
R_Date MD.17.13.D.250-251	1302	1190	95.4	1278	20	1283	1297	1187	95.4	1261	29	1271		59.6			71.7		110.00	0.59
		Warning! Poor agreement - A= 59.6%(A'c= 60.0%)																		
R_Date MD.14.05.A.276-277	1401	1326	95.4	1363	18	1363	1396	1321	95.4	1361	18	1361		97.8			99.9		75.00	0.11
R_Date JC.14.02.C.168.5-169.5	1695	1557	95.4	1618	41	1609	1690	1570	95.4	1628	34	1617		114.5			3.6		120.00	0.29
R_Date MD.14.05.B1.306.5-307.5	1707	1604	95.4	1654	30	1658	1692	1571	95.3	1630	33	1618		81			3.1		121.00	0.73
EQ4							1692	1571	95.4	1631	33	1618					3.1			
R_Date MR.14.02.A.297.5-298	1690	1544	95.4	1594	33	1588	1692	1572	95.4	1632	33	1618		58			3.2		120.00	1.15
		Warning! Poor agreement - A= 58.0%(A'c= 60.0%)																		
R_Date JC.14.02.C.170-171.5	1693	1561	95.4	1616	39	1606	1693	1572	95.5	1633	33	1619		106.6			3.1		121.00	0.52
R_Date MD.14.04.B.379.5-380.5	1709	1614	95.4	1659	28	1658	1695	1571	95.4	1636	33	1621		58.4			4.3		124.00	0.70
		Warning! Poor agreement - A= 58.4%(A'c= 60.0%)																		
R_Date MD.14.05.B1.308-309	1695	1565	95.4	1632	40	1622	1695	1572	95.4	1638	33	1621		127.8			5.2		123.00	0.18
Boundary base of section							1695	1572	95.4	1638	33	1621					5.2			
P_Sequence Northern Humboldt																		Mean=	89.12	0.76
																		StDev=	39.75	0.60

Table DR4. This table summarizes the raw OxCal P-sequence output using k = 0.007.

													Amodel=	69.9						Normalized Age Deviation[1]
	UNMODELLED (BP)						MODELLED (BP)						Aoverall=	77.6					Confidence Interval (yr)	
	from	**to**	**%**	**μ**	**σ**	**m**	**from**	**to**	**%**	**μ**	**σ**	**m**	**A_{comb}**	**A**	**L**	**P**	**C**			
2014																				
Boundary surface	-63	-64	95.4	-63	0	-63	-63	-64	95.4	-63	0	-63		100			100			
1700 CE							251	250	95.4	250	0	250					100			
R_Date MD.14.06.168.5-169.5	926	798	95.4	860	39	850	934	829	95.4	911	26	920		82.2			86		105.00	1.96
EQ2							935	851	95.4	919	17	923					88.1			
R_Date MR.14.02.B.225-226	955	802	95.4	902	40	921	934	914	95.4	924	6	925		159.4			92.6		20.00	3.67
R_Date MD.14.06.C.169.5-170.5	952	803	95.3	913	31	923	934	916	95.4	925	4	926		127.4			92.7		18.00	3.00
R_Date MR.14.05.B.188.5-189.5	959	910	95.4	926	19	927	939	916	95.4	927	5	927		119			91.3		23.00	0.20
R_Date MD.14.03.C.212.5-213.5	965	928	95.4	947	11	947	960	922	95.4	937	10	934		74			91.7		38.00	1.00
R_Date MR.14.02.A.273-273.5	1058	961	95.4	1008	30	1004	1057	972	95.4	1011	25	1008		97.3			36.7		85.00	0.12
R_Date JC.14.02.D.125.5-126	1072	969	95.4	1025	34	1021	1060	975	95.4	1016	25	1012		101.7			33.6		85.00	0.36
EQ3							1285	970	95.4	1143	115	1192					12.6			
R_Date JC.14.02.D.130-130.5	1278	1181	95.4	1229	29	1233	1284	1185	95.4	1248	30	1262		93.2			37.2		99.00	0.63
R_Date MR.14.05.C.246-247	1281	1182	95.4	1232	31	1240	1285	1186	95.4	1251	29	1264		101.1			38.5		99.00	0.66
R_Date MD.17.13.D.250-251	1302	1190	95.4	1278	20	1283	1297	1187	95.4	1263	28	1271		61.1			33		110.00	0.54
R_Date MD.14.05.A.276-277	1401	1326	95.4	1363	18	1363	1396	1321	95.4	1361	18	1361		98			99.9		75.00	0.11
R_Date JC.14.02.C.168.5-169.5	1695	1557	95.4	1618	41	1609	1693	1570	95.4	1644	36	1655		108.3			4.6		123.00	0.72
R_Date MD.14.05.B1.306.5-307.5	1707	1604	95.4	1654	30	1658	1694	1572	95.4	1648	35	1670		92.8			3.1		122.00	0.17
EQ4							1694	1573	95.4	1649	35	1673					2.7			
R_Date MR.14.02.A.297.5-298	1690	1544	95.4	1594	33	1588	1694	1574	95.4	1650	35	1674		49			2.5		120.00	1.60
		Warning! Poor agreement - A= 49.0%(A'c= 60.0%)																		
R_Date JC.14.02.C.170-171.5	1693	1561	95.4	1616	39	1606	1694	1575	95.5	1652	34	1674		100.7			2.3		119.00	1.06
R_Date MD.14.04.B.379.5-380.5	1709	1614	95.4	1659	28	1658	1695	1602	95.4	1654	33	1675		63.9			2		93.00	0.15
R_Date MD.14.05.B1.308-309	1695	1565	95.4	1632	40	1622	1695	1603	95.4	1654	33	1675		131.2			2.2		92.00	0.67
Boundary base of section							1695	1603	95.4	1654	33	1675					2.2			
P_Sequence Northern Humboldt																		Mean=	83.88	0.98
																		StDev=	36.72	1.03

Table DR5. This table summarizes the raw OxCal P-sequence output using k = 0.01.

													Amodel=	71.5						Normalized Age Deviation[1]
	UNMODELLED (BP)						MODELLED (BP)						Aoverall=	77.6					Confidence Interval (yr)	
	from	**to**	**%**	**μ**	**σ**	**m**	**from**	**to**	**%**	**μ**	**σ**	**m**	**A_{comb}**	**A**	**L**	**P**	**C**			
2014																				
Boundary surface	-63	-64	95.4	-63	0	-63	-63	-64	95.4	-63	0	-63		100			100			
1700 CE							251	250	95.4	250	0	250					100			
R_Date MD.14.06.168.5-169.5	926	798	95.4	860	39	850	934	834	95.4	912	22	920		78.6			48.6		100.00	2.36
EQ2							935	878	95.4	917	16	922					40.4			
R_Date MR.14.02.B.225-226	955	802	95.4	902	40	921	934	914	95.4	924	6	925		159.6			88.3		20.00	3.67
R_Date MD.14.06.C.169.5-170.5	952	803	95.3	913	31	923	934	917	95.4	926	4	926		127.8			88.6		17.00	3.25
R_Date MR.14.05.B.188.5-189.5	959	910	95.4	926	19	927	939	916	95.4	928	6	927		120.4			88.1		23.00	0.33
R_Date MD.14.03.C.212.5-213.5	965	928	95.4	947	11	947	959	921	95.4	937	10	933		71.7			75.9		38.00	1.00
R_Date MR.14.02.A.273-273.5	1058	961	95.4	1008	30	1004	1056	974	95.4	1012	24	1010		97.6			55.4		82.00	0.17
R_Date JC.14.02.D.125.5-126	1072	969	95.4	1025	34	1021	1059	977	95.4	1017	24	1017		103.5			53.7		82.00	0.33
EQ3							1285	973	95.4	1148	117	1194					19.7			
R_Date JC.14.02.D.130-130.5	1278	1181	95.4	1229	29	1233	1283	1185	95.4	1250	29	1262		93.1			67.4		98.00	0.72
R_Date MR.14.05.C.246-247	1281	1182	95.4	1232	31	1240	1285	1186	95.4	1254	27	1265		100			77		99.00	0.81
R_Date MD.17.13.D.250-251	1302	1190	95.4	1278	20	1283	1298	1187	95.4	1265	26	1272		64.9			81.4		111.00	0.50
R_Date MD.14.05.A.276-277	1401	1326	95.4	1363	18	1363	1397	1321	95.4	1361	18	1361		98			100		76.00	0.11
R_Date JC.14.02.C.168.5-169.5	1695	1557	95.4	1618	41	1609	1693	1569	95.4	1643	37	1631		109			27.6		124.00	0.68
R_Date MD.14.05.B1.306.5-307.5	1707	1604	95.4	1654	30	1658	1694	1571	95.4	1647	36	1668		90.5			27.5		123.00	0.19
EQ4							1694	1572	95.4	1649	35	1672					28.9			
R_Date MR.14.02.A.297.5-298	1690	1544	95.4	1594	33	1588	1694	1573	95.4	1650	35	1674		49.6			28.2		121.00	1.60
		Warning! Poor agreement - A= 49.6%(A'c= 60.0%)																		
R_Date JC.14.02.C.170-171.5	1693	1561	95.4	1616	39	1606	1694	1601	95.4	1652	34	1674		101.1			27.2		93.00	1.06
R_Date MD.14.04.B.379.5-380.5	1709	1614	95.4	1659	28	1658	1695	1574	95.4	1654	33	1675		63.7			30		121.00	0.15
R_Date MD.14.05.B1.308-309	1695	1565	95.4	1632	40	1622	1696	1603	95.4	1655	33	1676		130.6			29.3		93.00	0.70
Boundary base of section							1696	1603	95.4	1655	33	1676					29.3			
P_Sequence Northern Humboldt																		Mean=	83.59	1.04
																		StDev=	37.01	1.08

Table DR6. This table summarizes the raw OxCal P-sequence output using k = 0.02.

													Amodel=	68.4						Normalized Age
	UNMODELLED (BP)						MODELLED (BP)						Aoverall=	76.9					Confidence	Deviation[1]
	from	**to**	**%**	**μ**	**σ**	**m**	**from**	**to**	**%**	**μ**	**σ**	**m**	**A_{comb}**	**A**	**L**	**P**	**C**		Interval (yr)	
2014																				
Boundary surface	-63	-64	95.4	-63	0	-63	-63	-64	95.4	-63	0	-63		100			100			
1700 CE							251	250	95.4	250	0	250					100			
R_Date MD.14.06.168.5-169.5	926	798	95.4	860	39	850	934	805	95.4	907	30	919		83.2			69.3		129.00	1.57
EQ2							935	824	95.4	917	22	923					63.2			
R_Date MR.14.02.B.225-226	955	802	95.4	902	40	921	935	916	95.4	925	5	926		160.6			85.9		19.00	4.60
R_Date MD.14.06.C.169.5-170.5	952	803	95.3	913	31	923	934	917	95.4	926	4	926		126.8			87		17.00	3.25
R_Date MR.14.05.B.188.5-189.5	959	910	95.4	926	19	927	937	917	95.4	927	5	927		124.3			91.6		20.00	0.20
R_Date MD.14.03.C.212.5-213.5	965	928	95.4	947	11	947	957	921	95.4	935	9	932		64.2			50.2		36.00	1.33
R_Date MR.14.02.A.273-273.5	1058	961	95.4	1008	30	1004	1060	976	95.4	1019	25	1022		96.6			23.3		84.00	0.44
R_Date JC.14.02.D.125.5-126	1072	969	95.4	1025	34	1021	1060	980	95.4	1023	26	1026		102.5			21.5		80.00	0.08
EQ3							1284	976	95.4	1160	104	1196					40.5			
R_Date JC.14.02.D.130-130.5	1278	1181	95.4	1229	29	1233	1282	1184	95.4	1241	32	1255		98.4			24.5		98.00	0.38
R_Date MR.14.05.C.246-247	1281	1182	95.4	1232	31	1240	1284	1185	95.4	1246	32	1262		103			19.9		99.00	0.44
R_Date MD.17.13.D.250-251	1302	1190	95.4	1278	20	1283	1297	1186	95.4	1257	33	1270		57.9			16.8		111.00	0.64
		Warning! Poor agreement - A= 57.9%(A'c= 60.0%)																		
R_Date MD.14.05.A.276-277	1401	1326	95.4	1363	18	1363	1399	1322	95.4	1362	18	1362		98.8			99.9		77.00	0.06
R_Date JC.14.02.C.168.5-169.5	1695	1557	95.4	1618	41	1609	1692	1570	95.4	1636	36	1619		110.8			16.1		122.00	0.50
R_Date MD.14.05.B1.306.5-307.5	1707	1604	95.4	1654	30	1658	1694	1572	95.4	1641	34	1621		88.6			14.5		122.00	0.38
EQ4							1694	1572	95.4	1641	34	1622					12.5			
R_Date MR.14.02.A.297.5-298	1690	1544	95.4	1594	33	1588	1693	1574	95.3	1642	34	1622		52			12.2		119.00	1.41
		Warning! Poor agreement - A= 52.0%(A'c= 60.0%)																		
R_Date JC.14.02.C.170-171.5	1693	1561	95.4	1616	39	1606	1694	1574	95.4	1644	34	1623		102.3			12		120.00	0.82
R_Date MD.14.04.B.379.5-380.5	1709	1614	95.4	1659	28	1658	1695	1574	95.4	1647	34	1627		62.3			12.2		121.00	0.35
R_Date MD.14.05.B1.308-309	1695	1565	95.4	1632	40	1622	1695	1574	95.3	1648	34	1632		129.6			13		121.00	0.47
Boundary base of section							1695	1574	95.3	1648	34	1632					13			
P_Sequence Northern Humboldt																		Mean=	87.94	0.99
																		StDev=	40.49	1.21

Table DR7. This table summarizes the raw OxCal P-sequence output using k = 0.03.

													Amodel=	65.6						Normalized
	UNMODELLED (BP)						MODELLED (BP)						Aoverall=	75.8					Confidence	Age
	from	**to**	**%**	**μ**	**σ**	**m**	**from**	**to**	**%**	**μ**	**σ**	**m**	$\mathbf{A_{comb}}$	**A**	**L**	**P**	**C**		Interval (yr)	Deviation[1]
2014																				
Boundary surface	-63	-64	95.4	-63	0	-63	-63	-64	95.4	-63	0	-63		100			100			
1700 CE							251	250	95.4	250	0	250					100			
R_Date MD.14.06.168.5-169.5	926	798	95.4	860	39	850	933	835	95.4	908	25	918		86.4			12.8		98.00	1.92
EQ2							935	853	95.4	915	19	921					14.2			
R_Date MR.14.02.B.225-226	955	802	95.4	902	40	921	935	913	95.4	924	7	925		158.8			86.9		22.00	3.14
R_Date MD.14.06.C.169.5-170.5	952	803	95.3	913	31	923	935	916	95.4	926	4	926		126.5			78.5		19.00	3.25
R_Date MR.14.05.B.188.5-189.5	959	910	95.4	926	19	927	953	916	95.4	929	6	928		116.4			66.3		37.00	0.50
R_Date MD.14.03.C.212.5-213.5	965	928	95.4	947	11	947	956	922	95.4	935	9	932		70.9			79.7		34.00	1.33
R_Date MR.14.02.A.273-273.5	1058	961	95.4	1008	30	1004	1060	982	95.4	1028	23	1034		96			62.9		78.00	0.87
R_Date JC.14.02.D.125.5-126	1072	969	95.4	1025	34	1021	1062	986	95.4	1031	23	1037		102.1			62.4		76.00	0.26
EQ3							1285	980	95.4	1172	102	1206					48.1			
R_Date JC.14.02.D.130-130.5	1278	1181	95.4	1229	29	1233	1283	1185	95.4	1247	30	1261		94.5			77.4		98.00	0.60
R_Date MR.14.05.C.246-247	1281	1182	95.4	1232	31	1240	1285	1186	95.4	1250	30	1264		102.1			81.1		99.00	0.60
R_Date MD.17.13.D.250-251	1302	1190	95.4	1278	20	1283	1295	1187	95.4	1259	30	1269		54.5			79.7		108.00	0.63
		Warning! Poor agreement - A= 54.5%(A'c= 60.0%)																		
R_Date MD.14.05.A.276-277	1401	1326	95.4	1363	18	1363	1400	1324	95.4	1362	18	1363		99.4			99.9		76.00	0.06
R_Date JC.14.02.C.168.5-169.5	1695	1557	95.4	1618	41	1609	1691	1570	95.4	1638	37	1621		110.2			7.4		121.00	0.54
R_Date MD.14.05.B1.306.5-307.5	1707	1604	95.4	1654	30	1658	1693	1571	95.4	1643	36	1623		88.3			6.2		122.00	0.31
EQ4							1694	1571	95.4	1644	36	1624					6.5			
R_Date MR.14.02.A.297.5-298	1690	1544	95.4	1594	33	1588	1693	1574	95.4	1645	35	1625		52.6			7.3		119.00	1.46
		Warning! Poor agreement - A= 52.6%(A'c= 60.0%)																		
R_Date JC.14.02.C.170-171.5	1693	1561	95.4	1616	39	1606	1694	1575	95.3	1647	34	1630		101.9			7.7		119.00	0.91
R_Date MD.14.04.B.379.5-380.5	1709	1614	95.4	1659	28	1658	1694	1575	95.4	1648	34	1663		62.1			8.7		119.00	0.32
R_Date MD.14.05.B1.308-309	1695	1565	95.4	1632	40	1622	1695	1575	95.4	1650	33	1669		129.8			10.6		120.00	0.55
Boundary base of section							1695	1575	95.4	1650	33	1669					10.6			
P_Sequence Northern Humboldt																		Mean=	86.18	1.01
																		StDev=	36.94	0.95

Table DR8. This table summarizes the raw OxCal P-sequence output using k = 0.04.

													Amodel=	65.1						Normalized
	UNMODELLED (BP)						MODELLED (BP)						Aoverall=	74.6					Confidence	Age
	from	to	%	μ	σ	m	from	to	%	μ	σ	m	A_{comb}	A	L	P	C		Interval (yr)	Deviation[1]
2014																				
Boundary surface	-63	-64	95.4	-63	0	-63	-63	-64	95.4	-63	0	-63		100			100			
1700 CE							251	250	95.4	250	0	250		100			100			
R_Date MD.14.06.168.5-169.5	926	798	95.4	860	39	850	934	828	95.4	909	28	919		84			67.9		106.00	1.75
EQ2							935	836	95.4	915	22	923					72.3			
R_Date MR.14.02.B.225-226	955	802	95.4	902	40	921	935	912	95.4	923	11	925		157.3			90.2		23.00	1.91
R_Date MD.14.06.C.169.5-170.5	952	803	95.3	913	31	923	935	916	95.4	925	7	926		125			92		19.00	1.71
R_Date MR.14.05.B.188.5-189.5	959	910	95.4	926	19	927	939	917	95.4	928	5	928		120.2			86.8		22.00	0.40
R_Date MD.14.03.C.212.5-213.5	965	928	95.4	947	11	947	955	921	95.4	934	8	932		65.8			90.8		34.00	1.63
R_Date MR.14.02.A.273-273.5	1058	961	95.4	1008	30	1004	1060	985	95.4	1029	22	1034		92.3			17.9		75.00	0.95
R_Date JC.14.02.D.125.5-126	1072	969	95.4	1025	34	1021	1063	988	95.4	1031	22	1036		104.6			16		75.00	0.27
EQ3							1284	979	95.4	1131	104	1094					8.9			
R_Date JC.14.02.D.130-130.5	1278	1181	95.4	1229	29	1233	1282	1184	95.4	1244	32	1260		95.2			47.4		98.00	0.47
R_Date MR.14.05.C.246-247	1281	1182	95.4	1232	31	1240	1284	1185	95.4	1249	31	1264		102.1			48.6		99.00	0.55
R_Date MD.17.13.D.250-251	1302	1190	95.4	1278	20	1283	1295	1186	95.4	1259	30	1270		55.3			68.5		109.00	0.63
		Warning! Poor agreement - A= 55.3%(A'c= 60.0%)																		
R_Date MD.14.05.A.276-277	1401	1326	95.4	1363	18	1363	1400	1326	95.4	1363	18	1363		99.8			99.9		74.00	0.00
R_Date JC.14.02.C.168.5-169.5	1695	1557	95.4	1618	41	1609	1689	1570	95.4	1623	31	1615		116.2			2.8		119.00	0.16
R_Date MD.14.05.B1.306.5-307.5	1707	1604	95.4	1654	30	1658	1690	1572	95.4	1627	30	1617		79.5			2.1		118.00	0.90
EQ4							1690	1573	95.4	1628	30	1617					2			
R_Date MR.14.02.A.297.5-298	1690	1544	95.4	1594	33	1588	1691	1574	95.4	1629	30	1617		58.2			2		117.00	1.17
		Warning! Poor agreement - A= 58.2%(A'c= 60.0%)																		
R_Date JC.14.02.C.170-171.5	1693	1561	95.4	1616	39	1606	1692	1574	95.4	1631	30	1618		106.8			2		118.00	0.50
R_Date MD.14.04.B.379.5-380.5	1709	1614	95.4	1659	28	1658	1694	1573	95.4	1633	30	1619		57.7			2.5		121.00	0.87
		Warning! Poor agreement - A= 57.7%(A'c= 60.0%)																		
R_Date MD.14.05.B1.308-309	1695	1565	95.4	1632	40	1622	1695	1574	95.4	1634	30	1620		128.6			3.1		121.00	0.07
Boundary base of section							1695	1574	95.4	1634	30	1620					3.1			
P_Sequence Northern Humboldt																		Mean=	85.18	0.82
																		StDev=	38.26	0.62

Table DR9. This table summarizes the raw OxCal P-sequence output using k = 0.05.

													Amodel=	66.4						Normalized
	UNMODELLED (BP)						MODELLED (BP)						Aoverall=	75.2					Confidence	Age
	from	**to**	**%**	**μ**	**σ**	**m**	**from**	**to**	**%**	**μ**	**σ**	**m**	**A_{comb}**	**A**	**L**	**P**	**C**		Interval (yr)	Deviation[1]
2014																				
Boundary surface	-63	-64	95.4	-63	0	-63	-63	-64	95.4	-63	0	-63		100			100			
1700 CE							251	250	95.4	250	0	250					100			
R_Date MD.14.06.168.5-169.5	926	798	95.4	860	39	850	934	804	95.4	906	30	918		88.9			90.9		130.00	1.53
EQ2							935	828	95.4	916	22	923					87.3			
R_Date MR.14.02.B.225-226	955	802	95.4	902	40	921	935	915	95.4	924	9	925		159.2			91.4		20.00	2.44
R_Date MD.14.06.C.169.5-170.5	952	803	95.3	913	31	923	934	917	95.4	926	5	926		126.1			93.7		17.00	2.60
R_Date MR.14.05.B.188.5-189.5	959	910	95.4	926	19	927	936	918	95.4	928	4	928		123.6			92.6		18.00	0.50
R_Date MD.14.03.C.212.5-213.5	965	928	95.4	947	11	947	954	921	95.4	934	8	932		64.1			94.8		33.00	1.63
R_Date MR.14.02.A.273-273.5	1058	961	95.4	1008	30	1004	1061	987	95.4	1033	20	1039		97.6			79.4		74.00	1.25
R_Date JC.14.02.D.125.5-126	1072	969	95.4	1025	34	1021	1063	988	95.4	1035	21	1041		101			76.3		75.00	0.48
EQ3							1284	984	95.4	1150	101	1187					52.6			
R_Date JC.14.02.D.130-130.5	1278	1181	95.4	1229	29	1233	1282	1184	95.4	1243	32	1259		97.3			72.3		98.00	0.44
R_Date MR.14.05.C.246-247	1281	1182	95.4	1232	31	1240	1284	1185	95.4	1247	32	1263		104.4			72		99.00	0.47
R_Date MD.17.13.D.250-251	1302	1190	95.4	1278	20	1283	1295	1186	95.4	1254	33	1268		51.4			67.4		109.00	0.73
		Warning! Poor agreement - A= 51.4%(A'c= 60.0%)																		
R_Date MD.14.05.A.276-277	1401	1326	95.4	1363	18	1363	1400	1329	95.4	1363	17	1364		100.3			99.9		71.00	0.00
R_Date JC.14.02.C.168.5-169.5	1695	1557	95.4	1618	41	1609	1691	1570	95.4	1637	37	1620		109.2			18.5		121.00	0.51
R_Date MD.14.05.B1.306.5-307.5	1707	1604	95.4	1654	30	1658	1693	1573	95.4	1644	34	1625		91			14.1		120.00	0.29
EQ4							1694	1573	95.4	1645	34	1626					14.4			
R_Date MR.14.02.A.297.5-298	1690	1544	95.4	1594	33	1588	1694	1574	95.4	1646	34	1627		49.9			14.7		120.00	1.53
		Warning! Poor agreement - A= 49.9%(A'c= 60.0%)																		
R_Date JC.14.02.C.170-171.5	1693	1561	95.4	1616	39	1606	1694	1575	95.4	1647	34	1631		101.3			14.6		119.00	0.91
R_Date MD.14.04.B.379.5-380.5	1709	1614	95.4	1659	28	1658	1695	1601	95.4	1649	33	1664		62.7			15.3		94.00	0.30
R_Date MD.14.05.B1.308-309	1695	1565	95.4	1632	40	1622	1695	1602	95.4	1650	33	1670		130			17.3		93.00	0.55
Boundary base of section							1695	1602	95.4	1650	33	1670					17.3			
P_Sequence Northern Humboldt																		Mean=	83.00	0.95
																		StDev=	39.05	0.76

Table DR10. This table summarizes the raw OxCal P-sequence output using k = 0.06.

													Amodel=	60.6						Normalized
	UNMODELLED (BP)						MODELLED (BP)						Aoverall=	70.7					Confidence	Age
	from	to	%	μ	σ	m	from	to	%	μ	σ	m	A_{comb}	A	L	P	C		Interval (yr)	Deviation[1]
2014																				
Boundary surface	-63	-64	95.4	-63	0	-63	-63	-64	95.4	-63	0	-63		100			100			
1700 CE							251	250	95.4	250	0	250					100			
R_Date MD.14.06.168.5-169.5	926	798	95.4	860	39	850	934	828	95.4	909	27	919		84			92.8		106.00	1.81
EQ2							935	840	95.4	919	17	924					49.2			
R_Date MR.14.02.B.225-226	955	802	95.4	902	40	921	935	915	95.4	925	6	926		159.3			67.9		20.00	3.83
R_Date MD.14.06.C.169.5-170.5	952	803	95.3	913	31	923	935	917	95.4	926	4	927		124.9			75.1		18.00	3.25
R_Date MR.14.05.B.188.5-189.5	959	910	95.4	926	19	927	936	918	95.4	928	4	928		125.5			89.8		18.00	0.50
R_Date MD.14.03.C.212.5-213.5	965	928	95.4	947	11	947	954	921	95.4	933	8	931		60.1			85.7		33.00	1.75
R_Date MR.14.02.A.273-273.5	1058	961	95.4	1008	30	1004	1064	988	95.4	1039	17	1043		95			68.9		76.00	1.82
R_Date JC.14.02.D.125.5-126	1072	969	95.4	1025	34	1021	1065	1000	95.4	1041	18	1045		100.9			68.1		65.00	0.89
EQ3							1281	1002	95.5	1135	91	1142					34.9			
R_Date JC.14.02.D.130-130.5	1278	1181	95.4	1229	29	1233	1280	1182	95.4	1228	34	1234		105			28.4		98.00	0.03
R_Date MR.14.05.C.246-247	1281	1182	95.4	1232	31	1240	1282	1185	95.4	1232	35	1242		110.9			30.2		97.00	0.00
R_Date MD.17.13.D.250-251	1302	1190	95.4	1278	20	1283	1293	1185	95.4	1239	38	1259		38.8			29.8		108.00	1.03
		Warning! Poor agreement - A= 38.8%(A'c= 60.0%)																		
R_Date MD.14.05.A.276-277	1401	1326	95.4	1363	18	1363	1400	1330	95.4	1364	17	1364		100.4			99.8		70.00	0.06
R_Date JC.14.02.C.168.5-169.5	1695	1557	95.4	1618	41	1609	1690	1567	95.4	1629	35	1616		111.7			9.8		123.00	0.31
R_Date MD.14.05.B1.306.5-307.5	1707	1604	95.4	1654	30	1658	1693	1574	95.4	1637	33	1620		86.4			2.8		119.00	0.52
EQ4							1693	1575	95.4	1638	32	1620					2.8			
R_Date MR.14.02.A.297.5-298	1690	1544	95.4	1594	33	1588	1693	1599	95.4	1639	33	1621		52.9			0.4		94.00	1.36
		Warning! Poor agreement - A= 52.9%(A'c= 60.0%)																		
R_Date JC.14.02.C.170-171.5	1693	1561	95.4	1616	39	1606	1694	1600	95.4	1640	33	1621		104.1			0.4		94.00	0.73
R_Date MD.14.04.B.379.5-380.5	1709	1614	95.4	1659	28	1658	1694	1601	95.4	1642	32	1622		60.7			0.5		93.00	0.53
R_Date MD.14.05.B1.308-309	1695	1565	95.4	1632	40	1622	1695	1601	95.4	1644	32	1624		129.8			0.8		94.00	0.38
Boundary base of section							1695	1601	95.4	1644	32	1624					0.8			
P_Sequence Northern Humboldt																		Mean=	78.00	1.11
																		StDev=	35.33	1.10

Table DR11. This table summarizes the raw OxCal P-sequence output using k = 0.07.

													Amodel=	59.8						Normalized
	UNMODELLED (BP)						MODELLED (BP)						Aoverall=	69.9					Confidence	Age
	from	to	%	μ	σ	m	from	to	%	μ	σ	m	A_{comb}	A	L	P	C		Interval (yr)	Deviation[1]
2014																				
Boundary surface	-63	-64	95.4	-63	0	-63	-63	-64	95.4	-63	0	-63		100			100			
1700 CE							251	250	95.4	250	0	250					100			
R_Date MD.14.06.168.5-169.5	926	798	95.4	860	39	850	934	829	95.4	908	27	918		86.9			92.7		105.00	1.78
EQ2							935	839	95.4	919	18	923					82.9			
R_Date MR.14.02.B.225-226	955	802	95.4	902	40	921	935	915	95.4	925	6	926		157.9			91.9		20.00	3.83
R_Date MD.14.06.C.169.5-170.5	952	803	95.3	913	31	923	935	918	95.4	927	4	927		123.1			92.7		17.00	3.50
R_Date MR.14.05.B.188.5-189.5	959	910	95.4	926	19	927	936	919	95.4	928	4	928		126.9			96.1		17.00	0.50
R_Date MD.14.03.C.212.5-213.5	965	928	95.4	947	11	947	951	921	95.4	932	7	931		54.5			95		30.00	2.14
		Warning! Poor agreement - A= 54.5%(A'c= 60.0%)																		
R_Date MR.14.02.A.273-273.5	1058	961	95.4	1008	30	1004	1063	995	95.4	1037	19	1043		95.5			65.6		68.00	1.53
R_Date JC.14.02.D.125.5-126	1072	969	95.4	1025	34	1021	1065	985	95.4	1039	20	1044		100.5			66.2		80.00	0.70
EQ3							1283	996	95.3	1150	95	1187					62.1			
R_Date JC.14.02.D.130-130.5	1278	1181	95.4	1229	29	1233	1281	1183	95.4	1235	35	1252		100.8			60.1		98.00	0.17
R_Date MR.14.05.C.246-247	1281	1182	95.4	1232	31	1240	1283	1185	95.4	1239	35	1259		109.5			55		98.00	0.20
R_Date MD.17.13.D.250-251	1302	1190	95.4	1278	20	1283	1294	1185	95.4	1244	37	1265		42.4			52.4		109.00	0.92
		Warning! Poor agreement - A= 42.4%(A'c= 60.0%)																		
R_Date MD.14.05.A.276-277	1401	1326	95.4	1363	18	1363	1401	1330	95.4	1364	17	1365		100.6			99.9		71.00	0.06
R_Date JC.14.02.C.168.5-169.5	1695	1557	95.4	1618	41	1609	1625	1570	95.4	1607	14	1612		121.7			97.5		55.00	0.79
R_Date MD.14.05.B1.306.5-307.5	1707	1604	95.4	1654	30	1658	1629	1573	95.4	1612	11	1615		71.2			98.5		56.00	3.82
EQ4							1629	1573	95.4	1613	10	1615					98.6			
R_Date MR.14.02.A.297.5-298	1690	1544	95.4	1594	33	1588	1629	1574	95.4	1613	10	1616		64.1			98.6		55.00	1.90
R_Date JC.14.02.C.170-171.5	1693	1561	95.4	1616	39	1606	1630	1573	95.4	1614	10	1616		111.2			98.5		57.00	0.20
R_Date MD.14.04.B.379.5-380.5	1709	1614	95.4	1659	28	1658	1658	1571	95.4	1617	13	1617		53.7			98.5		87.00	3.23
		Warning! Poor agreement - A= 53.7%(A'c= 60.0%)																		
R_Date MD.14.05.B1.308-309	1695	1565	95.4	1632	40	1622	1682	1572	95.5	1619	16	1618		125			98.1		110.00	0.81
Boundary base of section							1682	1572	95.5	1619	16	1618					98.1			
P_Sequence Northern Humboldt																		Mean=	66.65	1.53
																		StDev=	32.26	1.34

Table DR12. This table summarizes the raw OxCal P-sequence output using k = 0.08.

													Amodel=	62.3						Normalized
	UNMODELLED (BP)						MODELLED (BP)						Aoverall=	71.9					Confidence	Age
	from	**to**	**%**	**μ**	**σ**	**m**	**from**	**to**	**%**	**μ**	**σ**	**m**	**A_{comb}**	**A**	**L**	**P**	**C**		Interval (yr)	Deviation[1]
2014																				
Boundary surface	-63	-64	95.4	-63	0	-63	-63	-64	95.4	-63	0	-63		100			100			
1700 CE							251	250	95.4	250	0	250					100			
R_Date MD.14.06.168.5-169.5	926	798	95.4	860	39	850	934	829	95.4	906	30	919		85.6			53.2		105.00	1.53
EQ2							935	832	95.4	916	23	924					47			
R_Date MR.14.02.B.225-226	955	802	95.4	902	40	921	935	916	95.4	925	9	926		160.4			95.4		19.00	2.56
R_Date MD.14.06.C.169.5-170.5	952	803	95.3	913	31	923	935	918	95.4	926	4	926		126.8			94.9		17.00	3.25
R_Date MR.14.05.B.188.5-189.5	959	910	95.4	926	19	927	935	918	95.4	927	4	928		127.1			90.9		17.00	0.25
R_Date MD.14.03.C.212.5-213.5	965	928	95.4	947	11	947	952	921	95.4	932	7	931		58.3			94.4		31.00	2.14
		Warning! Poor agreement - A= 58.3%(A'c= 60.0%)																		
R_Date MR.14.02.A.273-273.5	1058	961	95.4	1008	30	1004	1063	1005	95.4	1042	16	1045		94.8			92.2		58.00	2.13
R_Date JC.14.02.D.125.5-126	1072	969	95.4	1025	34	1021	1065	1004	95.4	1043	16	1047		100.7			92.3		61.00	1.13
EQ3							1283	1001	95.4	1141	95	1137					73.6			
R_Date JC.14.02.D.130-130.5	1278	1181	95.4	1229	29	1233	1282	1183	95.4	1238	34	1253		99.3			61		99.00	0.26
R_Date MR.14.05.C.246-247	1281	1182	95.4	1232	31	1240	1284	1185	95.4	1241	34	1259		106.5			59.8		99.00	0.26
R_Date MD.17.13.D.250-251	1302	1190	95.4	1278	20	1283	1293	1186	95.4	1248	36	1266		44.7			62.2		107.00	0.83
		Warning! Poor agreement - A= 44.7%(A'c= 60.0%)																		
R_Date MD.14.05.A.276-277	1401	1326	95.4	1363	18	1363	1401	1331	95.4	1365	17	1365		100.8			99.9		70.00	0.12
R_Date JC.14.02.C.168.5-169.5	1695	1557	95.4	1618	41	1609	1685	1567	95.4	1611	21	1612		119.7			81.6		118.00	0.33
R_Date MD.14.05.B1.306.5-307.5	1707	1604	95.4	1654	30	1658	1688	1572	95.5	1617	19	1615		74.9			82.8		116.00	1.95
EQ4							1688	1574	95.4	1618	19	1616					80.9			
R_Date MR.14.02.A.297.5-298	1690	1544	95.4	1594	33	1588	1689	1574	95.5	1619	19	1616		61.3			79.5		115.00	1.32
R_Date JC.14.02.C.170-171.5	1693	1561	95.4	1616	39	1606	1689	1574	95.4	1620	19	1617		109.2			79.8		115.00	0.21
R_Date MD.14.04.B.379.5-380.5	1709	1614	95.4	1659	28	1658	1690	1573	95.5	1621	19	1618		55.1			78.5		117.00	2.00
		Warning! Poor agreement - A= 55.1%(A'c= 60.0%)																		
R_Date MD.14.05.B1.308-309	1695	1565	95.4	1632	40	1622	1692	1574	95.4	1623	21	1619		127.2			77.7		118.00	0.43
Boundary base of section							1692	1574	95.4	1623	21	1619					77.7			
P_Sequence Northern Humboldt																		Mean=	81.29	1.22
																		StDev=	39.57	0.98

Table DR13. This table summarizes the raw OxCal P-sequence output using k = 0.09.

																				Normalized
													Amodel=	58.3						
	UNMODELLED (BP)						MODELLED (BP)						Aoverall=	67.7					Confidence	Age
	from	**to**	**%**	**μ**	**σ**	**m**	**from**	**to**	**%**	**μ**	**σ**	**m**	**A_{comb}**	**A**	**L**	**P**	**C**		Interval (yr)	Deviation[1]
2014																				
Boundary surface	-63	-64	95.4	-63	0	-63	-63	-64	95.4	-63	0	-63		100			100			
1700 CE							251	250	95.4	250	0	250					100			
R_Date MD.14.06.168.5-169.5	926	798	95.4	860	39	850	934	830	95.4	910	25	919		84.8			76.2		104.00	2.00
EQ2							935	862	95.4	919	16	923					87.8			
R_Date MR.14.02.B.225-226	955	802	95.4	902	40	921	934	916	95.4	925	5	926		160.4			93.7		18.00	4.60
R_Date MD.14.06.C.169.5-170.5	952	803	95.3	913	31	923	935	918	95.4	926	4	927		125.3			93.6		17.00	3.25
R_Date MR.14.05.B.188.5-189.5	959	910	95.4	926	19	927	935	918	95.4	928	4	928		126.4			88.1		17.00	0.50
R_Date MD.14.03.C.212.5-213.5	965	928	95.4	947	11	947	951	921	95.4	932	7	931		57.3			80.2		30.00	2.14
		Warning! Poor agreement - A= 57.3%(A'c= 60.0%)																		
R_Date MR.14.02.A.273-273.5	1058	961	95.4	1008	30	1004	1063	1000	95.4	1044	24	1045		95.6			35.3		63.00	1.50
R_Date JC.14.02.D.125.5-126	1072	969	95.4	1025	34	1021	1170	998	95.4	1046	25	1046		97.1			33.8		172.00	0.84
EQ3							1283	999	95.3	1137	89	1152					32.9			
R_Date JC.14.02.D.130-130.5	1278	1181	95.4	1229	29	1233	1281	1182	95.4	1225	34	1203		105.4			25.6		99.00	0.12
R_Date MR.14.05.C.246-247	1281	1182	95.4	1232	31	1240	1282	1185	95.4	1228	35	1206		113.4			23.4		97.00	0.11
R_Date MD.17.13.D.250-251	1302	1190	95.4	1278	20	1283	1291	1185	95.4	1233	38	1242		33.4			22.5		106.00	1.18
		Warning! Poor agreement - A= 33.4%(A'c= 60.0%)																		
R_Date MD.14.05.A.276-277	1401	1326	95.4	1363	18	1363	1401	1331	95.4	1365	17	1365		100.8			99.7		70.00	0.12
R_Date JC.14.02.C.168.5-169.5	1695	1557	95.4	1618	41	1609	1689	1566	95.4	1620	31	1614		115.4			78.7		123.00	0.06
R_Date MD.14.05.B1.306.5-307.5	1707	1604	95.4	1654	30	1658	1691	1572	95.4	1627	29	1617		80.7			75.3		119.00	0.93
EQ4							1691	1573	95.4	1628	29	1617					75.2			
R_Date MR.14.02.A.297.5-298	1690	1544	95.4	1594	33	1588	1691	1598	95.4	1629	29	1618		56.9			73.7		93.00	1.21
		Warning! Poor agreement - A= 56.9%(A'c= 60.0%)																		
R_Date JC.14.02.C.170-171.5	1693	1561	95.4	1616	39	1606	1692	1600	95.4	1631	29	1618		106.6			74.5		92.00	0.52
R_Date MD.14.04.B.379.5-380.5	1709	1614	95.4	1659	28	1658	1694	1574	95.3	1632	29	1619		57.4			75.4		120.00	0.93
		Warning! Poor agreement - A= 57.4%(A'c= 60.0%)																		
R_Date MD.14.05.B1.308-309	1695	1565	95.4	1632	40	1622	1695	1575	95.4	1634	30	1620		127.8			74.1		120.00	0.07
Boundary base of section							1695	1575	95.4	1634	30	1620					74.1			
P_Sequence Northern Humboldt																		Mean=	85.88	1.18
																		StDev=	44.25	1.24

Table DR14. This table summarizes the raw OxCal P-sequence output using k = 0.1.

																				Normalized
													Amodel=	56.5						
	UNMODELLED (BP)						MODELLED (BP)						Aoverall=	64.9					Confidence	Age
	from	**to**	**%**	**μ**	**σ**	**m**	**from**	**to**	**%**	**μ**	**σ**	**m**	A_{comb}	**A**	**L**	**P**	**C**		Interval (yr)	Deviation[1]
Boundary surface	-63	-64	95.4	-63	0	-63	-63	-64	95.4	-63	0	-63		100			100			
1700 CE							251	250	95.4	250	0	250					100			
R_Date MD.14.06.168.5-169.5	926	798	95.4	860	39	850	934	822	95.4	905	30	917		88.6			85.4		112.00	1.50
EQ2							935	825	95.4	914	24	923					89			
R_Date MR.14.02.B.225-226	955	802	95.4	902	40	921	935	916	95.4	925	7	926		159			98.8		19.00	3.29
R_Date MD.14.06.C.169.5-170.5	952	803	95.3	913	31	923	935	918	95.4	927	4	927		124			96.9		17.00	3.50
R_Date MR.14.05.B.188.5-189.5	959	910	95.4	926	19	927	935	920	95.4	928	4	928		127.5			98.1		15.00	0.50
R_Date MD.14.03.C.212.5-213.5	965	928	95.4	947	11	947	949	921	95.4	932	6	931		54.7			97.4		28.00	2.50
		Warning! Poor agreement - A= 54.7%(A'c= 60.0%)																		
R_Date MR.14.02.A.273-273.5	1058	961	95.4	1008	30	1004	1167	1000	95.4	1045	25	1045		93			66.1		167.00	1.48
R_Date JC.14.02.D.125.5-126	1072	969	95.4	1025	34	1021	1169	999	95.4	1047	25	1047		97.3			60.6		170.00	0.88
EQ3							1280	1003	95.4	1139	85	1165					60.4			
R_Date JC.14.02.D.130-130.5	1278	1181	95.4	1229	29	1233	1280	1182	95.4	1218	33	1199		109			45.5		98.00	0.33
R_Date MR.14.05.C.246-247	1281	1182	95.4	1232	31	1240	1281	1184	95.4	1220	34	1199		117.3			48.7		97.00	0.35
R_Date MD.17.13.D.250-251	1302	1190	95.4	1278	20	1283	1291	1183	95.3	1224	37	1200		27.8			46.3		108.00	1.46
		Warning! Poor agreement - A= 27.8%(A'c= 60.0%)																		
R_Date MD.14.05.A.276-277	1401	1326	95.4	1363	18	1363	1401	1331	95.4	1365	17	1365		100.8			99.6		70.00	0.12
R_Date JC.14.02.C.168.5-169.5	1695	1557	95.4	1618	41	1609	1690	1567	95.4	1626	34	1615		111.2			35		123.00	0.24
R_Date MD.14.05.B1.306.5-307.5	1707	1604	95.4	1654	30	1658	1693	1592	95.4	1635	31	1619		86.2			27.3		101.00	0.61
EQ4							1693	1595	95.4	1637	32	1620					29.2			
R_Date MR.14.02.A.297.5-298	1690	1544	95.4	1594	33	1588	1692	1601	95.4	1638	32	1620		52.2			30.3		91.00	1.38
		Warning! Poor agreement - A= 52.2%(A'c= 60.0%)																		
R_Date JC.14.02.C.170-171.5	1693	1561	95.4	1616	39	1606	1692	1602	95.4	1639	32	1621		103.1			30.1		90.00	0.72
R_Date MD.14.04.B.379.5-380.5	1709	1614	95.4	1659	28	1658	1693	1603	95.4	1640	31	1621		60.8			30.2		90.00	0.61
R_Date MD.14.05.B1.308-309	1695	1565	95.4	1632	40	1622	1695	1603	95.4	1642	32	1622		129.2			32		92.00	0.31
Boundary base of section							1695	1603	95.4	1642	32	1622					32			
P_Sequence Northern Humboldt																		Mean=	87.53	1.16
																		StDev=	46.50	1.04

Table DR15. This table summarizes the raw OxCal P-sequence output using k = 0.2.

													Amodel=	34.1						Normalized
	UNMODELLED (BP)						MODELLED (BP)						Aoverall=	29.3					Confidence	Age
	from	to	%	μ	σ	m	from	to	%	μ	σ	m	A_{comb}	A	L	P	C		Interval (yr)	Deviation[1]
2014																				
Boundary surface	-63	-64	95.4	-63	0	-63	-63	-64	95.4	-63	0	-63		100			100			
1700 CE							251	250	95.4	250	0	250					100			
R_Date MD.14.06.168.5-169.5	926	798	95.4	860	39	850	933	831	95.4	909	24	917		92.3			96.7		102.00	2.04
EQ2							935	837	95.4	918	17	923					94.5			
R_Date MR.14.02.B.225-226	955	802	95.4	902	40	921	935	916	95.4	926	5	926		160.6			94		19.00	4.80
R_Date MD.14.06.C.169.5-170.5	952	803	95.3	913	31	923	935	918	95.4	926	4	927		125.8			95		17.00	3.25
R_Date MR.14.05.B.188.5-189.5	959	910	95.4	926	19	927	935	919	95.4	928	4	928		127.5			95.8		16.00	0.50
R_Date MD.14.03.C.212.5-213.5	965	928	95.4	947	11	947	949	921	95.4	932	6	931		55.9			92.4		28.00	2.50
		Warning! Poor agreement - A= 55.9%(A'c= 60.0%)																		
R_Date MR.14.02.A.273-273.5	1058	961	95.4	1008	30	1004	1175	1029	95.4	1138	50	1165		19.1			43.9		146.00	2.60
		Warning! Poor agreement - A= 19.1%(A'c= 60.0%)																		
R_Date JC.14.02.D.125.5-126	1072	969	95.4	1025	34	1021	1175	1027	95.4	1139	50	1165		33.5			43.7		148.00	2.28
		Warning! Poor agreement - A= 33.5%(A'c= 60.0%)																		
EQ3							1274	1030	95.4	1172	43	1183					72.2			
R_Date JC.14.02.D.130-130.5	1278	1181	95.4	1229	29	1233	1274	1180	95.4	1199	19	1194		117.1			56.5		94.00	1.58
R_Date MR.14.05.C.246-247	1281	1182	95.4	1232	31	1240	1273	1181	95.4	1200	20	1195		126.7			50.1		92.00	1.60
R_Date MD.17.13.D.250-251	1302	1190	95.4	1278	20	1283	1277	1182	95.4	1201	22	1195		11.6			55.6		95.00	3.50
		Warning! Poor agreement - A= 11.6%(A'c= 60.0%)																		
R_Date MD.14.05.A.276-277	1401	1326	95.4	1363	18	1363	1401	1334	95.4	1366	17	1366		101.2			99.9		67.00	0.18
R_Date JC.14.02.C.168.5-169.5	1695	1557	95.4	1618	41	1609	1689	1566	95.4	1625	35	1614		106.8			35.8		123.00	0.20
R_Date MD.14.05.B1.306.5-307.5	1707	1604	95.4	1654	30	1658	1692	1572	95.4	1638	33	1621		86.8			21.8		120.00	0.48
EQ4							1693	1573	95.4	1640	33	1621					22.2		120.00	49.70
R_Date MR.14.02.A.297.5-298	1690	1544	95.4	1594	33	1588	1693	1574	95.4	1642	34	1622		51.2			23.7		119.00	1.41
		Warning! Poor agreement - A= 51.2%(A'c= 60.0%)																		
R_Date JC.14.02.C.170-171.5	1693	1561	95.4	1616	39	1606	1694	1574	95.4	1642	33	1622		101.2			22.8		120.00	0.79
R_Date MD.14.04.B.379.5-380.5	1709	1614	95.4	1659	28	1658	1694	1574	95.3	1643	33	1623		60.8			23.2		120.00	0.48
R_Date MD.14.05.B1.308-309	1695	1565	95.4	1632	40	1622	1696	1576	95.4	1646	33	1627		126			25.5		120.00	0.42
Boundary base of section							1696	1576	95.4	1646	33	1627					25.5			
P_Sequence Northern Humboldt																		Mean=	92.56	4.35
																		StDev=	44.21	11.39

Table DR16. This table summarizes the raw OxCal P-sequence output using k = 0.3.

													Amodel=	14.2						
	UNMODELLED (BP)						MODELLED (BP)						Aoverall=	9.8					Confidence Interval (yr)	Normalized Age Deviation[1]
	from	to	%	μ	σ	m	from	to	%	μ	σ	m	A_{comb}	A	L	P	C			
2014																				
Boundary surface	-63	-64	95.4	-63	0	-63	-63	-64	95.4	-63	0	-63		100			100			
1700 CE							251	250	95.4	250	0	250					100			
R_Date MD.14.06.168.5-169.5	926	798	95.4	860	39	850	932	834	95.4	909	22	916		94.2			92		98.00	2.23
EQ2							935	855	95.4	918	16	923					93.5			
R_Date MR.14.02.B.225-226	955	802	95.4	902	40	921	935	918	95.4	926	4	927		158.1			90.6		17.00	6.00
R_Date MD.14.06.C.169.5-170.5	952	803	95.3	913	31	923	935	919	95.4	927	3	928		122.5			93.7		16.00	4.67
R_Date MR.14.05.B.188.5-189.5	959	910	95.4	926	19	927	935	920	95.4	928	3	929		130.8			98		15.00	0.67
R_Date MD.14.03.C.212.5-213.5	965	928	95.4	947	11	947	945	921	95.4	930	5	930		47.2			94.8		24.00	3.40
		Warning! Poor agreement - A= 47.2%(A'c= 60.0%)																		
R_Date MR.14.02.A.273-273.5	1058	961	95.4	1008	30	1004	1175	1160	95.4	1166	10	1167		0.8			98		15.00	15.80
		Warning! Poor agreement - A= 0.8%(A'c= 60.0%)																		
R_Date JC.14.02.D.125.5-126	1072	969	95.4	1025	34	1021	1175	1161	95.4	1166	10	1167		11.4			97.9		14.00	14.10
		Warning! Poor agreement - A= 11.4%(A'c= 60.0%)																		
EQ3							1202	1161	95.4	1180	16	1180					95.6			
R_Date JC.14.02.D.130-130.5	1278	1181	95.4	1229	29	1233	1206	1181	95.4	1195	11	1193		118.3			85.6		25.00	3.09
R_Date MR.14.05.C.246-247	1281	1182	95.4	1232	31	1240	1205	1182	95.4	1195	11	1194		128.2			83.5		23.00	3.36
R_Date MD.17.13.D.250-251	1302	1190	95.4	1278	20	1283	1206	1183	95.4	1196	12	1194		8.7			86.9		23.00	6.83
		Warning! Poor agreement - A= 8.7%(A'c= 60.0%)																		
R_Date MD.14.05.A.276-277	1401	1326	95.4	1363	18	1363	1400	1335	95.4	1366	16	1367		101.9			99.3		65.00	0.19
R_Date JC.14.02.C.168.5-169.5	1695	1557	95.4	1618	41	1609	1686	1565	95.4	1616	31	1610		109.9			16.6		121.00	0.06
R_Date MD.14.05.B1.306.5-307.5	1707	1604	95.4	1654	30	1658	1690	1572	95.3	1629	30	1617		80.4			5		118.00	0.83
EQ4							1690	1574	95.4	1631	30	1618					4.8			
R_Date MR.14.02.A.297.5-298	1690	1544	95.4	1594	33	1588	1692	1576	95.4	1633	31	1619		54.3			5.2		116.00	1.26
		Warning! Poor agreement - A= 54.3%(A'c= 60.0%)																		
R_Date JC.14.02.C.170-171.5	1693	1561	95.4	1616	39	1606	1692	1578	95.5	1634	30	1619		104			5.2		114.00	0.60
R_Date MD.14.04.B.379.5-380.5	1709	1614	95.4	1659	28	1658	1693	1577	95.4	1634	30	1620		57.6			5.2		116.00	0.83
		Warning! Poor agreement - A= 57.6%(A'c= 60.0%)																		
R_Date MD.14.05.B1.308-309	1695	1565	95.4	1632	40	1622	1695	1577	95.3	1637	31	1622		124.4			6		118.00	0.16
Boundary base of section							1695	1577	95.3	1637	31	1622					6			
P_Sequence Northern Humboldt																		Mean=	61.06	3.77
																		StDev=	47.63	4.69

Table DR17. This table summarizes the raw OxCal P-sequence output using k = 0.4.

													Amodel=	6.6						Normalized
	UNMODELLED (BP)						MODELLED (BP)						Aoverall=	7.1					Confidence	Age
	from	to	%	μ	σ	m	from	to	%	μ	σ	m	A_{comb}	A	L	P	C		Interval (yr)	Deviation[1]
2014																				
Boundary surface	-63	-64	95.4	-63	0	-63	-63	-64	95.4	-63	0	-63		100			100			
1700 CE							251	250	95.4	250	0	250					100			
R_Date MD.14.06.168.5-169.5	926	798	95.4	860	39	850	932	836	95.4	910	20	916		97.6			99.1		96.00	2.50
EQ2							935	856	95.4	919	15	923					97.9			61.27
R_Date MR.14.02.B.225-226	955	802	95.4	902	40	921	935	918	95.4	926	4	927		159.2			95.2		17.00	6.00
R_Date MD.14.06.C.169.5-170.5	952	803	95.3	913	31	923	935	919	95.4	927	3	928		122.6			93.8		16.00	4.67
R_Date MR.14.05.B.188.5-189.5	959	910	95.4	926	19	927	936	920	95.4	928	3	929		131.7			98.4		16.00	0.67
R_Date MD.14.03.C.212.5-213.5	965	928	95.4	947	11	947	942	921	95.4	930	5	930		44.3			97.3		21.00	3.40
		Warning! Poor agreement - A= 44.3%(A'c= 60.0%)																		
R_Date MR.14.02.A.273-273.5	1058	961	95.4	1008	30	1004	1174	1161	95.4	1167	3	1167		0.3			96.7		13.00	53.00
		Warning! Poor agreement - A= 0.3%(A'c= 60.0%)																		
R_Date JC.14.02.D.125.5-126	1072	969	95.4	1025	34	1021	1174	1161	95.4	1167	3	1167		10.9			96.5		13.00	47.33
		Warning! Poor agreement - A= 10.9%(A'c= 60.0%)																		
EQ3							1200	1161	95.4	1180	13	1179					95.7			
R_Date JC.14.02.D.130-130.5	1278	1181	95.4	1229	29	1233	1204	1183	95.4	1194	7	1193		118.8			95.7		21.00	5.00
R_Date MR.14.05.C.246-247	1281	1182	95.4	1232	31	1240	1205	1184	95.4	1194	7	1194		129			95.8		21.00	5.43
R_Date MD.17.13.D.250-251	1302	1190	95.4	1278	20	1283	1205	1184	95.4	1195	8	1194		8			95.7		21.00	10.38
		Warning! Poor agreement - A= 8.0%(A'c= 60.0%)																		
R_Date MD.14.05.A.276-277	1401	1326	95.4	1363	18	1363	1401	1336	95.4	1367	16	1367		102.5			99.2		65.00	0.25
R_Date JC.14.02.C.168.5-169.5	1695	1557	95.4	1618	41	1609	1684	1564	95.4	1611	28	1607		111.9			11.8		120.00	0.25
R_Date MD.14.05.B1.306.5-307.5	1707	1604	95.4	1654	30	1658	1689	1574	95.3	1625	27	1616		75.7			2		115.00	1.07
EQ4							1690	1575	95.4	1627	27	1617					1.7			
R_Date MR.14.02.A.297.5-298	1690	1544	95.4	1594	33	1588	1691	1595	95.4	1629	28	1618		56.4			1.8		96.00	1.25
		Warning! Poor agreement - A= 56.4%(A'c= 60.0%)																		
R_Date JC.14.02.C.170-171.5	1693	1561	95.4	1616	39	1606	1691	1597	95.4	1629	28	1618		106.6			1.8		94.00	0.46
R_Date MD.14.04.B.379.5-380.5	1709	1614	95.4	1659	28	1658	1692	1598	95.4	1629	28	1618		54.7			1.7		94.00	1.07
		Warning! Poor agreement - A= 54.7%(A'c= 60.0%)																		
R_Date MD.14.05.B1.308-309	1695	1565	95.4	1632	40	1622	1695	1598	95.4	1633	28	1621		123.5			1.9		97.00	0.04
Boundary base of section							1695	1598	95.4	1633	28	1621					1.9			
P_Sequence Northern Humboldt																		Mean=	55.06	11.34
																		StDev=	42.38	19.90

Table DR18. This table summarizes the raw OxCal P-sequence output using k = 0.5.

													Amodel=	8.7						Normalized
	UNMODELLED (BP)						MODELLED (BP)						Aoverall=	7.5					Confidence	Age
	from	to	%	μ	σ	m	from	to	%	μ	σ	m	A_{comb}	A	L	P	C		Interval (yr)	Deviation[1]
2014																				
Boundary surface	-63	-64	95.4	-63	0	-63	-63	-64	95.4	-63	0	-63		100			100			
1700 CE							251	250	95.4	250	0	250					100			
R_Date MD.14.06.168.5-169.5	926	798	95.4	850	39	850	931	840	95.4	911	18	916		99.5			99.6		91.00	2.83
EQ2							935	895	95.4	919	14	923					98.8			
R_Date MR.14.02.B.225-226	955	802	95.4	902	40	921	935	918	95.4	927	4	927		159.3			99.3		17.00	6.25
R_Date MD.14.06.C.169.5-170.5	952	803	95.3	913	31	923	935	920	95.4	927	3	928		123			99.4		15.00	4.67
R_Date MR.14.05.B.188.5-189.5	959	910	95.4	926	19	927	936	920	95.4	928	3	929		131.9			96.1		16.00	0.67
R_Date MD.14.03.C.212.5-213.5	965	928	95.4	947	11	947	941	921	95.4	930	4	930		42			97.3		20.00	4.25
		Warning! Poor agreement - A= 42.0%(A'c= 60.0%)																		
R_Date MR.14.02.A.273-273.5	1058	961	95.4	1008	30	1004	1174	1161	95.4	1167	6	1167		0.4			97.2		13.00	26.50
		Warning! Poor agreement - A= 0.4%(A'c= 60.0%)																		
R_Date JC.14.02.D.125.5-126	1072	969	95.4	1025	34	1021	1174	1161	95.4	1167	6	1167		10.9			97.8		13.00	23.67
		Warning! Poor agreement - A= 10.9%(A'c= 60.0%)																		
EQ3							1199	1162	95.4	1180	12	1180					94.4			
R_Date JC.14.02.D.130-130.5	1278	1181	95.4	1229	29	1233	1203	1183	95.4	1193	5	1193		118.7			82.8		20.00	7.20
R_Date MR.14.05.C.246-247	1281	1182	95.4	1232	31	1240	1203	1184	95.4	1193	5	1193		128.3			86		19.00	7.80
R_Date MD.17.13.D.250-251	1302	1190	95.4	1278	20	1283	1204	1184	95.4	1193	5	1193		7.8			89		20.00	17.00
		Warning! Poor agreement - A= 7.8%(A'c= 60.0%)																		
R_Date MD.14.05.A.276-277	1401	1326	95.4	1363	18	1363	1400	1338	95.4	1368	16	1368		102.6			99.3		62.00	0.31
R_Date JC.14.02.C.168.5-169.5	1695	1557	95.4	1618	41	1609	1683	1565	95.4	1613	29	1607		108			40.5		118.00	0.17
R_Date MD.14.05.B1.306.5-307.5	1707	1604	95.4	1654	30	1658	1689	1574	95.4	1627	28	1616		77			27.4		115.00	0.96
EQ4							1690	1575	95.5	1629	29	1617					26.1			
R_Date MR.14.02.A.297.5-298	1690	1544	95.4	1594	33	1588	1692	1594	95.4	1631	29	1618		54.8			25.6		98.00	1.28
		Warning! Poor agreement - A= 54.8%(A'c= 60.0%)																		
R_Date JC.14.02.C.170-171.5	1693	1561	95.4	1616	39	1606	1692	1594	95.4	1632	29	1619		104.1			25.7		98.00	0.55
R_Date MD.14.04.B.379.5-380.5	1709	1614	95.4	1659	28	1658	1693	1595	95.4	1632	29	1619		56.3			25.7		98.00	0.93
		Warning! Poor agreement - A= 56.3%(A'c= 60.0%)																		
R_Date MD.14.05.B1.308-309	1695	1565	95.4	1632	40	1622	1695	1598	95.4	1636	29	1622		122.1			25.5		97.00	0.14
Boundary base of section							1695	1598	95.4	1636	29	1622					25.5			
P_Sequence Northern Humboldt																		Mean=	54.71	6.19
																		StDev=	42.78	8.31

Table DR19. This table summarizes the raw OxCal P-sequence output using k = 0.6.

													Amodel=	6.1						
	UNMODELLED (BP)						MODELLED (BP)						Aoverall=	6.9					Confidence Interval (yr)	Normalized Age Deviation[1]
	from	**to**	**%**	**μ**	**σ**	**m**	**from**	**to**	**%**	**μ**	**σ**	**m**	**A_{comb}**	**A**	**L**	**P**	**C**			
2014																				
Boundary surface	-63	-64	95.4	-63	0	-63	-63	-64	95.4	-63	0	-63		100			100			
1700 CE							251	250	95.4	250	0	250					100			
R_Date MD.14.06.168.5-169.5	926	798	95.4	860	39	850	930	829	95.4	910	20	915		101.2			97		101.00	2.50
EQ2							935	832	95.4	917	17	922					96.9			53.94
R_Date MR.14.02.B.225-226	955	802	95.4	902	40	921	935	916	95.4	925	14	927		157.4			95.4		19.00	1.64
R_Date MD.14.06.C.169.5-170.5	952	803	95.3	913	31	923	935	918	95.4	925	14	927		121.5			93.9		17.00	0.86
R_Date MR.14.05.B.188.5-189.5	959	910	95.4	926	19	927	936	920	95.4	926	14	928		130.4			97.3		16.00	0.00
R_Date MD.14.03.C.212.5-213.5	965	928	95.4	947	11	947	943	920	95.4	927	14	929		38.5			96.1		23.00	1.43
		Warning! Poor agreement - A= 38.5%(A'c= 60.0%)																		
R_Date MR.14.02.A.273-273.5	1058	961	95.4	1008	30	1004	1174	1161	95.4	1167	5	1167		0.3			91.8		13.00	31.80
		Warning! Poor agreement - A= 0.3%(A'c= 60.0%)																		
R_Date JC.14.02.D.125.5-126	1072	969	95.4	1025	34	1021	1174	1161	95.4	1167	5	1167		10.8			89.9		13.00	28.40
		Warning! Poor agreement - A= 10.8%(A'c= 60.0%)																		
EQ3							1199	1162	95.4	1180	11	1180					93.3			
R_Date JC.14.02.D.130-130.5	1278	1181	95.4	1229	29	1233	1204	1183	95.4	1193	6	1192		118.6			78.1		21.00	6.00
R_Date MR.14.05.C.246-247	1281	1182	95.4	1232	31	1240	1204	1183	95.4	1193	6	1193		127.1			76.3		21.00	6.50
R_Date MD.17.13.D.250-251	1302	1190	95.4	1278	20	1283	1205	1184	95.4	1194	6	1193		7.7			76.3		21.00	14.00
		Warning! Poor agreement - A= 7.7%(A'c= 60.0%)																		
R_Date MD.14.05.A.276-277	1401	1326	95.4	1363	18	1363	1400	1340	95.4	1369	15	1369		102.8			97.3		60.00	0.40
R_Date JC.14.02.C.168.5-169.5	1695	1557	95.4	1618	41	1609	1682	1564	95.4	1611	29	1606		106.9			10.8		118.00	0.24
R_Date MD.14.05.B1.306.5-307.5	1707	1604	95.4	1654	30	1658	1689	1572	95.4	1625	29	1616		73.6			2.1		117.00	1.00
EQ4							1690	1572	95.4	1627	29	1617					1.9			
R_Date MR.14.02.A.297.5-298	1690	1544	95.4	1594	33	1588	1691	1573	95.4	1630	30	1618		56.9			2.2		118.00	1.20
		Warning! Poor agreement - A= 56.9%(A'c= 60.0%)																		
R_Date JC.14.02.C.170-171.5	1693	1561	95.4	1616	39	1606	1692	1573	95.4	1630	30	1618		105			2.2		119.00	0.47
R_Date MD.14.04.B.379.5-380.5	1709	1614	95.4	1659	28	1658	1692	1573	95.3	1631	30	1619		54.2			2.2		119.00	0.93
		Warning! Poor agreement - A= 54.2%(A'c= 60.0%)																		
R_Date MD.14.05.B1.308-309	1695	1565	95.4	1632	40	1622	1695	1575	95.4	1634	30	1622		120.7			2.5		120.00	0.07
Boundary base of section							1695	1575	95.4	1634	30	1622					2.5			
P_Sequence Northern Humboldt																		Mean=	60.94	8.41
																		StDev=	48.75	14.84

Table DR20. This table summarizes the raw OxCal P-sequence output using k = 0.8.

													Amodel=	8.2						Normalized
	UNMODELLED (BP)						MODELLED (BP)						Aoverall=	7					Confidence	Age
	from	to	%	μ	σ	m	from	to	%	μ	σ	m	A_{comb}	A	L	P	C		Interval (yr)	Deviation[1]
2014																				
Boundary surface	-63	-64	95.4	-63	0	-63	-63	-64	95.4	-63	0	-63		100			100			
1700 CE							251	250	95.4	250	0	250					100			
R_Date MD.14.06.168.5-169.5	926	798	95.4	860	39	850	930	893	95.4	913	13	915		103.7			99.8		37.00	4.08
EQ2							934	904	95.4	920	10	922					99.3			
R_Date MR.14.02.B.225-226	955	802	95.4	902	40	921	935	919	95.4	927	3	927		162.3			97.4		16.00	8.33
R_Date MD.14.06.C.169.5-170.5	952	803	95.3	913	31	923	934	921	95.4	927	3	927		126.3			95.1		13.00	4.67
R_Date MR.14.05.B.188.5-189.5	959	910	95.4	926	19	927	935	921	95.4	928	3	928		134.4			93.1		14.00	0.67
R_Date MD.14.03.C.212.5-213.5	965	928	95.4	947	11	947	938	921	95.4	929	3	929		35			98.1		17.00	6.00
		Warning! Poor agreement - A= 35.0%(A'c= 60.0%)																		
R_Date MR.14.02.A.273-273.5	1058	961	95.4	1008	30	1004	1174	1162	95.4	1167	5	1168		0.3			97.6		12.00	31.80
		Warning! Poor agreement - A= 0.3%(A'c= 60.0%)																		
R_Date JC.14.02.D.125.5-126	1072	969	95.4	1025	34	1021	1174	1162	95.4	1168	5	1168		10.5			96.3		12.00	28.60
		Warning! Poor agreement - A= 10.5%(A'c= 60.0%)																		
EQ3							1197	1164	95.4	1180	10	1180					98.5			
R_Date JC.14.02.D.130-130.5	1278	1181	95.4	1229	29	1233	1202	1183	95.4	1192	5	1192		118.4			92.3		19.00	7.40
R_Date MR.14.05.C.246-247	1281	1182	95.4	1232	31	1240	1202	1184	95.4	1193	5	1192		127.1			90.2		18.00	7.80
R_Date MD.17.13.D.250-251	1302	1190	95.4	1278	20	1283	1203	1184	95.4	1193	5	1192		7.7			90		19.00	17.00
		Warning! Poor agreement - A= 7.7%(A'c= 60.0%)																		
R_Date MD.14.05.A.276-277	1401	1326	95.4	1363	18	1363	1401	1341	95.4	1370	15	1371		102.2			96		60.00	0.47
R_Date JC.14.02.C.168.5-169.5	1695	1557	95.4	1618	41	1609	1680	1563	95.4	1612	30	1605		102.9			2.9		117.00	0.20
R_Date MD.14.05.B1.306.5-307.5	1707	1604	95.4	1654	30	1658	1688	1572	95.4	1626	29	1615		72.7			0.3		116.00	0.97
EQ4							1689	1573	95.4	1628	30	1617					0.2			
R_Date MR.14.02.A.297.5-298	1690	1544	95.4	1594	33	1588	1690	1573	95.4	1631	30	1618		56.9			0.2		117.00	1.23
		Warning! Poor agreement - A= 56.9%(A'c= 60.0%)																		
R_Date JC.14.02.C.170-171.5	1693	1561	95.4	1616	39	1606	1690	1573	95.4	1631	30	1618		104.6			0.2		117.00	0.50
R_Date MD.14.04.B.379.5-380.5	1709	1614	95.4	1659	28	1658	1691	1573	95.4	1632	30	1619		54.2			0.2		118.00	0.90
		Warning! Poor agreement - A= 54.2%(A'c= 60.0%)																		
R_Date MD.14.05.B1.308-309	1695	1565	95.4	1632	40	1622	1695	1576	95.4	1636	30	1622		120.4			0.3		119.00	0.13
Boundary base of section							1695	1576	95.4	1636	30	1622					0.3			
P_Sequence Northern Humboldt																		Mean=	55.35	7.10
																		StDev=	48.56	9.76

Table DR20. This table summarizes the raw OxCal P-sequence output using k = 1.

													Amodel=	5.9						Normalized
	UNMODELLED (BP)						MODELLED (BP)						Aoverall=	6					Confidence	Age
	from	to	%	μ	σ	m	from	to	%	μ	σ	m	A_{comb}	A	L	P	C		Interval (yr)	Deviation[1]
Boundary surface	-63	-64	95.4	-63	0	-63	-63	-64	95.4	-63	0	-63		100			100			
1700 CE							251	250	95.4	250	0	250					100			
R_Date MD.14.06.168.5-169.5	926	798	95.4	860	39	850	930	830	95.4	911	17	915		105.3			97.7		100.00	3.00
EQ2							935	901	95.4	918	15	922					97.4			
R_Date MR.14.02.B.225-226	955	802	95.4	902	40	921	935	918	95.4	925	14	927		158.8			97.8		17.00	1.64
R_Date MD.14.06.C.169.5-170.5	952	803	95.3	913	31	923	935	919	95.4	925	14	927		122.5			97.5		16.00	0.86
R_Date MR.14.05.B.188.5-189.5	959	910	95.4	926	19	927	935	919	95.4	926	14	928		132.2			97.5		16.00	0.00
R_Date MD.14.03.C.212.5-213.5	965	928	95.4	947	11	947	938	920	95.4	926	14	929		29.4			96.1		18.00	1.50
		Warning! Poor agreement - A= 29.4%(A'c= 60.0%)																		
R_Date MR.14.02.A.273-273.5	1058	961	95.4	1008	30	1004	1174	1161	95.4	1167	8	1168		0.2			98		13.00	19.88
		Warning! Poor agreement - A= 0.2%(A'c= 60.0%)																		
R_Date JC.14.02.D.125.5-126	1072	969	95.4	1025	34	1021	1175	1161	95.4	1167	8	1168		10.2			98.5		14.00	17.75
		Warning! Poor agreement - A= 10.2%(A'c= 60.0%)																		
EQ3							1196	1164	95.4	1179	10	1180					99.5			
R_Date JC.14.02.D.130-130.5	1278	1181	95.4	1229	29	1233	1202	1182	95.4	1192	6	1191		118.4			95.1		20.00	6.17
R_Date MR.14.05.C.246-247	1281	1182	95.4	1232	31	1240	1202	1183	95.4	1192	6	1192		126.5			94		19.00	6.67
R_Date MD.17.13.D.250-251	1302	1190	95.4	1278	20	1283	1202	1184	95.4	1192	6	1192		7.6			93.7		18.00	14.33
		Warning! Poor agreement - A= 7.6%(A'c= 60.0%)																		
R_Date MD.14.05.A.276-277	1401	1326	95.4	1363	18	1363	1400	1343	95.4	1371	15	1372		101.5			94.4		57.00	0.53
R_Date JC.14.02.C.168.5-169.5	1695	1557	95.4	1618	41	1609	1679	1562	95.4	1610	30	1604		100.4			8.5		117.00	0.27
R_Date MD.14.05.B1.306.5-307.5	1707	1604	95.4	1654	30	1658	1686	1572	95.4	1625	30	1615		69.8			4.5		114.00	0.97
EQ4							1688	1573	95.4	1627	30	1616					4.5			
R_Date MR.14.02.A.297.5-298	1690	1544	95.4	1594	33	1588	1690	1574	95.4	1630	31	1618		58.7			4.7		116.00	1.16
		Warning! Poor agreement - A= 58.7%(A'c= 60.0%)																		
R_Date JC.14.02.C.170-171.5	1693	1561	95.4	1616	39	1606	1690	1574	95.4	1630	31	1618		104.6			4.7		116.00	0.45
R_Date MD.14.04.B.379.5-380.5	1709	1614	95.4	1659	28	1658	1690	1574	95.4	1630	31	1618		52.5			4.8		116.00	0.94
		Warning! Poor agreement - A= 52.5%(A'c= 60.0%)																		
R_Date MD.14.05.B1.308-309	1695	1565	95.4	1632	40	1622	1695	1578	95.4	1635	31	1622		119.8			5		117.00	0.10
Boundary base of section							1695	1578	95.4	1635	31	1622					5			
P_Sequence Northern Humboldt																		Mean=	59.06	4.48
																		StDev=	48.26	6.49

Table DR21. This table summarizes the raw OxCal P-sequence output using k = 2.

	UNMODELLED (BP)						MODELLED (BP)						Amodel=	4.2					Confidence	Normalized Age
													Aoverall=	2.4						
	from	to	%	μ	σ	m	from	to	%	μ	σ	m	A_{comb}	A	L	P	C		Interval (yr)	Deviation[1]
Boundary surface	-63	-64	95.4	-63	0	-63	-63	-64	95.4	-63	0	-63		100			100			
1700 CE							251	250	95.4	250	0	250					100			
R_Date MD.14.06.168.5-169.5	926	798	95.4	860	39	850	926	803	95.4	865	44	836		99			17.7		123.00	0.11
EQ2							930	815	95.4	871	44	838					15			
R_Date MR.14.02.B.225-226	955	802	95.4	902	40	921	934	830	95.4	876	45	841		97.5			14.1		104.00	0.58
R_Date MD.14.06.C.169.5-170.5	952	803	95.3	913	31	923	934	831	95.4	877	45	841		67.8			14.1		103.00	0.80
R_Date MR.14.05.B.188.5-189.5	959	910	95.4	926	19	927	934	831	95.4	877	45	841		61.6			14		103.00	1.09
R_Date MD.14.03.C.212.5-213.5	965	928	95.4	947	11	947	934	831	95.4	877	45	842		8.6			13.9		103.00	1.56
		Warning! Poor agreement - A= 8.6%(A'c= 60.0%)																		
R_Date MR.14.02.A.273-273.5	1058	961	95.4	1008	30	1004	1175	1161	95.4	1168	5	1169		0.2			94.1		14.00	32.00
		Warning! Poor agreement - A= 0.2%(A'c= 60.0%)																		
R_Date JC.14.02.D.125.5-126	1072	969	95.4	1025	34	1021	1175	1161	95.4	1168	5	1169		9.6			95.5		14.00	28.60
		Warning! Poor agreement - A= 9.6%(A'c= 60.0%)																		
EQ3							1195	1165	95.4	1179	8	1180					99.7			
R_Date JC.14.02.D.130-130.5	1278	1181	95.4	1229	29	1233	1200	1181	95.4	1191	5	1191		117.8			98.2		19.00	7.60
R_Date MR.14.05.C.246-247	1281	1182	95.4	1232	31	1240	1200	1182	95.4	1191	5	1191		122.3			98.4		18.00	8.20
R_Date MD.17.13.D.250-251	1302	1190	95.4	1278	20	1283	1200	1182	95.4	1191	5	1191		7.1			98.4		18.00	17.40
		Warning! Poor agreement - A= 7.1%(A'c= 60.0%)																		
R_Date MD.14.05.A.276-277	1401	1326	95.4	1363	18	1363	1400	1345	95.4	1372	13	1373		103.5			96.2		55.00	0.69
R_Date JC.14.02.C.168.5-169.5	1695	1557	95.4	1618	41	1609	1665	1555	95.4	1593	22	1594		105.2			72.7		110.00	1.14
R_Date MD.14.05.B1.306.5-307.5	1707	1604	95.4	1654	30	1658	1678	1566	95.4	1606	23	1608		44.1			72		112.00	2.09
		Warning! Poor agreement - A= 44.1%(A'c= 60.0%)																		
EQ4							1680	1569	95.4	1609	23	1610					72.8			
R_Date MR.14.02.A.297.5-298	1690	1544	95.4	1594	33	1588	1684	1571	95.4	1612	23	1613		78.2			73.7		113.00	0.78
R_Date JC.14.02.C.170-171.5	1693	1561	95.4	1616	39	1606	1684	1571	95.4	1612	23	1613		113.5			73.7		113.00	0.17
R_Date MD.14.04.B.379.5-380.5	1709	1614	95.4	1659	28	1658	1684	1571	95.4	1612	23	1613		35.7			73.6		113.00	2.04
		Warning! Poor agreement - A= 35.7%(A'c= 60.0%)																		
R_Date MD.14.05.B1.308-309	1695	1565	95.4	1632	40	1622	1689	1574	95.4	1617	23	1618		111.7			76.2		115.00	0.65
Boundary base of section							1689	1574	95.4	1617	23	1618					76.2			
P_Sequence Northern Humboldt																		Mean=	79.41	6.21
																		StDev=	44.14	10.10

Table DR22. This table summarizes the raw OxCal P-sequence output using k = 3.

													Amodel=	3.6						Normalized
	UNMODELLED (BP)						MODELLED (BP)						Aoverall=	3					Confidence	Age
	from	to	%	μ	σ	m	from	to	%	μ	σ	m	A_{comb}	A	L	P	C		Interval (yr)	Deviation[1]
Boundary surface	-63	-64	95.4	-63	0	-63	-63	-64	95.4	-63	0	-63		100			100			
1700 CE							251	250	95.4	250	0	250					100			
R_Date MD.14.06.168.5-169.5	926	798	95.4	860	39	850	926	821	95.4	904	26	912		113.4					105.00	1.69
EQ2							930	826	95.4	910	26	918								
R_Date MR.14.02.B.225-226	955	802	95.4	902	40	921	934	832	95.4	916	26	924		158					102.00	0.54
R_Date MD.14.06.C.169.5-170.5	952	803	95.3	913	31	923	934	832	95.4	916	26	925		125					102.00	0.12
R_Date MR.14.05.B.188.5-189.5	959	910	95.4	926	19	927	934	832	95.4	916	26	925		110.1					102.00	0.38
R_Date MD.14.03.C.212.5-213.5	965	928	95.4	947	11	947	934	832	95.4	917	26	925		10.1					102.00	1.15
		Warning! Poor agreement - A= 10.1%(A'c= 60.0%)																		
R_Date MR.14.02.A.273-273.5	1058	961	95.4	1008	30	1004	1178	1163	95.4	1170	5	1170		0.2			98.2		15.00	32.40
		Warning! Poor agreement - A= 0.2%(A'c= 60.0%)																		
R_Date JC.14.02.D.125.5-126	1072	969	95.4	1025	34	1021	1176	1163	95.4	1170	5	1170		8.2			98.5		13.00	29.00
		Warning! Poor agreement - A= 8.2%(A'c= 60.0%)																		
EQ3							1190	1169	95.4	1179	6	1180					99.4			
R_Date JC.14.02.D.130-130.5	1278	1181	95.4	1229	29	1233	1197	1182	95.4	1189	3	1189		116.2			91.1		15.00	13.33
R_Date MR.14.05.C.246-247	1281	1182	95.4	1232	31	1240	1197	1182	95.4	1189	3	1190		115.2			90.4		15.00	14.33
R_Date MD.17.13.D.250-251	1302	1190	95.4	1278	20	1283	1198	1182	95.4	1189	3	1190		6.3			91.3		16.00	29.67
		Warning! Poor agreement - A= 6.3%(A'c= 60.0%)																		
R_Date MD.14.05.A.276-277	1401	1326	95.4	1363	18	1363	1396	1347	95.4	1372	12	1372		107.5			99.3		49.00	0.75
R_Date JC.14.02.C.168.5-169.5	1695	1557	95.4	1618	41	1609	1610	1556	95.4	1585	16	1587		103.2			90.3		54.00	2.06
R_Date MD.14.05.B1.306.5-307.5	1707	1604	95.4	1654	30	1658	1620	1567	95.4	1597	17	1602		30.5			89		53.00	3.35
		Warning! Poor agreement - A= 30.5%(A'c= 60.0%)																		
EQ4							1623	1570	95.4	1600	17	1605					89.4			
R_Date MR.14.02.A.297.5-298	1690	1544	95.4	1594	33	1588	1625	1571	95.4	1602	17	1608		92.1			89.7		54.00	0.47
R_Date JC.14.02.C.170-171.5	1693	1561	95.4	1616	39	1606	1625	1571	95.4	1602	17	1608		118.1			89.9		54.00	0.82
R_Date MD.14.04.B.379.5-380.5	1709	1614	95.4	1659	28	1658	1625	1571	95.4	1602	17	1608		24.6			89.8		54.00	3.35
		Warning! Poor agreement - A= 24.6%(A'c= 60.0%)																		
R_Date MD.14.05.B1.308-309	1695	1565	95.4	1632	40	1622	1631	1576	95.4	1608	17	1613		105.9			91.4		55.00	1.41
Boundary base of section							1631	1576	95.4	1608	17	1613					91.4			
P_Sequence Northern Humboldt																		Mean=	56.47	7.93
																		StDev=	34.85	11.51

Table DR23. This table summarizes the raw OxCal P-sequence output using k = 4.

	UNMODELLED (BP)						MODELLED (BP)													
													Amodel=	1.2						
													Aoverall=	0.5					Confidence Interval (yr)	Normalized Age Deviation[1]
	from	to	%	µ	σ	m	from	to	%	µ	σ	m	A_{comb}	A	L	P	C			
Boundary surface	-63	-64	95.4	-63	0	-63	-63	-64	95.4	-63	0	-63		100			100			
1700 CE							251	250	95.4	250	0	250					100			
R_Date MD.14.06.168.5-169.5	926	798	95.4	860	39	850	919	804	95.4	839	34	828		77					115.00	0.62
EQ2							925	814	95.4	845	34	832							111.00	24.85
R_Date MR.14.02.B.225-226	955	802	95.4	902	40	921	928	828	95.4	851	34	836		61.1						
R_Date MD.14.06.C.169.5-170.5	952	803	95.3	913	31	923	929	828	95.4	851	34	836		34.7					101.00	1.82
		Warning! Poor agreement - A= 34.7%(A'c= 60.0%)																		
R_Date MR.14.05.B.188.5-189.5	959	910	95.4	926	19	927	929	828	95.4	851	34	836		21.2					101.00	2.21
		Warning! Poor agreement - A= 21.2%(A'c= 60.0%)																		
R_Date MD.14.03.C.212.5-213.5	965	928	95.4	947	11	947	929	828	95.4	851	34	836		1					101.00	2.82
		Warning! Poor agreement - A= 1.0%(A'c= 60.0%)																		
R_Date MR.14.02.A.273-273.5	1058	961	95.4	1008	30	1004	1178	1162	95.4	1170	3	1170		0.2			94.7		16.00	54.00
		Warning! Poor agreement - A= 0.2%(A'c= 60.0%)																		
R_Date JC.14.02.D.125.5-126	1072	969	95.4	1025	34	1021	1176	1163	95.4	1170	3	1170		8.3			94.6		13.00	48.33
		Warning! Poor agreement - A= 8.3%(A'c= 60.0%)																		
EQ3							1190	1169	95.4	1179	5	1179					98.9			
R_Date JC.14.02.D.130-130.5	1278	1181	95.4	1229	29	1233	1196	1181	95.4	1188	3	1189		115			79.8		15.00	13.67
R_Date MR.14.05.C.246-247	1281	1182	95.4	1232	31	1240	1196	1181	95.4	1189	3	1189		110.3			77.9		15.00	14.33
R_Date MD.17.13.D.250-251	1302	1190	95.4	1278	20	1283	1196	1181	95.4	1189	3	1189		5.8			79.3		15.00	29.67
		Warning! Poor agreement - A= 5.8%(A'c= 60.0%)																		
R_Date MD.14.05.A.276-277	1401	1326	95.4	1363	18	1363	1393	1347	95.4	1370	11	1370		112.6			94.9		46.00	0.64
R_Date JC.14.02.C.168.5-169.5	1695	1557	95.4	1618	41	1609	1605	1554	95.4	1576	16	1571		89.1			69.3		51.00	2.63
R_Date MD.14.05.B1.306.5-307.5	1707	1604	95.4	1654	30	1658	1617	1566	95.4	1588	17	1581		21.3			67.5		51.00	3.88
		Warning! Poor agreement - A= 21.3%(A'c= 60.0%)																		
EQ4							1619	1568	95.4	1590	18	1583					65.7			
R_Date MR.14.02.A.297.5-298	1690	1544	95.4	1594	33	1588	1622	1570	95.4	1593	18	1586		108.1			63.8		52.00	0.06
R_Date JC.14.02.C.170-171.5	1693	1561	95.4	1616	39	1606	1622	1571	95.4	1593	18	1586		119.4			63.7		51.00	1.28
R_Date MD.14.04.B.379.5-380.5	1709	1614	95.4	1659	28	1658	1622	1571	95.4	1593	18	1587		13.5			63.8		51.00	3.67
		Warning! Poor agreement - A= 13.5%(A'c= 60.0%)																		
R_Date MD.14.05.B1.308-309	1695	1565	95.4	1632	40	1622	1626	1575	95.4	1598	18	1592		93.1			61.5		51.00	1.89
Boundary base of section							1626	1575	95.4	1598	18	1592					61.5			
P_Sequence Northern Humboldt																		Mean=	56.24	12.14
																		StDev=	36.50	17.13

Table DR24. This table summarizes the raw OxCal P-sequence output using k = 5.

													Amodel=	1.1						Normalized
	UNMODELLED (BP)						MODELLED (BP)						Aoverall=	0.4					Confidence	Age
	from	to	%	μ	σ	m	from	to	%	μ	σ	m	A_{comb}	A	L	P	C		Interval (yr)	Deviation[1]
Boundary surface	-63	-64	95.4	-63	0	-63	-63	-64	95.4	-63	0	-63		100			100			
1700 CE							251	250	95.4	250	0	250					100			
R_Date MD.14.06.168.5-169.5	926	798	95.4	860	39	850	919	806	95.4	856	42	830		80.1			1.2		113.00	0.10
EQ2							924	817	95.4	862	42	834					0.9			
R_Date MR.14.02.B.225-226	955	802	95.4	902	40	921	928	829	95.4	868	41	837		75.7			0.6		99.00	0.83
R_Date MD.14.06.C.169.5-170.5	952	803	95.3	913	31	923	928	829	95.4	868	41	837		47.5			0.6		99.00	1.10
		Warning! Poor agreement - A= 47.5%(A'c= 60.0%)																		
R_Date MR.14.05.B.188.5-189.5	959	910	95.4	926	19	927	928	828	95.4	868	41	837		28.2			0.6		100.00	1.41
		Warning! Poor agreement - A= 28.2%(A'c= 60.0%)																		
R_Date MD.14.03.C.212.5-213.5	965	928	95.4	947	11	947	928	828	95.4	868	41	837		0.6			0.6		100.00	1.93
		Warning! Poor agreement - A= 0.6%(A'c= 60.0%)																		
R_Date MR.14.02.A.273-273.5	1058	961	95.4	1008	30	1004	1178	1165	95.4	1170	4	1171		0.2			86		13.00	40.50
		Warning! Poor agreement - A= 0.2%(A'c= 60.0%)																		
R_Date JC.14.02.D.125.5-126	1072	969	95.4	1025	34	1021	1179	1165	95.4	1170	4	1171		7.1			84.5		14.00	36.25
		Warning! Poor agreement - A= 7.1%(A'c= 60.0%)																		
EQ3							1190	1168	95.4	1180	6	1179					95.5			
R_Date JC.14.02.D.130-130.5	1278	1181	95.4	1229	29	1233	1198	1180	95.4	1189	8	1187		112.1			88.8		18.00	5.00
R_Date MR.14.05.C.246-247	1281	1182	95.4	1232	31	1240	1197	1180	95.4	1189	8	1188		99.7			88.7		17.00	5.38
R_Date MD.17.13.D.250-251	1302	1190	95.4	1278	20	1283	1197	1180	95.4	1189	8	1188		4.6			87.7		17.00	11.13
		Warning! Poor agreement - A= 4.6%(A'c= 60.0%)																		
R_Date MD.14.05.A.276-277	1401	1326	95.4	1363	18	1363	1392	1347	95.4	1369	11	1369		114.5			93.4		45.00	0.55
R_Date JC.14.02.C.168.5-169.5	1695	1557	95.4	1618	41	1609	1602	1553	95.4	1573	15	1568		82.1			97.7		49.00	3.00
R_Date MD.14.05.B1.306.5-307.5	1707	1604	95.4	1654	30	1658	1616	1565	95.4	1584	16	1578		19.2			97.4		51.00	4.38
		Warning! Poor agreement - A= 19.2%(A'c= 60.0%)																		
EQ4							1617	1567	95.4	1587	17	1581					97.2			
R_Date MR.14.02.A.297.5-298	1690	1544	95.4	1594	33	1588	1621	1570	95.4	1590	17	1582		111.8			96.8		51.00	0.24
R_Date JC.14.02.C.170-171.5	1693	1561	95.4	1616	39	1606	1621	1570	95.4	1590	17	1583		119.9			96.7		51.00	1.53
R_Date MD.14.04.B.379.5-380.5	1709	1614	95.4	1659	28	1658	1621	1570	95.4	1590	17	1583		11.1			96.7		51.00	4.06
		Warning! Poor agreement - A= 11.1%(A'c= 60.0%)																		
R_Date MD.14.05.B1.308-309	1695	1565	95.4	1632	40	1622	1625	1574	95.4	1595	17	1588		88			96.9		51.00	2.18
Boundary base of section							1625	1574	95.4	1595	17	1588					96.9			
P_Sequence Northern Humboldt																		Mean=	55.24	7.03
																		StDev=	32.31	12.38

Table DR25. This table summarizes the raw OxCal P-sequence output using k = 6.

													Amodel=	0.6						
	UNMODELLED (BP)						MODELLED (BP)						Aoverall=	0.1					Confidence	Normalized Age
	from	to	%	μ	σ	m	from	to	%	μ	σ	m	A_{comb}	A	L	P	C		Interval (yr)	Deviation[1]
2014																				
Boundary surface	-63	-64	95.4	-63	0	-63	-63	-64	95.4	-63	0	-63		100			100			
1700 CE							251	250	95.4	250	0	250					100			
R_Date MD.14.06.168.5-169.5	926	798	95.4	860	39	850	912	805	95.4	830	25	825		59.5					107.00	1.20
		Warning! Poor agreement - A= 59.5%(A'c= 60.0%)																		
EQ2							917	815	95.4	836	24	830								
R_Date MR.14.02.B.225-226	955	802	95.4	902	40	921	922	826	95.4	842	24	835		42.6					96.00	2.50
		Warning! Poor agreement - A= 42.6%(A'c= 60.0%)																		
R_Date MD.14.06.C.169.5-170.5	952	803	95.3	913	31	923	922	826	95.4	842	24	835		18.3					96.00	2.96
		Warning! Poor agreement - A= 18.3%(A'c= 60.0%)																		
R_Date MR.14.05.B.188.5-189.5	959	910	95.4	926	19	927	922	826	95.4	842	24	835		6.7					96.00	3.50
		Warning! Poor agreement - A= 6.7%(A'c= 60.0%)																		
R_Date MD.14.03.C.212.5-213.5	965	928	95.4	947	11	947	922	828	95.4	842	24	835							94.00	4.38
		Warning! Poor agreement - A= 0.0%(A'c= 60.0%)																		
R_Date MR.14.02.A.273-273.5	1058	961	95.4	1008	30	1004	1178	1165	95.4	1170	7	1171		0.3			60.1		13.00	23.14
		Warning! Poor agreement - A= 0.3%(A'c= 60.0%)																		
R_Date JC.14.02.D.125.5-126	1072	969	95.4	1025	34	1021	1179	1165	95.4	1170	7	1171		7			59.2		14.00	20.71
		Warning! Poor agreement - A= 7.0%(A'c= 60.0%)																		
EQ3							1189	1171	95.4	1179	5	1179					96.2			
R_Date JC.14.02.D.130-130.5	1278	1181	95.4	1229	29	1233	1195	1181	95.4	1187	3	1187		110.6			90.8		14.00	14.00
R_Date MR.14.05.C.246-247	1281	1182	95.4	1232	31	1240	1195	1181	95.4	1187	3	1187		95.5			89.6		14.00	15.00
R_Date MD.17.13.D.250-251	1302	1190	95.4	1278	20	1283	1195	1181	95.4	1187	3	1187		4.1			89.6		14.00	30.33
		Warning! Poor agreement - A= 4.1%(A'c= 60.0%)																		
R_Date MD.14.05.A.276-277	1401	1326	95.4	1363	18	1363	1387	1348	95.4	1367	10	1367		120.4			98.4		39.00	0.40
R_Date JC.14.02.C.168.5-169.5	1695	1557	95.4	1618	41	1609	1596	1552	95.4	1568	11	1565		71.8			96.1		44.00	4.55
R_Date MD.14.05.B1.306.5-307.5	1707	1604	95.4	1654	30	1658	1609	1564	95.4	1579	12	1576		15.3			96.2		45.00	6.25
		Warning! Poor agreement - A= 15.3%(A'c= 60.0%)																		
EQ4							1613	1566	95.4	1581	12	1578					96			
R_Date MR.14.02.A.297.5-298	1690	1544	95.4	1594	33	1588	1615	1569	95.4	1584	12	1580		118.3			95.6		46.00	0.83
R_Date JC.14.02.C.170-171.5	1693	1561	95.4	1616	39	1606	1615	1569	95.4	1584	12	1580		121.1			95.6		46.00	2.67
R_Date MD.14.04.B.379.5-380.5	1709	1614	95.4	1659	28	1658	1615	1569	95.4	1584	12	1580		6.8			95.6		46.00	6.25
		Warning! Poor agreement - A= 6.8%(A'c= 60.0%)																		
R_Date MD.14.05.B1.308-309	1695	1565	95.4	1632	40	1622	1620	1573	95.4	1589	12	1586		80.9			95.1		47.00	3.58
Boundary base of section							1620	1573	95.4	1589	12	1586					95.1			
P_Sequence Northern Humboldt																		Mean=	51.24	8.37
																		StDev=	33.82	8.95

Table DR26. This table summarizes the raw OxCal P-sequence output using k = 8.

													Amodel=	0						Normalized
	UNMODELLED (BP)						MODELLED (BP)						Aoverall=	0					Confidence	Age
	from	to	%	μ	σ	m	from	to	%	μ	σ	m	A_{comb}	A	L	P	C		Interval (yr)	Deviation[1]
2014																				
Boundary surface	-63	-64	95.4	-63	0	-63	-63	-64	95.4	-63	0	-63		100			100			
1700 CE							251	250	95.4	250	0	250					100			
R_Date MD.14.06.168.5-169.5	926	798	95.4	860	39	850	833	809	95.4	821	6	822		48.9			99.9		24.00	6.50
		Warning! Poor agreement - A= 48.9%(A'c= 60.0%)																		
EQ2							836	818	95.4	827	4	828					99.9			
R_Date MR.14.02.B.225-226	955	802	95.4	902	40	921	840	827	95.4	834	2	834		34			99.8		13.00	34.00
		Warning! Poor agreement - A= 34.0%(A'c= 60.0%)																		
R_Date MD.14.06.C.169.5-170.5	952	803	95.3	913	31	923	840	827	95.4	834	2	834		12			99.9		13.00	39.50
		Warning! Poor agreement - A= 12.0%(A'c= 60.0%)																		
R_Date MR.14.05.B.188.5-189.5	959	910	95.4	926	19	927	840	828	95.4	834	2	834		3.1			99.9		12.00	46.00
		Warning! Poor agreement - A= 3.1%(A'c= 60.0%)																		
R_Date MD.14.03.C.212.5-213.5	965	928	95.4	947	11	947	840	828	95.4	834	2	834					99.9		12.00	56.50
		Warning! Poor agreement - A= 0.0%(A'c= 60.0%)																		
R_Date MR.14.02.A.273-273.5	1058	961	95.4	1008	30	1004	1178	1166	95.4	1171	5	1171		0.1			96.4		12.00	32.60
		Warning! Poor agreement - A= 0.1%(A'c= 60.0%)																		
R_Date JC.14.02.D.125.5-126	1072	969	95.4	1025	34	1021	1179	1166	95.4	1171	5	1171		5.9			95.9		13.00	29.20
		Warning! Poor agreement - A= 5.9%(A'c= 60.0%)																		
EQ3							1188	1171	95.4	1179	4	1179					99.7			
R_Date JC.14.02.D.130-130.5	1278	1181	95.4	1229	29	1233	1195	1180	95.4	1186	3	1186		108.4			97.9		15.00	14.33
R_Date MR.14.05.C.246-247	1281	1182	95.4	1232	31	1240	1194	1181	95.4	1186	3	1186		88.5			97.8		13.00	15.33
R_Date MD.17.13.D.250-251	1302	1190	95.4	1278	20	1283	1194	1181	95.4	1186	3	1186		3.4			98		13.00	30.67
		Warning! Poor agreement - A= 3.4%(A'c= 60.0%)																		
R_Date MD.14.05.A.276-277	1401	1326	95.4	1363	18	1363	1382	1349	95.4	1365	8	1365		125.1			99.8		33.00	0.25
R_Date JC.14.02.C.168.5-169.5	1695	1557	95.4	1618	41	1609	1578	1551	95.4	1563	7	1563		58			99.3		27.00	7.86
		Warning! Poor agreement - A= 58.0%(A'c= 60.0%)																		
R_Date MD.14.05.B1.306.5-307.5	1707	1604	95.4	1654	30	1658	1588	1562	95.4	1574	7	1574		13.5			99.1		26.00	11.43
		Warning! Poor agreement - A= 13.5%(A'c= 60.0%)																		
EQ4							1594	1565	95.4	1577	7	1576					98.8			
R_Date MR.14.02.A.297.5-298	1690	1544	95.4	1594	33	1588	1593	1567	95.4	1579	7	1579		121.8			99		26.00	2.14
R_Date JC.14.02.C.170-171.5	1693	1561	95.4	1616	39	1606	1593	1567	95.4	1579	7	1579		123			99		26.00	5.29
R_Date MD.14.04.B.379.5-380.5	1709	1614	95.4	1659	28	1658	1593	1567	95.4	1579	7	1579		4.7			99.1		26.00	11.43
		Warning! Poor agreement - A= 4.7%(A'c= 60.0%)																		
R_Date MD.14.05.B1.308-309	1695	1565	95.4	1632	40	1622	1599	1572	95.4	1585	7	1584		75.6			99.2		27.00	6.71
Boundary base of section							1599	1572	95.4	1585	7	1584					99.2			
P_Sequence Northern Humboldt																		Mean=	19.47	20.57
																		StDev=	7.43	16.90

Table DR27. This table summarizes the raw OxCal P-sequence output using k = 10.

													Amodel=	0						Normalized
	UNMODELLED (BP)						MODELLED (BP)						Aoverall=	0					Confidence	Age
	from	to	%	μ	σ	m	from	to	%	μ	σ	m	A_{comb}	A	L	P	C		Interval (yr)	Deviation[1]
2014																				
Boundary surface	-63	-64	95.4	-63	0	-63	-63	-64	95.4	-63	0	-63		100			100			
1700 CE							251	250	95.4	250	0	250					100			
R_Date MD.14.06.168.5-169.5	926	798	95.4	860	39	850	830	809	95.4	820	5	821		44.1			99.7		21.00	8.00
		Warning! Poor agreement - A= 44.1%(A'c= 60.0%)																		
EQ2							835	817	95.4	827	4	827					99.5			
R_Date MR.14.02.B.225-226	955	802	95.4	902	40	921	839	827	95.4	833	3	833		31.6			98.2		12.00	23.00
		Warning! Poor agreement - A= 31.6%(A'c= 60.0%)																		
R_Date MD.14.06.C.169.5-170.5	952	803	95.3	913	31	923	839	827	95.4	833	3	833		11			98.6		12.00	26.67
		Warning! Poor agreement - A= 11.0%(A'c= 60.0%)																		
R_Date MR.14.05.B.188.5-189.5	959	910	95.4	926	19	927	839	828	95.4	833	3	833		2.8			98.3		11.00	31.00
		Warning! Poor agreement - A= 2.8%(A'c= 60.0%)																		
R_Date MD.14.03.C.212.5-213.5	965	928	95.4	947	11	947	839	828	95.4	833	3	834					98.1		11.00	38.00
		Warning! Poor agreement - A= 0.0%(A'c= 60.0%)																		
R_Date MR.14.02.A.273-273.5	1058	961	95.4	1008	30	1004	1178	1166	95.4	1171	7	1172		0.1			61.2		12.00	23.29
		Warning! Poor agreement - A= 0.1%(A'c= 60.0%)																		
R_Date JC.14.02.D.125.5-126	1072	969	95.4	1025	34	1021	1179	1166	95.4	1171	7	1172		5.1			59.2		13.00	20.86
		Warning! Poor agreement - A= 5.1%(A'c= 60.0%)																		
EQ3							1188	1171	95.4	1179	5	1180					97.8			
R_Date JC.14.02.D.130-130.5	1278	1181	95.4	1229	29	1233	1195	1179	95.4	1187	5	1186		107			27.5		16.00	8.40
R_Date MR.14.05.C.246-247	1281	1182	95.4	1232	31	1240	1195	1178	95.4	1187	5	1186		86.3			27.5		17.00	9.00
R_Date MD.17.13.D.250-251	1302	1190	95.4	1278	20	1283	1195	1178	95.4	1187	5	1186		3.2			26.9		17.00	18.20
		Warning! Poor agreement - A= 3.2%(A'c= 60.0%)																		
R_Date MD.14.05.A.276-277	1401	1326	95.4	1363	18	1363	1380	1350	95.4	1365	8	1365		126.5			98.7		30.00	0.25
R_Date JC.14.02.C.168.5-169.5	1695	1557	95.4	1618	41	1609	1575	1551	95.4	1562	6	1562		51.2			98.8		24.00	9.33
		Warning! Poor agreement - A= 51.2%(A'c= 60.0%)																		
R_Date MD.14.05.B1.306.5-307.5	1707	1604	95.4	1654	30	1658	1584	1563	95.4	1573	5	1573		12.7			97.8		21.00	16.20
		Warning! Poor agreement - A= 12.7%(A'c= 60.0%)																		
EQ4							1589	1565	95.4	1576	6	1575					98.4			
R_Date MR.14.02.A.297.5-298	1690	1544	95.4	1594	33	1588	1589	1568	95.4	1578	6	1578		121.8			96.9		21.00	2.67
R_Date JC.14.02.C.170-171.5	1693	1561	95.4	1616	39	1606	1589	1568	95.4	1578	6	1578		124.1			97		21.00	6.33
R_Date MD.14.04.B.379.5-380.5	1709	1614	95.4	1659	28	1658	1590	1567	95.4	1578	6	1578		4.7			97		23.00	13.50
		Warning! Poor agreement - A= 4.7%(A'c= 60.0%)																		
R_Date MD.14.05.B1.308-309	1695	1565	95.4	1632	40	1622	1595	1572	95.4	1583	6	1583		76.3			98		23.00	8.17
Boundary base of section							1595	1572	95.4	1583	6	1583					98			
P_Sequence Northern Humboldt																		Mean=	17.94	15.46
																		StDev=	5.61	10.46

Table DR28. This table summarizes fossil foraminifera counts across contact A.

Depth	Hs	Bp	Ti	Jm	Mf	Rn	Mp	Ab	Tt	SUM
108.5	18	49	49	63	27	5		2		213
109.5	10	43	51	57	26	3		1		191
110.5	12	25	49	113	10	1				210
111.5	9	61	57	53	30	1				211
112.5	11	35	38	119	25	8				236
113.5	8	36	35	101	25	6		3		214
115.5	54	114	18	22	11					219
116.5	87	125	20	32	5		5		2	276
117.5	31	119	55	14	3					222
118.5	72	55	47	11	20					205
119.5		57	82	70	4				2	215

Hs - *Haplophragmoides* spp.
BP – Balticammina *pseudomacrescens*
Ti – Trochammina *inflata*
Jm – Jadammina *macrescens*
Mf – Miliammina *fusca*
Rn – *Reophax* spp.
Mp – Miliammina *petila*
Ab – *Amobaculites* spp.
Tt – Trochamminita *irregularis*

Table DR29. This table summarizes fossil foraminifera counts across contact B.

Depth	Hs	Bp	Ti	Jm	Mf	Rn	Mp	Ab	Tt	SUM
159.5	12	45	28	23	2					111
160.5	10	49	29	37	4					129
161.5	16	70	36	58					1	182
162.5	12	49	16	23	1					115
159.5	12	45	28	23	2					111
160.5	10	49	29	37	4					129

Hs - *Haplophragmoides* spp.
BP – Balticammina *pseudomacrescens*
Ti – Trochammina *inflata*
Jm – Jadammina *macrescens*
Mf – Miliammina *fusca*
Rn – *Reophax* spp.
Mp – Miliammina *petila*
Ab – *Amobaculites* spp.
Tt – Trochamminita *irregularis*

Table DR30. This table summarizes fossil foraminifera counts across contact C.

Depth	Hs	Bp	Ti	Jm	Mf	Rn	Mp	Ab	Tt	SUM
165.5	12	13	60	78	45	2				210
166.5	25	19	59	50	56	1				210
168.5	13	21	57	57	65	1		1		215
169.5	6	2	11	14	16					49
171.5	15	85	49	28	31					208
173.5	11	75	75	45	5					211
174.5	37	24	72	63	13					209
175.5	14	81	59	51	6		1			212

Hs - *Haplophragmoides* spp.
BP – Balticammina *pseudomacrescens*
Ti – Trochammina *inflata*
Jm – Jadammina *macrescens*
Mf – Miliammina *fusca*
Rn – *Reophax* spp.
Mp – Miliammina *petila*
Ab – *Amobaculites* spp.
Tt – Trochamminita *irregularis*

Table DR31. This table summarizes fossil foraminifera counts across contact D.

Depth	Hs	Bp	Ti	Jm	Mf	Rn	Mp	Ab	Tt	SUM
242.5	8	36	32	79	25	15	0	9		204
245.5	9	24	33	73	33	13	0	12		197
246.5	14	38	44	62	32	16	1	15		222
249.5	38	105	20	56					3	222
251.5	4	12	33	54					2	105
253.5	7	7	149	46						209

Hs - *Haplophragmoides* spp.
BP – Balticammina *pseudomacrescens*
Ti – Trochammina *inflata*
Jm – Jadammina *macrescens*
Mf – Miliammina *fusca*
Rn – *Reophax* spp.
Mp – Miliammina *petila*
Ab – *Amobaculites* spp.
Tt – Trochamminita *irregularis*

Table DR32. This table summarizes fossil foraminifera counts across contact E.

Depth	Hs	Bp	Ti	Jm	Mf	Rn	Mp	Ab	Tt	SUM
302.5	1		61	6	131	10		6		215
304.5	1	1	65	7	119	12		2		207
306.5	1	0	50	1	130	15		3		200
309.5	5	1	57	6	84	7				160
311.5	1	1	23	2	29	2		2		60

Hs - *Haplophragmoides* spp.
BP – Balticammina *pseudomacrescens*
Ti – Trochammina *inflata*
Jm – Jadammina *macrescens*
Mf – Miliammina *fusca*
Rn – *Reophax* spp.
Mp – Miliammina *petila*
Ab – *Amobaculites* spp.
Tt – Trochamminita *irregularis*

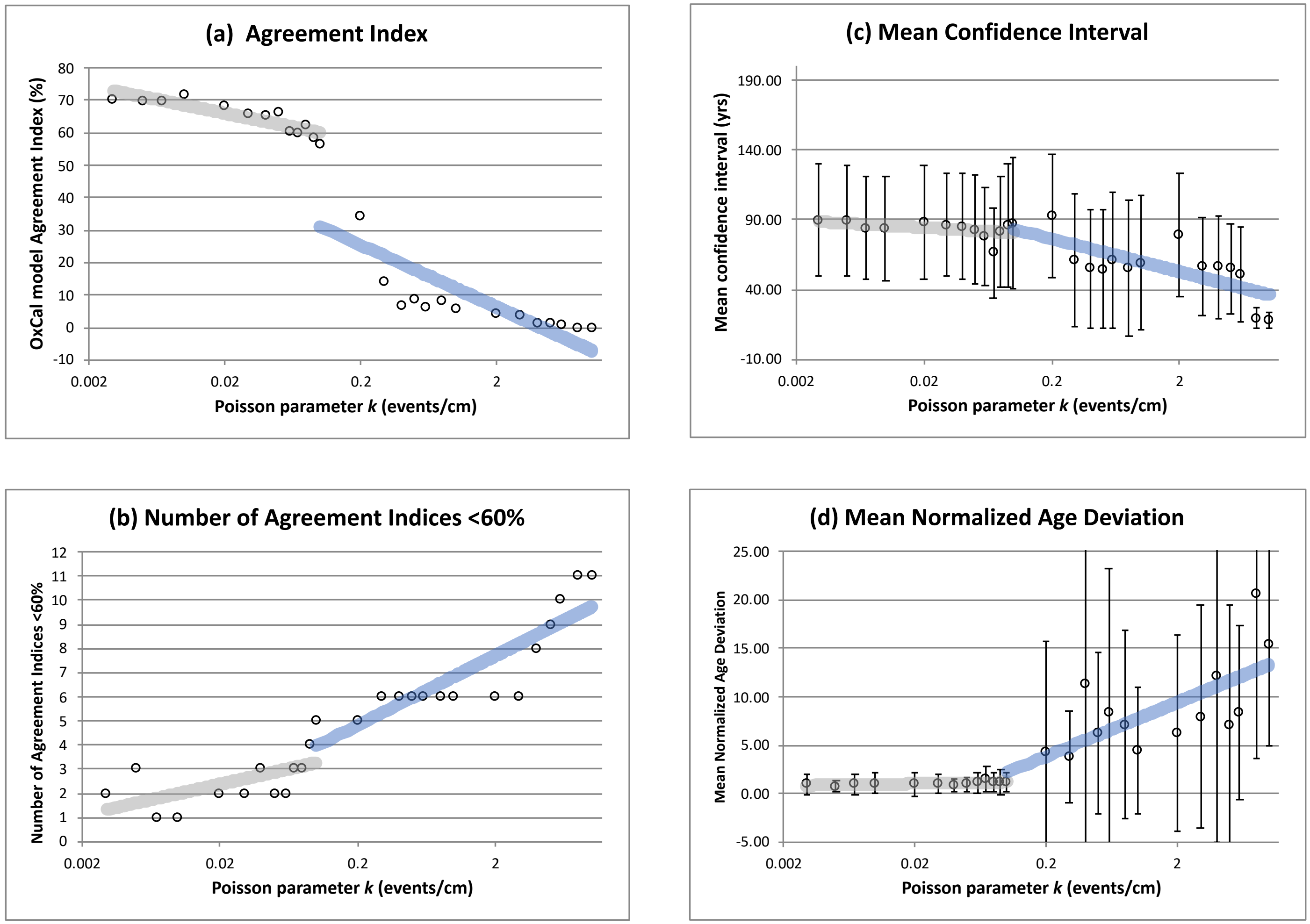

Figure DR1. The plots on this page show clear inflections in the various criteria where the Poisson value is k=0.1. Model results for all twenty six runs using the appropriate k value can be found Table DR1-27.

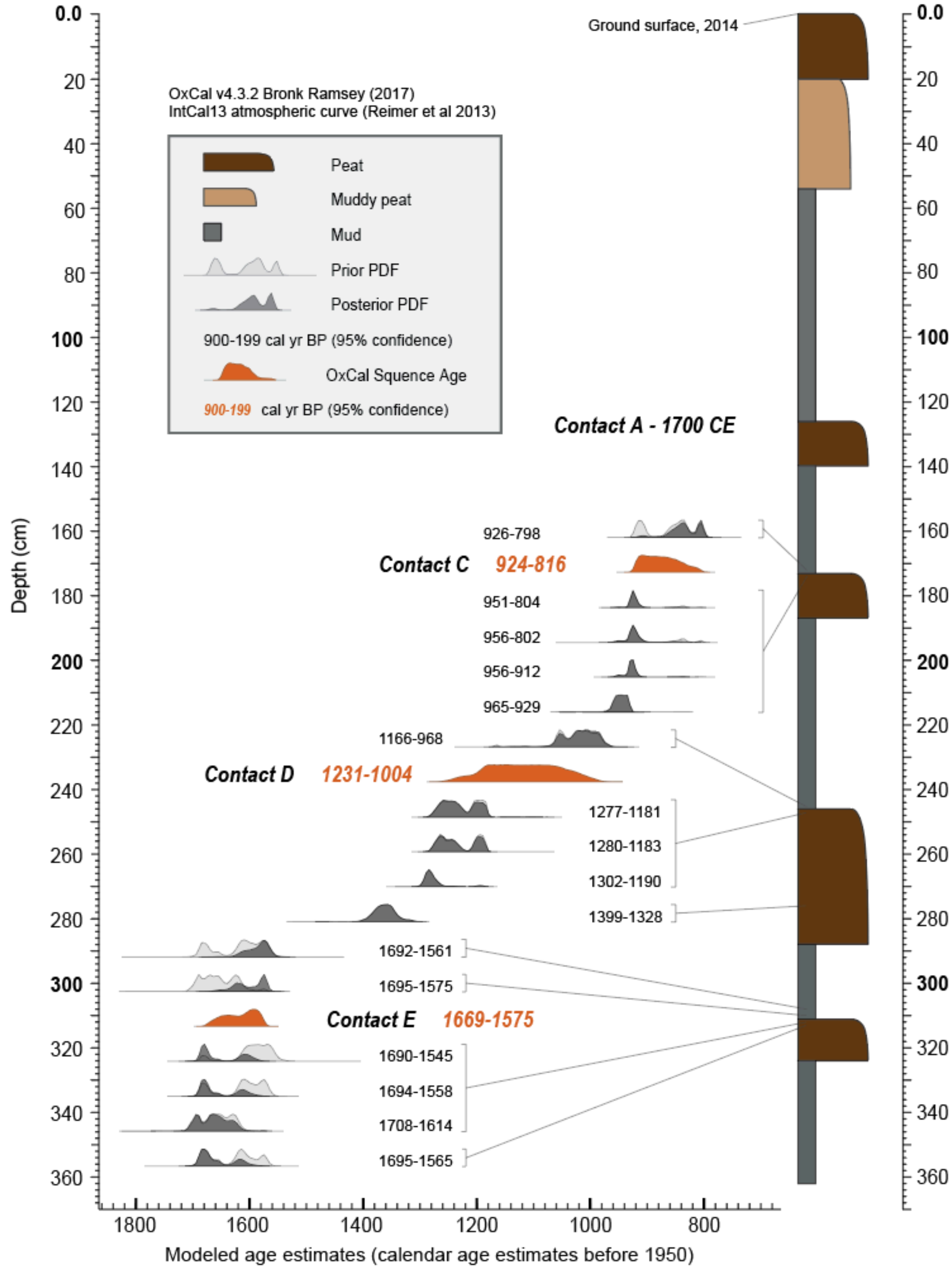

Figure DR2. Composite simplified lithostratigraphy and age constraints used in the development of northern Humboldt Bay age-depth models. Calibrated radiocarbon likelihood distributions and posterior age model are shown in light grey and dark grey (95% confidence interval). The age probability distributions (95% confidence) are the results from OxCal 'Sequence' model are shown in orange. Results of Bayesian age model implemented with OxCal version 4.3.2 (Bronk Ramsey 2017) that used the IntCal13 atmospheric calibration curve (Reimer et al., 2013). Tie-lines connect radiocarbon age PDF's to the appropriate depths on the composite simplified lithostratigraphic column.

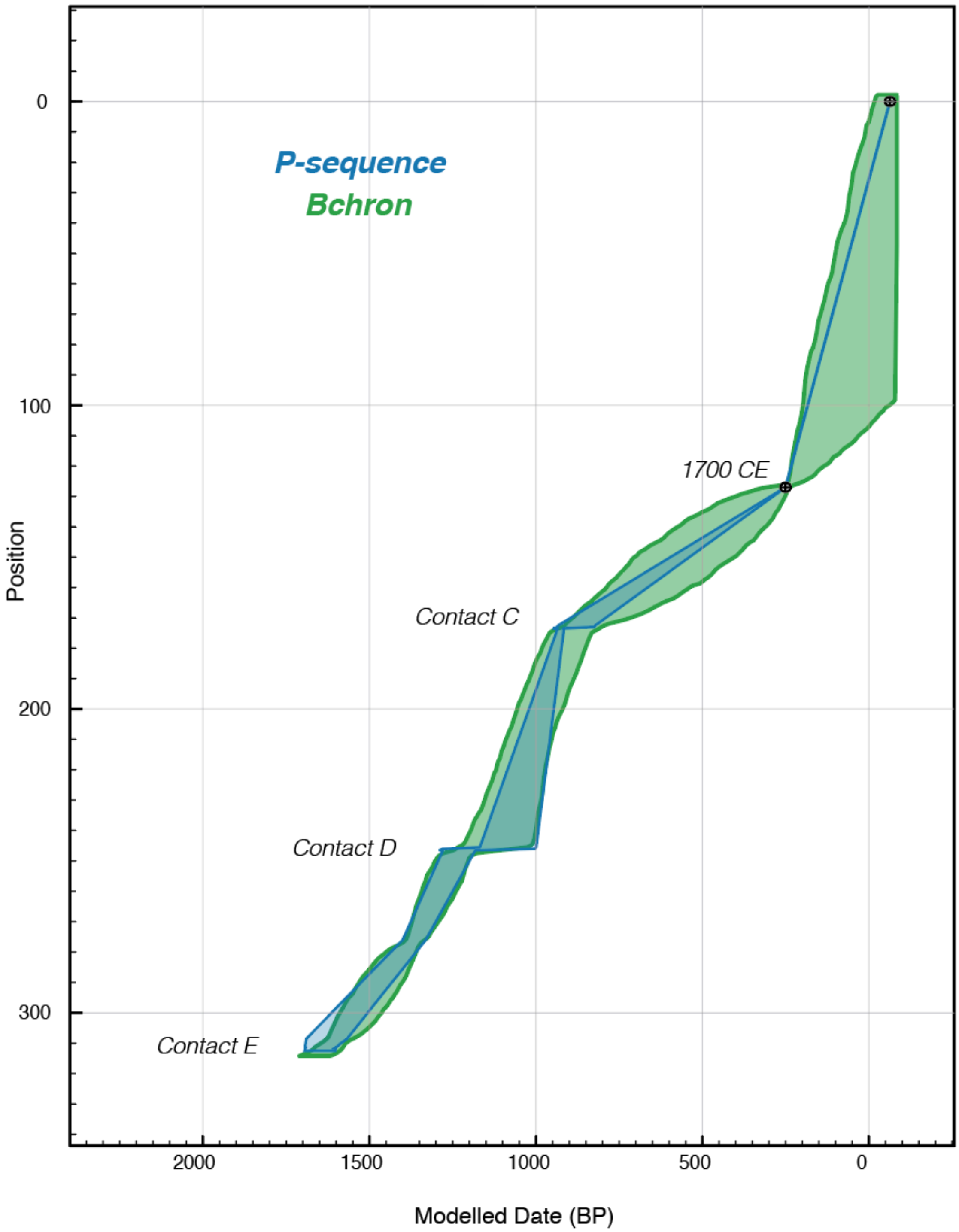

Figure DR3. Plot of overlapping age-depth models of Bchron and OxCal “P-sequence’ (where *k*=0.1).

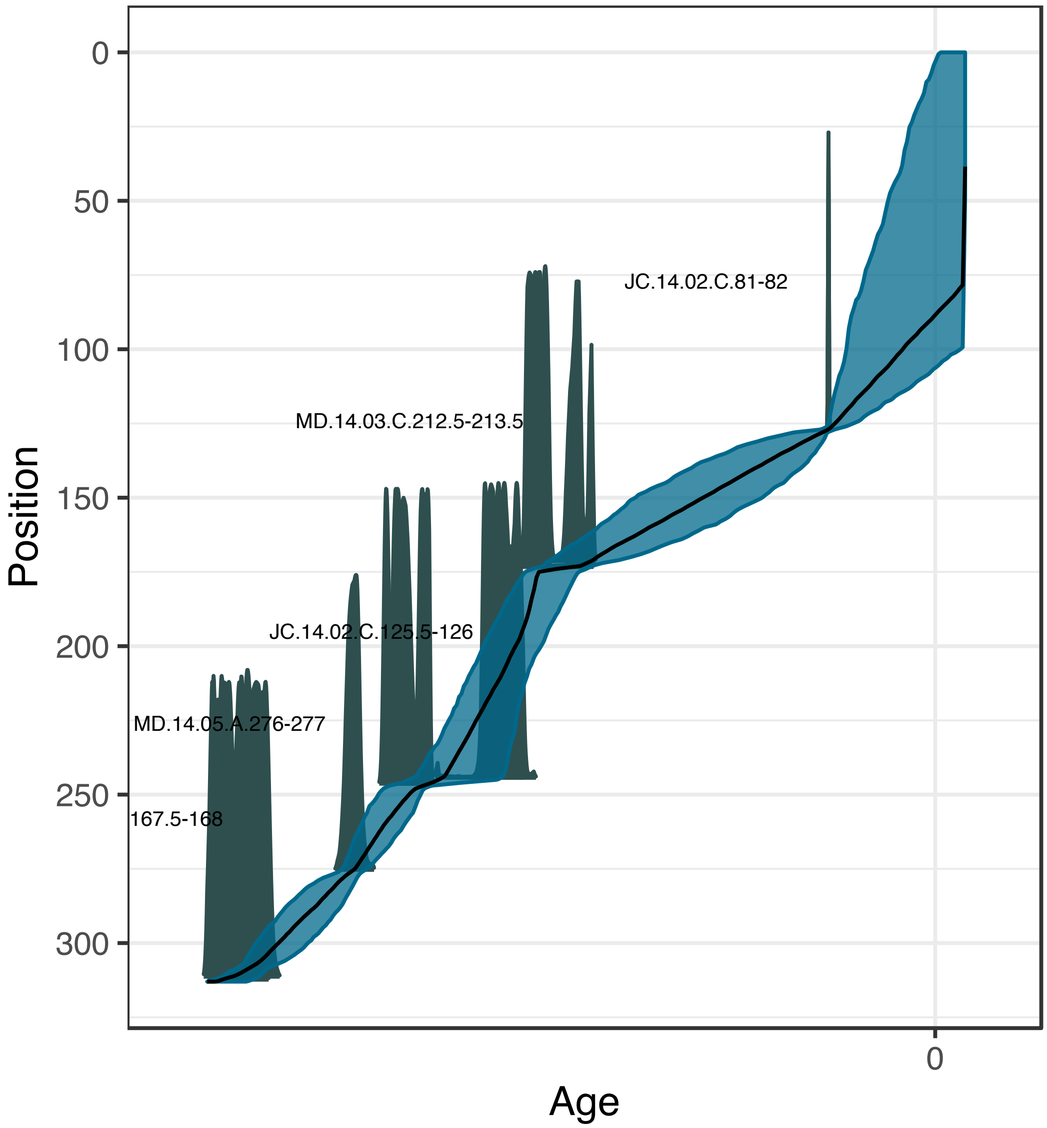

Figure DR4. Plot of Bchron age-depth model.

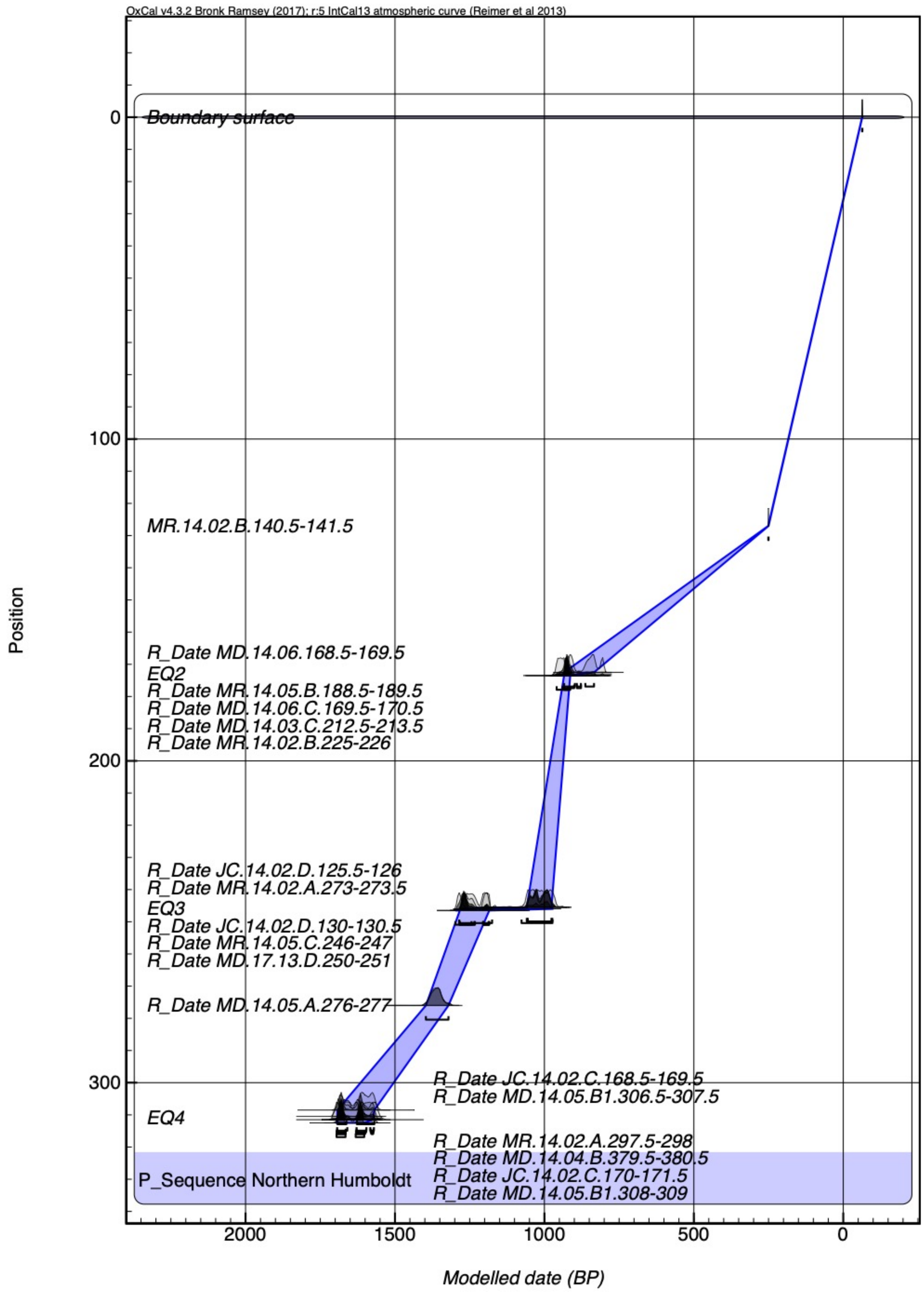

Figure DR5. Plot of OxCal "P-sequence' age-depth model (where *k*=0.1).

```
Plot(P-Sequence)
{
 P_Sequence("Northern Humboldt", 0.1)
 {
  Boundary("base of section");
  R_Date("MD.14.05.B1.308-309", 1720, 15)
  {
   z=312.5;
  };
  R_Date("MD.14.04.B.379.5-380.5", 1750, 15)
  {
   z=311.5;
  };
  R_Date("JC.14.02.C.170-171.5", 1710, 15)
  {
   z=311.5;
  };
  R_Date("MR.14.02.A.297.5-298", 1690, 20)
  {
   z=311.5;
  };
  Date("EQ4")
  {
   z=311;
  };
  R_Date("MD.14.05.B1.306.5-307.5", 1740, 15)
  {
   z=310.5;
  };
  R_Date("JC.14.02.C.168.5-169.5", 1710, 20)
  {
   z=308.5;
  };
  R_Date("MD.14.05.A.276-277", 1480, 15)
  {
   z=276;
  };
  R_Date("MD.17.13.D.250-251", 1340, 20)
  {
   z=246.5;
  };
  R_Date("MR.14.05.C.246-247", 1290, 15)
  {
   z=246.5;
  };
  R_Date("JC.14.02.D.130-130.5", 1280, 20)
  {
   z=246.5;
  };
  Date("EQ3")
  {
   z=246;
  };
  R_Date("JC.14.02.D.125.5-126", 1130, 20)
  {
   z=245.5;
  };
  R_Date("MR.14.02.A.273-273.5", 1100, 20)
  {
   z=245.5;
  };
  R_Date("MD.14.03.C.212.5-213.5", 1040, 15)
  {
   z=173.5;
  };
  R_Date("MR.14.05.B.188.5-189.5", 1000, 15)
  {
   z=173.5;
  };
  R_Date("MD.14.06.C.169.5-170.5", 990, 15)
  {
   z=173.5;
  };
  R_Date("MR.14.02.B.225-226", 990, 20)
  {
   z=173.5;
  };
  Date ("EQ2")
  {
   z=173;
  };
  R_Date("MD.14.06.168.5-169.5", 955, 15)
  {
   z=172.5;
  };
  Date("1700 CE", 1700.1)
  {
   z=127;
  };
  Boundary ("surface", 2014)
  {
   z=0;
  };
 };
};
```

Figure DR6. The OxCal P-sequence model code (using k=0.1).

```
Plot(Sequence)
 {
  Sequence("Northern Humboldt Bay")
  {
   Boundary("base");
   Phase("contact 4 max")
   {
    R_Date("JC.14.02.C.170-171.5", 1710, 15);
    R_Date("MD.14.05.B1.308-309", 1720, 15);
    R_Date("MD.14.04.B.379.5-380.5", 1750, 15);
    R_Date("MR.14.02.A.297.5-298", 1690, 20);
   };
   Date("contact 4");
   Phase("contact 4 min")
   {
    R_Date("JC.14.02.C.168.5-169.5", 1710, 20);
    R_Date("MD.14.05.B1.306.5-307.5", 1740, 15);
   };
   Phase("contact 3 max")
   {
    R_Date("JC.14.02.D.130-130.5", 1280, 20);
    R_Date("MD.14.05.A.276-277", 1480, 15);
    R_Date("MR.14.05.C.246-247", 1290, 15);
    R_Date("MR.17.13.d.250-251", 1340, 20);
   };
   Date("contact 3");
   Phase("contact 3 min")
   {
    R_Date("JC.14.02.D.125.5-126", 1130, 20);
   };
   Phase("contact 2 max")
   {
    R_Date("MD.14.06.C.169.5-170.5", 990, 15);
    R_Date("MD.14.03.C.212.5-213.5", 1040, 15);
    R_Date("MR.14.05.B.188.5-189.5", 1000, 15);
    R_Date("MR.14.02.B.225-226", 990, 20);
   };
   Date("contact 2");
   Phase("contact 2 min")
   {
    R_Date("MD.14.06.168.5-169.5", 955, 15);
   };
   Phase("contact 1 max")
   {
    Date("1700 CE", 1700.1);
   };
   Date("contact 1");
   Boundary("settlement", 1850);
  };
 };
```

Figure DR7. The OxCal ‘Sequence’ model code.